1985

Finline horn antennas.

Haq, Mumtaz ul

NAVAL POSTGRADUATE SCHOOL
Monterey, California

THESIS

FINLINE HORN
ANTENNAS

by

Mumtaz ul Haq

September 1985

Thesis Advisor: J.B. Knorr

SECURITY CLASSIFICATION OF THIS PAGE (When Data Entered)

REPORT DOCUMENTATION PAGE		READ INSTRUCTIONS BEFORE COMPLETING FORM
1. REPORT NUMBER	2. GOVT ACCESSION NO.	3. RECIPIENT'S CATALOG NUMBER
4. TITLE (and Subtitle) Finline Horn Antennas		5. TYPE OF REPORT & PERIOD COVERED Master's Thesis; September 1985
		6. PERFORMING ORG. REPORT NUMBER
7. AUTHOR(s) Mumtaz ul Haq		8. CONTRACT OR GRANT NUMBER(s)
9. PERFORMING ORGANIZATION NAME AND ADDRESS Naval Postgraduate School Monterey, California 93943-5100		10. PROGRAM ELEMENT, PROJECT, TASK AREA & WORK UNIT NUMBERS
11. CONTROLLING OFFICE NAME AND ADDRESS Naval Postgraduate School Monterey, California 93943-5100		12. REPORT DATE September 1985
		13. NUMBER OF PAGES 123
14. MONITORING AGENCY NAME & ADDRESS (if different from Controlling Office)		15. SECURITY CLASS. (of this report) UNCLASSIFIED
		15a. DECLASSIFICATION DOWNGRADING SCHEDULE

16. DISTRIBUTION STATEMENT (of this Report)

Approved for public release; distribution is unlimited

17. DISTRIBUTION STATEMENT (of the abstract entered in Block 20, if different from Report)

18. SUPPLEMENTARY NOTES

19. KEY WORDS (Continue on reverse side if necessary and identify by block number)

Finline Horn Antennas; Printed Circuit Antennas; Finline Monopulse Comparator; Printed Circuit-Monopulse Comparator

20. ABSTRACT (Continue on reverse side if necessary and identify by block number)

This thesis presents the results of an experimental investigation of the finline horn antennas. Both near-field and far-field measurements were made for horns with different physical and electrical parameters. This revealed the influence of the various parameters on the radiation pattern and led to a design which appears to be

close to the optimum with respect to gain and sidelobe levels. The application of these horns in a printed circuit monopulse comparator is also demonstrated.

Approved for public release; distribution is unlimited.

Finline Horn Antennas

by

Mumtaz ul Haq
Lt.Commander Pakistan Navy
B.E., Karachi University Pakistan, 1976

Submitted in partial fulfillment of the requirements for the degree of

MASTER OF SCIENCE IN ELECTRICAL ENGINEERING

from the

NAVAL POSTGRADUATE SCHOOL
September 1985

ABSTRACT

This thesis presents the results of an experimental investigation of the finline horn antennas. Both near-field and far-field measurements were made for horns with different physical and electrical parameters. This revealed the influence of the various parameters on the radiation pattern and led to a design which appears to be close to the optimum with respect to gain and sidelobe levels. The application of these horns in a printed circuit monopulse comparator is also demonstrated.

TABLE OF CONTENTS

LIST OF TABLES

LIST OF FIGURES

ACKNOWLEDGEMENTS

I would like to sincerely thank to my thesis adviser, Professor Jefferey B. Knorr, for his guidance and encouragement throughout this work.

Thanks is also given to my second reader, Professor H.M. Lee, for his suggestions on the microstrip to coaxial cable transition for the monopulse comparator; to my partner in the monopulse comaparator development, LCDR James W. Rowley, for his invaluable suggestions, encouragement, and friendship, without which, this project would not have been as successful as it was. I would also like to thank Microwave Laboratory Supervisor, Gray Rediske and Etching Laboratory Technician, Marc Brown, for their day to day assistance.

Last but not the least, I would like to thank my wife and children for their moral support, tolerance and understanding throughout Naval Postgraduate School stay.

This thesis is dedicated to my father.

I. INTRODUCTION

A. BACKGROUND

Millimeter wave systems offer many advantages over microwave systems such as broad bandwidth, higher spatial and frequency resolution, low probability of interference or interception and small component size. The manufacturing and interfacing of conventional components at these frequencies can lead to tolarence problems. The integrated circuit approach at millimeter wavelengths offers great advantages in terms of design, low insertion losses, compatibility with hybride IC devices, cost and transition to the waveguide instruments. Meier [Ref. 1] showed that many components like a wide band SPST switch, balance mixer, an endfire antenna and a four-port forward coupler could be manufactured using finline technology.

This thesis investigates the possibility of using the near-field antenna testing technique to improve the design of the finline horn antenna and to optimize the gain. It also introduces a new concept, a finline monopulse comparator and presents the experimental results.

1. Electromagnetic Horn Antennas

An open-ended waveguide can act as an antenna at microwave frequencies with a very wide beam and low gain. Basically there is an impedance mismatch at the open-end of the waveguide with respect to free space. If the dimensions of the waveguide are progressively increased to create a considerably larger radiating aperture, a highly directive radiation pattern can be achieved. This type of antenna is called an electromagnetic horn.

There are many types of horn antennas but Pyramid and Sectoral are more commonly used and are shown in Figure 1.1.

The pyramid horns start from a rectangular waveguide and are flared both in the E-plane and in the H-plane. The width of the radiating aperture in the H-plane is denoted by "A", and the height of the radiating aperture in the E-plane is denoted by "B". The flared length of the horn in the H-plane is denoted by "Lh" and flared length of the horn in the E-plane is denoted by "Le" as shown in Figure 1.1(a).

The sectoral horns are a special class of pyramid horns. These are flared either in the E-plane or in the H-plane. The terminology used for pyramid horns is also applicable to the sectoral horns.

2. Finline Horn Antennas

In finline, a dielectric substrate with metal strips on one or both sides is suspended in the E-plane of a rectangular waveguide. Sharma [Ref. 2] classified finline with metal on one side of the dielectric as unilateral finline and that with metal on both sides of the dielectric as bilateral finline. A bilateral finline is shown in Figure 1.2. If the fins are made $\lambda/4$, the open circuit from the waveguide opening should reflect back as a short at the edge of the fins. Thus, it can be modeled as a ridged waveguide.

According to Meier [Ref. 1], if the dielectric in the E-plane of the waveguide is extended beyond the wave-guide open end and the metal strip is flared to a sufficiently large radiating aperture in the E-plane, the resulting antenna can produce a nice radiating pattern. This type of antenna has the potential to mate with MIC's (micro-wave integrated circuit). Integrating an antenna with a receiver can provide advantages in term of size, weight and production cost. Such integration is specially desireable,

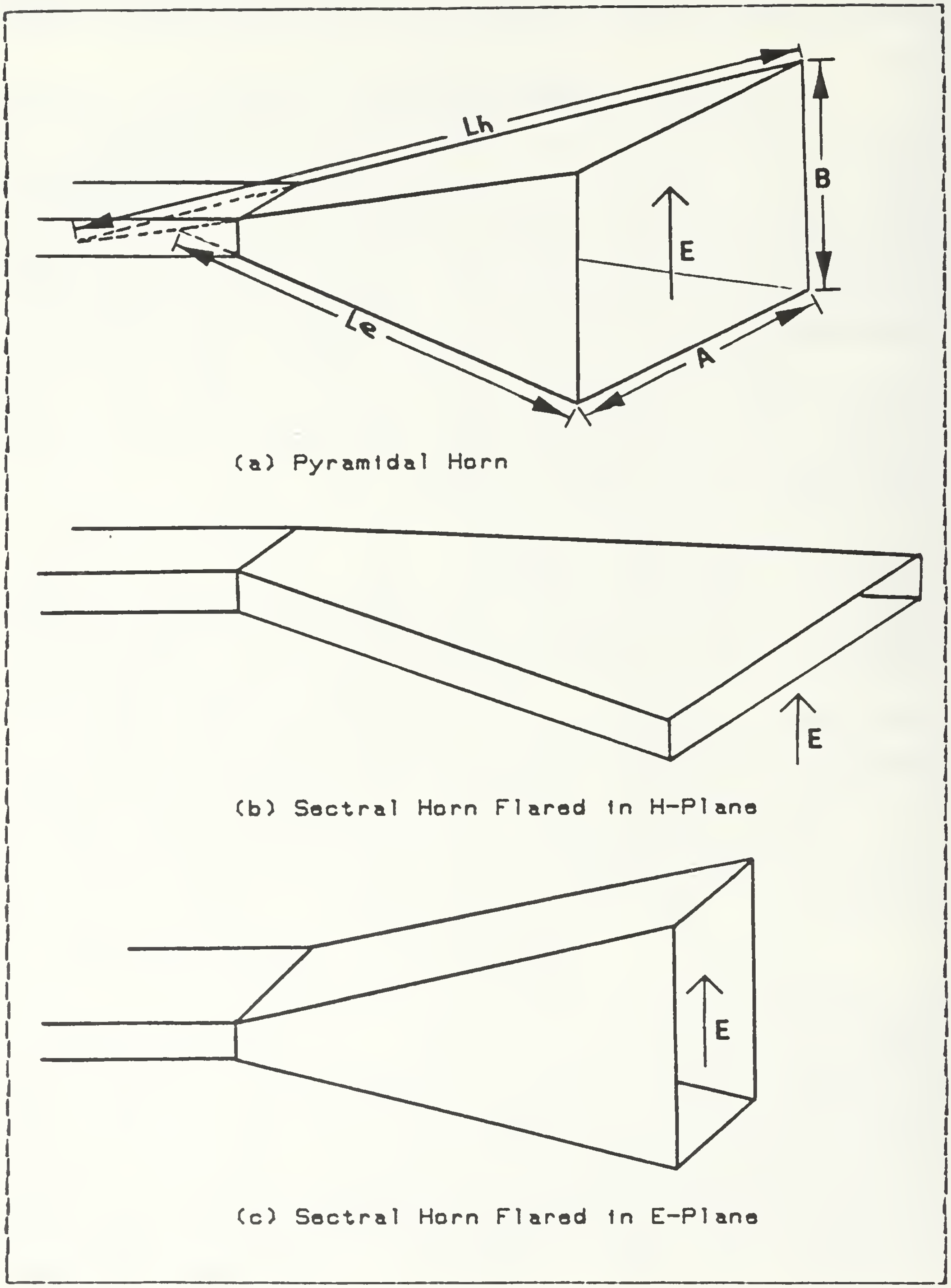

(a) Pyramidal Horn

(b) Sectral Horn Flared in H-Plane

(c) Sectral Horn Flared in E-Plane

Figure 1.1 Types of Horn Antennas.

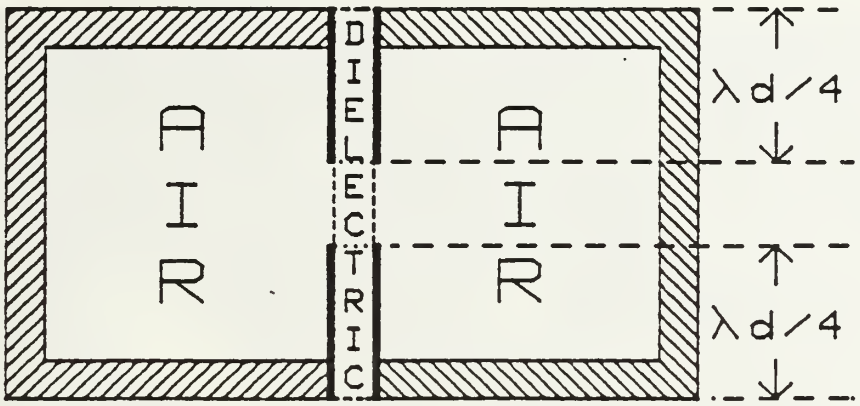

The quarter wavelength sections that reflect the opens at the top and bottom of the dielectric to apperant shorts across the tips of the fins (dotted lines).

Figure 1.2 Bilateral Finline.

when a large number of antenna / receiver modules are required, as in a phased array or multichannel direction finding system.

B. RELATED WORK

1. Near-Field Antenna Testing

Near-field antenna testing has not been very commonly used in the past to improve antenna design. At present only a few near-field measurement ranges are operational, but this technique appears to be heading for an exponential growth in the immediate future.

Harmening [Ref. 3] presented the results of near-field measurement made on the AN/SPY-1 phase array antenna at RCA Government System division in 1979. Stubenrauch and Newell [Ref. 4] published the results of some of the near-field antenna measurements performed at National Bureau of Standards and they particularly mentioned the results of measurements made on a large microstrip phased array for space born synthetic aperture radar (SAR) applications and also provided a comparison between far-field patterns obtained from conventional techniques and those calculated from near-field data.

2. Finline Horn Antenna

In the finline structure, longitudinal metal strips and dielectric layers are suspended in the E-plane of a rectangular waveguide housing to provide capacitive loading to the quasi TE10 mode. This loading widens the single mode bandwidth as in a similar structure, ridged waveguide. [Ref. 1]

Meier [Ref. 1] demonstrated that by extending the finline beyond the rectangular waveguide and flaring it in the E-plane, a suitable radiation pattern with sufficient gain can be achieved. The Ka band finline antenna reported by Meier had a gain of 13.5 dB. The half power beam widths were 44 deg. in the H-plane, and 27 deg. in the E-plane. A simple finline taper between the aperture and the waveguide feed provided an input VSWR of 1.8 across a 4.0 GHz band centered at 35.0 GHz.

Musitano [Ref. 5] measured a series of radiation patterns for finline horns already designed by Prof. J.B.Knorr as shown in Figure 1.3. For different flare lengths and angles he measured gain and 3 dB beam widths in the E and H-planes. Most of the radiation patterns were unsatisfactory and did not have clear main beams and the side lobes were far too high. The radiation pattern of E-plane and of H-plane are shown in Figure 1.4 and Figure 1.5 respectively.

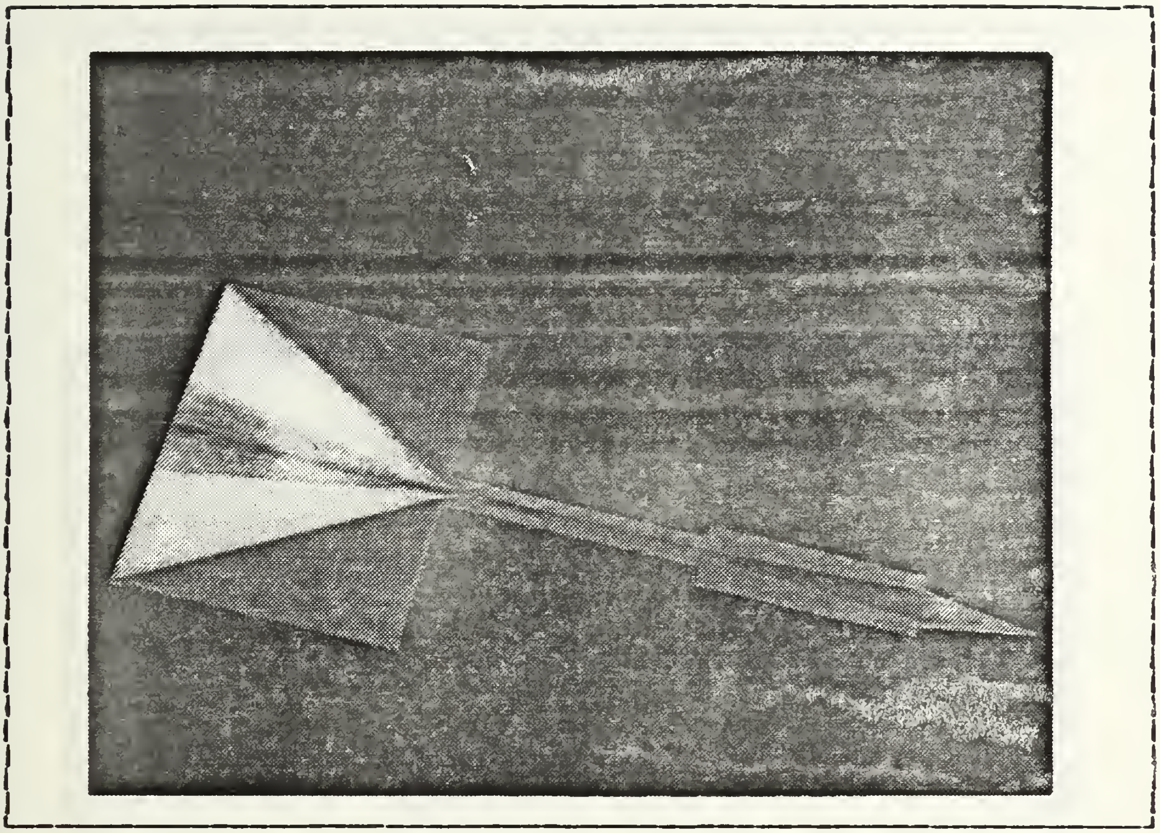

Figure 1.3 Finline Horn Antenna.

C. PURPOSE

The main purpose of this thesis is to perform near-field measurements on the finline horn antenna already designed by Prof. J.B.Knorr and to highlight the causes for the unsatisfactory far-field radiation pattern and using the near-field measurement observation, redesign the finline horn antenna with a uniform phase front. A secondary purpose is, to combine two finline horn antennas with a finline magic-tee to form a monopulse comparator and demonstrate sum and difference radiation patterns.

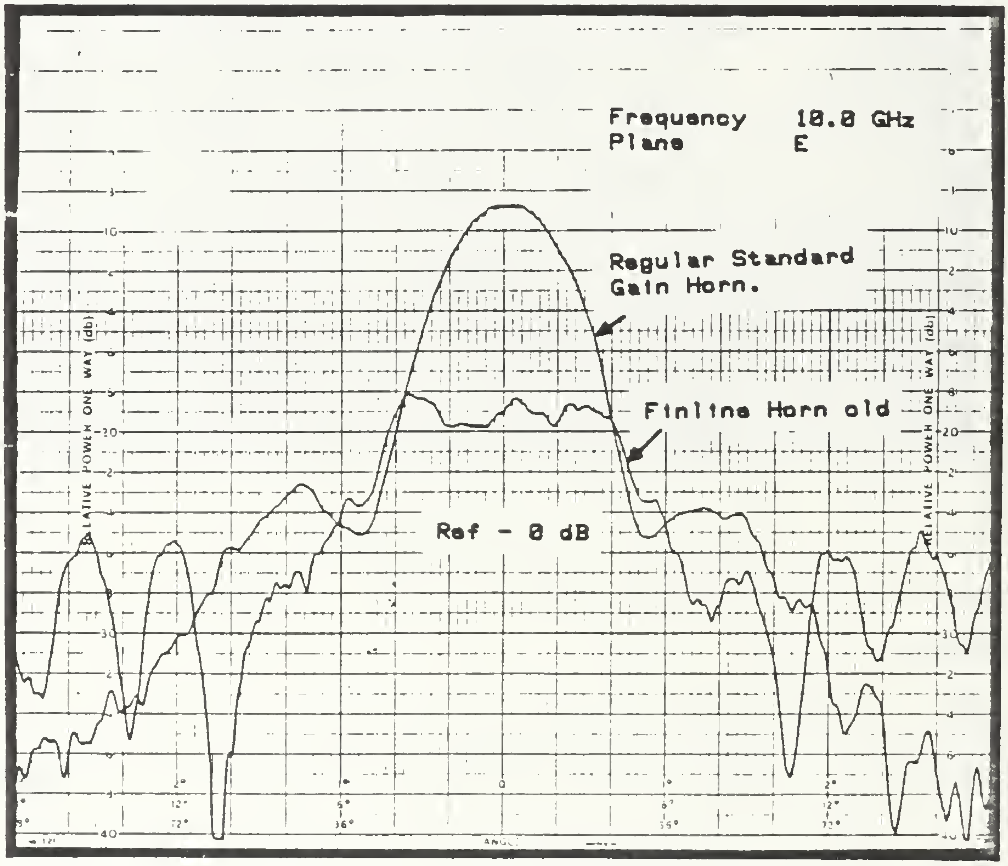

Figure 1.4 E-Plane Radiation Pattern of Old Finline Horn.

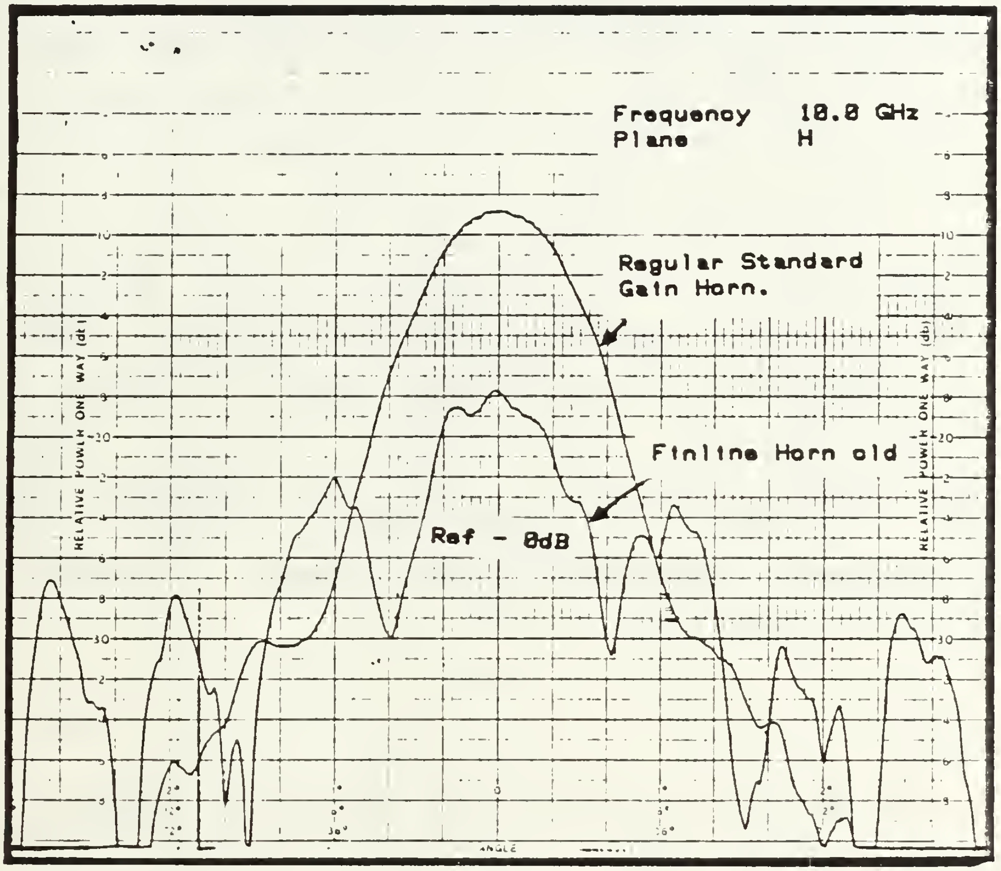

Figure 1.5 H-Plane Radiation Pattern of Old Finline Horn.

II. THEORY

A. NEAR-FIELD ANTENNA TESTING

1. Near-Field Testing Process

Near-field antenna testing is based on the accurate characterisaton of the RF field (phase and amplitude) of an antenna under test over a measurement plane parallel to and displaced a few wavelengths from the antenna aperture plane. The RF field is measured by precisely positioning an RF probe at uniformly spaced points in the aperture plane. This near-field is then transformed by fast Fourier transform to an E-plane far-field radiation pattern. [Ref. 3]

The area of the measurement plane is finite, and the resulting truncation of the measured RF field defines the maximum angles that will yield an accurate far-field pattern. A schematic relationship and far-field cutoff angle criterion for a planer near-field pattern range is shown in Figure 2.1. From Figure 2.1

$$Qc = \tan^{-1} (Lx-a)/2D \qquad \text{(eqn 2.1)}$$

Qc is the maximum angle to which far-field patterns can be accurately determined.

2. Error Sources

There are many error sources which contribute to the inaccuracy of the near-field measurement. These are discussed in the following paragraphs.

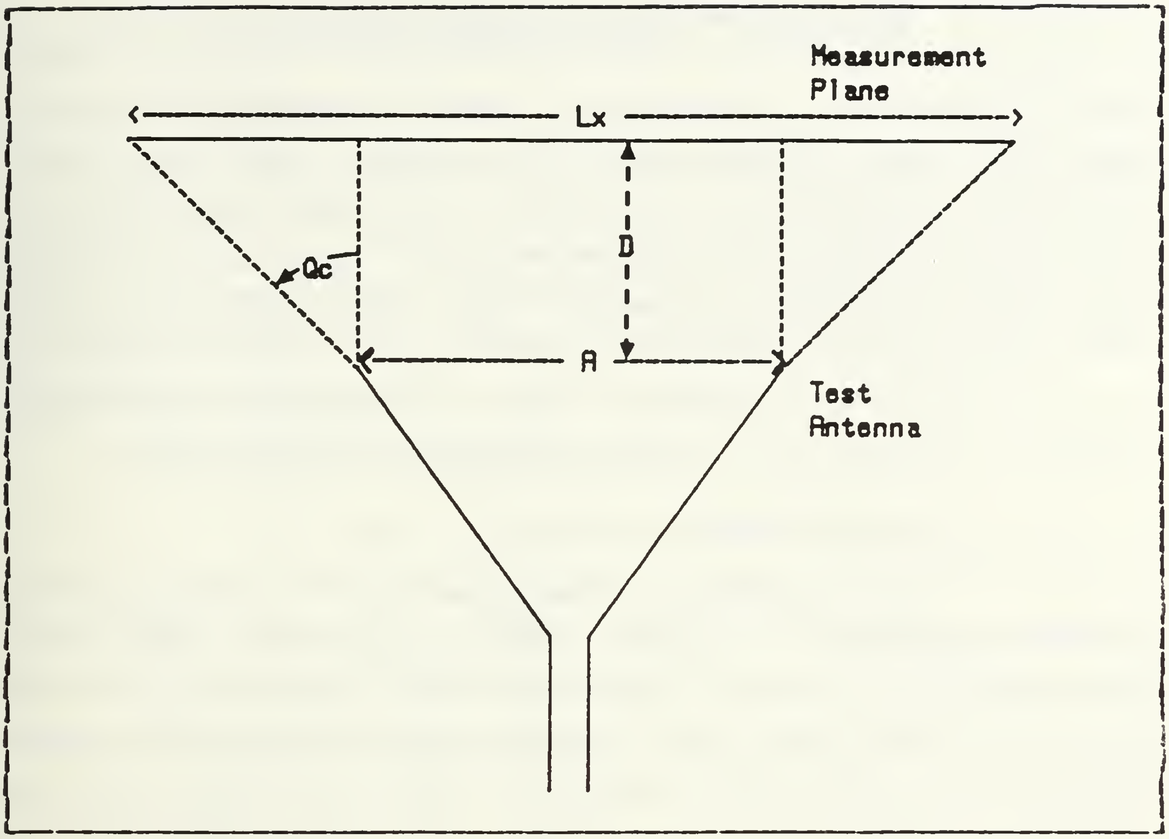

Figure 2.1 Near-Field Pattern Range Geometry.

a. Probe Position Error

The main contribution to the total fractional far-field error is due to the probe position error. There are two type of probe positioning error, the first is out of plane displacement (z-direction) of the RF probe and the second is in plane horizontal (x) direction and / or vertical (y) direction displacement of the probe. The probe is modeled as being at a point $p+\Delta p$ on the plane $Z = d + \Delta z$ in front of the test antenna. There exists an error pattern due to the difference between the desired near electric field at the point (p,d) and the field actually measured by the probe at the point $(p+\Delta p, d+\Delta z)$ as given by:

$$\Delta \bar{E}_t(\bar{\rho},\alpha) = \bar{E}_t(\bar{\rho}+\Delta\bar{\rho},\alpha+\Delta z) - \bar{E}_t(\bar{\rho},\alpha)$$

The displacement of the probe from a measurement plane at the instant of measurement will cause an error in phase as well as in magnitude, which in turn when transformed to far-field pattern will introduce error which is a function of antenna frequency, aperture size, illumination function and gain. In the near-field measurement, probe positioning is so critical that Warmening [Ref. 6] suggested probe positioning by Lasers for precise near-field measurements.

b. Probe Pattern Errors

The probe that measures the near-field of an antenna possesses a response which weights the field of the probe over its volume to produce a net signal and this can introduce some error when transforming the near-field measurement to the far-field pattern. There are many different ways to overcome this error. Huss [Ref. 7] suggested that if the probe antenna characteristics are known then probe pattern correction should be applied when transforming the near-field measurements in to far-field pattern or the separation distance between the measurement plane and antenna face should be increased to several wavelengths to avoid any probe pattern error.

The probe pattern is more important for small probes and when the measurement plane is within 1-2 wavelengths from the antenna face.

c. Probe Polarization Error

The probe's output not only depends upon its position on the measurement plane but is also a function of its polarization. If the polarization of the probe and the antenna are not matched, the probe will not respond to all the field present at that point. It is hard to know the polarization of the probe and the antenna both before hand. Hammening [Ref. 6] suggested that if it is assumed that the probe and antenna are not well matched, two separate scans with the probe mounted in the co-polarized and cross-polarized configuration should be performed. This would double the scan time and increase data reduction time. Then data from both scan polarizations as well as from probe calibration (if any) should be combined to obtain final antenna RF performance.

d. Multiple Reflections

The determination of test antenna radiation pattern from near-field measurement assumes that the measured data does not include multiple reflections from the near by objects or testing probe etc. Both amplitude and phase variations arising from multiple reflections can mask the desired field distribution along the scan plane. This is particularly true for a probe / test antenna separation distance on the order of one wavelength and for frequencies where the probe becomes electrically large. Grimm [Ref. 8] suggested that error due to multiple reflections could be avoided either by increasing the probe to test antenna separation distance or by averaging several sets of near field data taken at various multiples of $\lambda/8$ separation.

e. Instrumentation Errors

A final source of far-field error is due to the imprecision of the near field test instruments. As stated by Grimm [Ref. 8], typical microwave receivers measures RF phase to within 0.05 deg for maximum amplitude input and to within 0.5 deg when the RF signal amplitude is 20 dB down from the maximum. Such a small phase variation contributes negligibe error to the far-field pattern. However, the typical receiver's inability to measure RF amplitude accurately contributes significantly to the far-field pattern error.

B. HORN ANTENNAS

The standard electromagnetic horn can be used either as a primary antenna or as a reflector feed driven from a waveguide. Horns are flared in the E and or H-planes according to the design requirements. When the energy is transmitted from the horn there may or may not be a reflection of energy. A reflected wave will inevitably disturb the incident wave and give rise to a standing wave. If this ratio is equal to 1, there is no reflected energy; i.e all the energy provided by the waveguide is transmitted into space by the horn and there is a perfect impedance match of the horn with free space. From the Reciprocity Theorem, it follows that under such circumstances, all the energy arriving from free space and entering the horn will be passed to the waveguide. The horn may therefore be considered as a transformer between waveguide and space.

The mouth of the horn is a radiating aperture and the the radiation from this aperture would depend upon the distribution of amplitude and phase in the aperture plane. In fact, it is more complicated because the external walls of the horn contain currents which influence the far-field radiation pattern. Therefore it is very difficult if not impossible to make precise calculations. For horns with large aperture, it is the amplitude and phase distribution of the aperture field which has the predominating influence on the radiation pattern. For horns with dimensions which do not exceed one or two wavelengths the effect of currents circulating on the external walls becomes appreciable. [Ref. 9]

The field variation across the aperture of an electromagnetic horn is similar to the field distribution of the TE10 mode across a rectangular waveguide. The field amplitude distribution is uniform in the E-plane and obeys approximately a cosine law in the H-plane. If we consider the aperture of a horn in the H-plane the field intensity is maximum at the center of the horn and falls gradually to the sides and at the side wall of the horn, the field vanishes. Therefore we can define the aperture of a horn in the H-plane in another way; half the radiating aperture (A/2) is equal the distance from the point of maximum field amplitude to the point where the field amplitude becomes sufficiently negligible.

According to Thourel [Ref. 9], the beam width in the E-plane and in the H-plane for a regular horn antenna can be approximated by $51*\lambda/B$ and $69*\lambda/A$ respectively. According to Ghandi [Ref. 10: p. 140] for the optimum design the gain of a pyramid horn can be approximated by $0.5*4\pi*(AB/\lambda^2)$, the gain of a sectoral horn flared in the H- plane can be approximated by $0.63*4\pi*(AB/\lambda^2)$, and the gain of a sectoral horn flared in the E-plane can be approximated by $0.65*4\pi*(AB/\lambda^2)$. The constant terms 0.5, 0.63 and 0.65 are illumination factors. Therefore, the gain of any pyramid or sectoral horn can be approximated by

$$\text{Gain} = (\text{constant})*4\pi*(AB/\lambda^2) \qquad \text{(eqn 2.2)}$$

where the constant is the illumination efficiency.

Equation 2.2 can also be written as

$$\text{Gain} = C*(AB/\lambda^2) \qquad \text{(eqn 2.3)}$$

where $C = (\text{Illumination efficiency}) * 4\pi$.

1. Finline Horn Antenna

The theory and design considerations for a finline horn are not altogether different from those for a standard electromagnetic horn. For the standard electromagnetic horn the medium of propagation is air , where as in the finline horn the medium of propagation is partially dielectric material and partially air.

Basically the finline horn is fed from a slot and the slot can be transitioned from waveguide, coaxial cable or from another microwave device e.g. finline magic-tee, depending upon the design requirements. The width of the slot is very critical. If it is fed from a coaxial cable it should match the impedance of the coaxial cable, if it is fed from another microwave device it should match the impedance of that device and if it is transitioned from a waveguide, then the width of the slot is a variable parameter. The waveguide can be matched to the desired width of the slot by taper design as described by Adalbert and Ingo [Ref. 11].

In addition to the slot width, the height of fins in the waveguide is also an important factor in the design of finline horns. For the ideal design the height of fins should be $\lambda/2$, so that the short from the waveguide wall should reflect back as a short at the edge of the fins. In that case the finline can be modeled as a riged waveguide. The ideal design requirement for the slot width and the fin height are difficult to meet, but through suitable selection of dielectric material both conditions can be satisfied. If under some circumstances the condition of $\lambda/2$ for fins can not be satisfied, then the finline cannot exactly be modeled as a ridged waveguide but it can be visualized as two fins in the waveguide and most of the field will concentrate between the fins depending upon the dielectric constant of the material. In our experiment, we will consider finline horn driven with different slot widths and discuss the results obtain from these changes.

For the finline horn, we have physical control of the flare length, flare angle and radiating aperture in the E-plane, but we have no physical control on the parameters in the H-plane. However by using different dielectric material, we can control the effective aperture length in the H-plane.

As mentioned in the preceding paragraphs, half of the radiating aperture (A/2) in the H-plane can be defined from the maximum field strength point to the point where the field becomes negligible. If we use the higher dielectric constant material, more field will be concentrating in the dielectric and the point of negligible field strength will move closer to the center, thereby reducing the aperture size in the H-plane. Therefore, we can control the radiating aperture in the H-plane by using different dielectric materials. Mathematically we can define the H-plane radiating aperture (A) by the following equation,

$$A = K1 * 1 / (Er)^{K2} \quad \text{or} \quad A / \lambda = K1 * 1 / (Er)^{K2} \qquad \text{(eqn 2.4)}$$

where K1 and K2 are constants.

Now considering the simplified gain equation of 2.3, we know the physical dimensions of B/λ of the finline horn and we can approximate the dimensions of A/λ from Equation 2.4 . If we substitute the A/λ from Equation 2.4 into Equation 2.3 , we get

$$\text{Gain} = C1 * \frac{B}{\lambda * (Er)^{C2}} \qquad \text{(eqn 2.5)}$$

Where C1 and C2 are constants.

If by some means we can find the values of the constants C1 and C2, then we can approximate the gain of a finline horn antenna. We will use the experimental approach to find the values of C1 and C2 in the next chapter. Similarly the beamwidth in E and H-planes can be approximated by $K1*\lambda/B$ and $K2*(Er)^{K3}$ respectively and constant terms can be found from the experimental results.

2. Design Considerations for the Finline Horn Antenna

There are many design parameters which need to be considered for the design of a finline horn antenna. In the following paragraphs we will discuss each one of them.

Given the gain and beamwidth of the finline horn antenna, we need to calculate the flare length (Le), flare angle, radiating aperture (B) and Er. The flare length is normally defined in terms of number of wavelengths in the dielectric. The Le normally depends upon the gain we want and how long a horn antenna we can afford to make. A series of curves for different Le's has been shown by Jasik [Ref. 12:p. 10-6]. These curves are plotted for b/λ vs $Ge*(\lambda/a)$. For a specific le, the $Ge*(\lambda/a)$ increases with an increase in b/λ and reaches an optimum value and any further increase in b/λ beyond the optimum value decreases the $Ge*(\lambda/a)$. As mentioned previously, we have no physical dimensions in the H-plane, however we have established an equivalence in terms of dielectric constant. We can still use these curves but cannot calculate the exact gain. One might consider taking b/λ for the optimum value, but this is not always the best solution because in addition to high gain we need a well defined main beam and low side lobes. Jasik [Ref. 12:p. 10-4] shows the universal radiation patterns in the E and H-planes. These Figures have been replotted in Figures 2.2 and 2.3. As shown in Figure 2.2, for lower side lobes we need to have a lower value of maximum phase deviation in wavelength (S), which is defined by

$$S = B^2 / (8 * \lambda * Le) \qquad \text{(eqn 2.6)}$$

Where B is radiation aperture in E-plane
Le is flare length in E-plane
and λ is wavelength in air.

From Figure 2.2, we can see that for a good radiation pattern, we need to have S < 0.125. A higher value of S will give a completely distorted radiation pattern. These curves of Figures 2.2 and 2.3 are for design of regular horn antennas. Now the question arises as to wether we can use these curves for a finline horn and if so wether we should take the wavelength in air or dielectric. We will show in our experiment that these curves are still applicable. We sould use the wavelength in air for calculation of S because when waves leaves the radiating plane they are in the air. The Figure 2.3 shows the universal radiation patterns in the H-plane. These patterns are also functions of maximum phase deviation (in wavelengths) in the H-plane. Maximum phase deviation in wavelengths (T) is defined by

$$T = A^2 / (8 * \lambda * Lh) \qquad \text{(eqn 2.7)}$$

Where A is radiation aperture in H-plane
Lh is flare length in H-plane
and λ is wavelength in air.

In equation 2.7, most of the terms are unknown in the case of a finline horn. We can see from Figure 2.3 that for this case also a lower value of T is desireable. However, a higher value of T will not seriously distort the pattern, but will give a wide pattern, which can be controlled by suitable choise of dielectric material.

From the above paragraphs we can concluded that radiating aperture (B), flare length (Le), flare angle and Er are interrelated and they need to be carefully selected according to the design requirements.

3. Uniform Phase Front Finline Horn Antenna

The radiation from an aperture is governed by the distribution of the fields on it. A reflector may be considered as an aperture, and its radiation pattern is governed by its illumination. In the most general case this illumination is supplied by the horn radiating towards the reflector. The distribution of the field at the aperture thus depends upon the shape of the horn's radiating plane.

The field distribution at the aperture of a regular horn antenna is quite difficult to change. However, some methods have been discussed by Thoural [Ref. 9]. In the case of a finline horn antenna, the field distribution at the radiating aperture can very effectively be varied.

Under normal circumstances the field distribution at the aperture has a semicirclar shape and the direction of propagation is perpendicular to the field. If we visualize, we have a diverging field. To achieve a uniform phase front at the radiating aperture, then the field must be propagating parallel to the Z-direction. In the following paragraphs, we will discuss a method to obtain a uniform phase front on a finline horn antenna.

For a uniform phase front, basically what we want is to slow down the field in the center or make the field at the edges to go fast, so that at the horn mouth, all the wave elements have the same phase. This can be done in several ways. One of the methods we considered was to drill holes in the dielectric edges to make the wave move faster on the edges and gradually slow down in the center. This concept is quite difficult to implement because it is hard

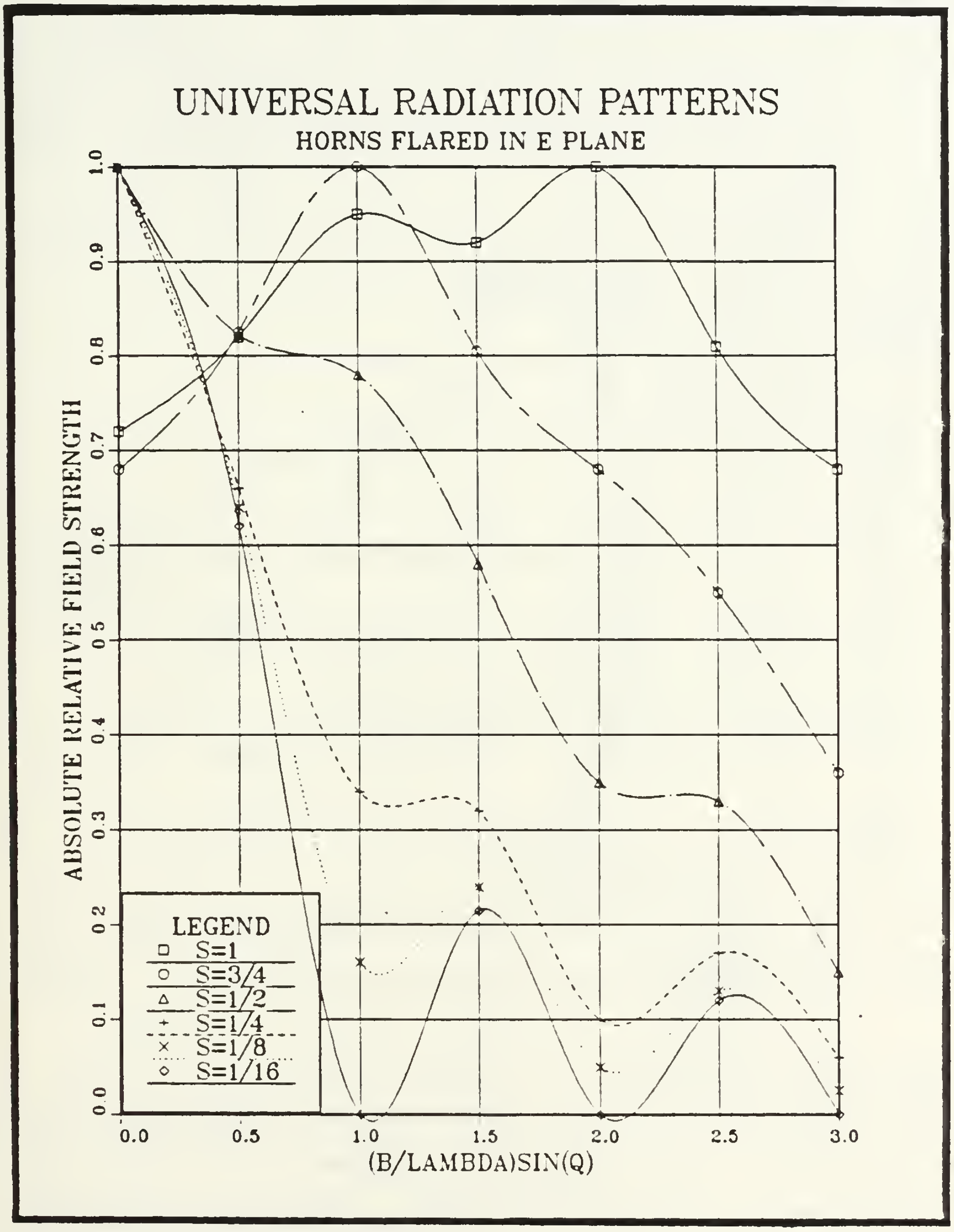

Figure 2.2 Universal Radiation Pattern in E-Plane (After Jasik, ref. 12).

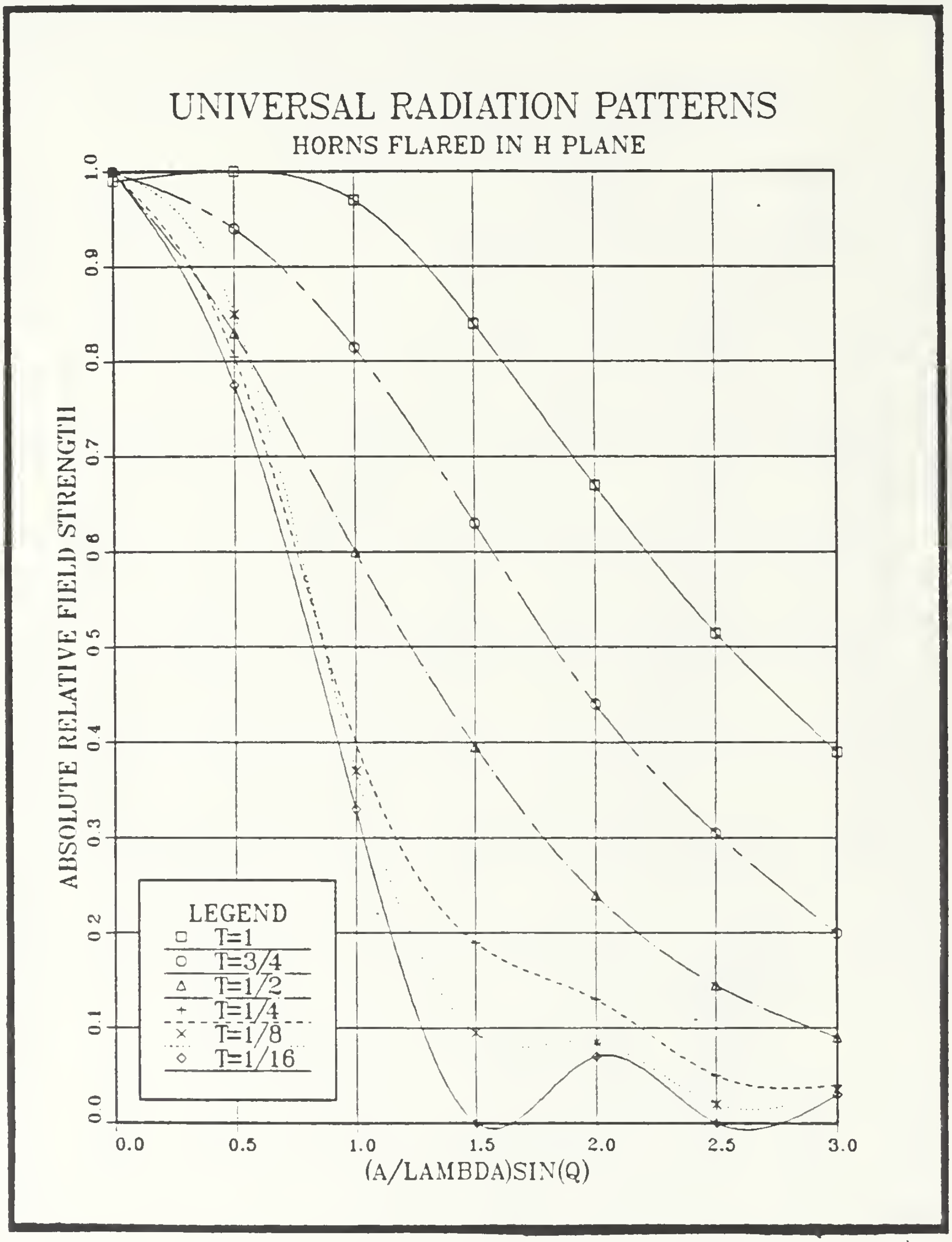

Figure 2.3 Universal Radiation Pattern in H-Plane (After Jasik, ref. 12).

to calculate the exact size, numbers and position of the holes. The second method we considered was to extend the dielectric beyond the horn mouth in a particular shape, so that the waves in center should keep on moving at the speed in the dielectric and at the edges the wave should move at the speed in the air and in some plane in front of the horn antenna, the field will have a uniform phase front.

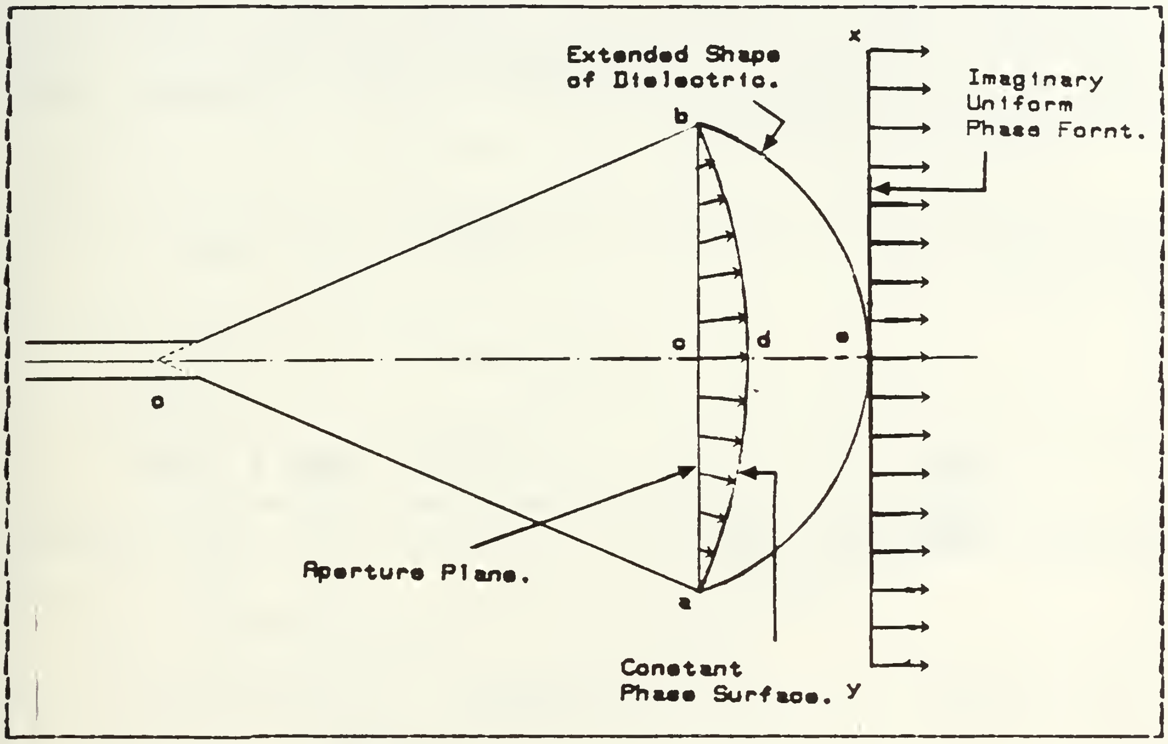

Figure 2.4 Finline Horn Antenna with Uniform Phase Front.

The finline horn antenna with extended dielectric is shown in Figure 2.4. Where plane acb is the aperture plane, the curve adb is a constant phase surface, and curve aeb is the extended dielectric shape to produce a uniform phase front at an imaginary plane xey. If we carefully visualize the Figure 2.4, we are introducing a converging lens in front of the aperture plane.

The lens theory is not a new concept. It has been previously considered by Fradin [Ref. 13], but he put a particular shape of dielectric in the mouth of the regular horn antenna in order to change the phase front in a desired way. In that method the wave was transitioning from air to dielectric and back to air. In the finline horn antenna, we are extending the dielectric and it is the shape of the dielectric which produces the uniform phase front at an imaginary plane. In the following section we will derive the equation to calculate the precise length of extended dielectric beyond the aperture.

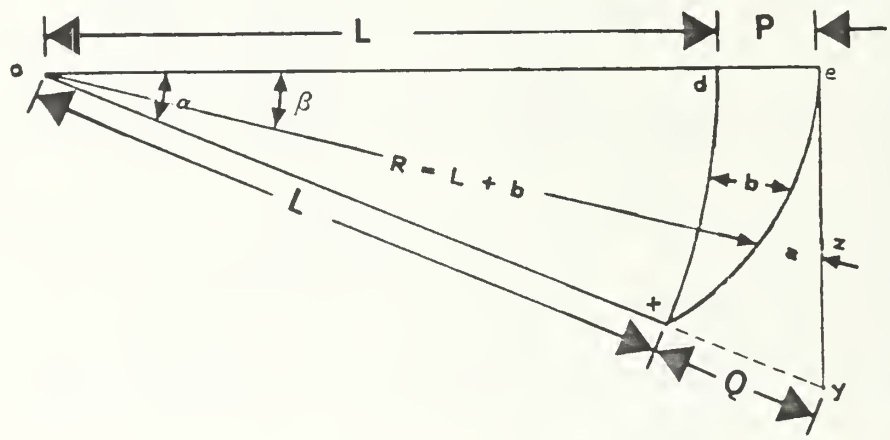

Figure 2.5 Geometry of Uniform Phase Front.

The finline horn antenna is symmetrical about its center axis, therefore we will only consider half as shown in Figure 2.5. Here L is the flare length from origin to the constant phase surface, is the flare angle, ey is the uniform phase surface, P is the length of the extended dielectric at the center, Q is the radial length from edge of horn to the uniform phase front and b is the radial length of the extended dielectric at an angle .

We need to calculate the radial extension (b) in terms of angle from the origin. In order to obtain a uniform phase front at plane ey as shown in Figure 2.5, we need to make the distances P , Q and a + b electrically the same. It was assumed during these calculations that incident field at the edge of dielectric is perpendicular to the dielectric shape, therefore reflection can be neglected.

$$Q = P\sqrt{Er} = a + b\sqrt{Er} \qquad \text{(eqn 2.8)}$$

From triangle oye of Figure 2.5,

$$L + P = (L + Q) * \cos(\alpha) \qquad \text{(eqn 2.9)}$$

Substituting P in term of Q from Equation 2.8 in Equation 2.9.

$$L + P = (L + P\sqrt{Er}) * \cos(\alpha) \qquad \text{(eqn 2.10)}$$

From Equation 2.10,

$$P = \frac{(1-\cos\alpha)}{(\sqrt{Er}\cos\alpha - 1)} * L \qquad \text{(eqn 2.11)}$$

This will give us the maximum height of dielectric at the center, In order to calculate the height "b" in term of angle β. From triangle oze of Figure 2.5,

$$(L + P) = (L + a + b) * \cos(\beta) \qquad \text{(eqn 2.12)}$$

where $0 \leqslant \beta \leqslant \alpha$

From Figure 2.5, when $\beta = 0$

$$R = L + P \quad \text{or} \quad b = P$$

and when $\beta = \alpha$

$$R = L \quad \text{or} \quad b = 0$$

From Equation 2.12,

$$a + b = \frac{L(1-\cos\beta) + P}{\cos\beta} \qquad \text{(eqn 2.13)}$$

From Equation 2.8, we know that

$$a + b\sqrt{Er} = P\sqrt{Er} \qquad \text{(eqn 2.14)}$$

Solving simultaneously the Equation 2.13 and Equation 2.14, we get

$$b = \frac{L(1-\cos\beta) + P(1-\sqrt{Er}\cos\beta)}{\cos\beta(1-\sqrt{Er})} \qquad \text{(eqn 2.15)}$$

Substituting value of P from Equation 2.11 into Equation 2.15,

$$b = \frac{(1-\cos\beta) + \dfrac{(1-\sqrt{Er}\cos\beta)(1-\cos\alpha)}{(\sqrt{Er}\cos\alpha-1)}}{\cos\beta(1-\sqrt{Er})} * L \qquad \text{(eqn 2.16)}$$

This formula for "b" can be evaluated in some computer, which can draw the exact shape of the extended dielectric for the uniform phase front.

C. MONOPULSE RADAR ANTENNAS

The typical monopulse radar antenna system consists of four identical reflector feeds, interconnected with three or more magic-tees. The signals to and from the four feeds are added and subtracted in various combinations to produce three outputs.

All four of the feeds are summed together in phase to produce the sum channel. This signal is connected to the radar via a traditional T/R (transmit/receive) device.

The two difference channels provide the tracking information. The elevation port developes the difference of the upper and lower feeds, while the azimuth port produces the difference between the left and right elements. If a monopulse antenna is pointing exactly at a target there will be a strong signal in the sum channel and absolutely no signal in either the elevation or azimuth channels. The null in the difference channels is the result of shifting two identical signals 180 degrees from each other, and then adding them together. The phase shifting and addition is accomplished in the magic-tees.

The radar return from a target that is slightly left of the monopulse antenna extended center line will reach the left elements of the antenna before it reaches the right elements. This will produce a slight phase shift between the two returning pulses in the azimuth channel.

With this alignment, there will not be complete cancellation after the two signals are shifted by 180 degrees and then added. The resulting "difference" signal will increase in amplitude and shift in phase as the target gets farther away from the antenna boresight. There will also be a 180 degree phase shift in the difference channel as a target crosses the antenna boresight. [Ref. 14]

Since the null in the difference port can only occur with exact target/ antenna alignment, it signifies the exact center of both the sum and difference antenna patterns.

When this information is combined with range data, the target's location can be limited to an arc on the plane that bisects the two halves of the antenna. The point where the elevation and azimuth arcs cross, is directly in front of the antenna. The line between the monopulse antenna and this point is commonly referred to as the boresight of the antenna.

If the outputs of the difference channels are monitored while a target is within the main beam of the sum pattern; the target can be classified as exactly centered, a little left, a little right, a little low, a little high, or a combination of these directions.

As defined by Skolinik [Ref. 14], both amplitude and phase comparison monopulse systems use the phase of the difference signal to determine which side of boresight the target is on. The amplitude comparison system uses the relative amplitude of the difference channel (as compared to the sum channel) to determine how far a target is from the extended center line, while the phase comparison system obtains this information from the exact phase of the difference channel.

These techniques were initially called simultaneous lobing, since all four lobes are sampled during each and every returning radar echo. The trait of obtaining a complete tracking solution in only one pulse, finally led to the current designation of "Monopulse". [Ref. 14]

Earlier tracking radars such as conical scanning and lobe switching systems required numerous pulses to obtain the same information. The accuracy of these older systems was often degraded by the pulse to pulse amplitude variations. Monopulse systems, which are free of distortion, have achieved tracking accuracies of 0.003 degrees. [Ref. 14]

Two popular forms of amplitude comparison monopulse antenna systems are illustrated in Figures 2.6 and 2.7. [Ref. 14]

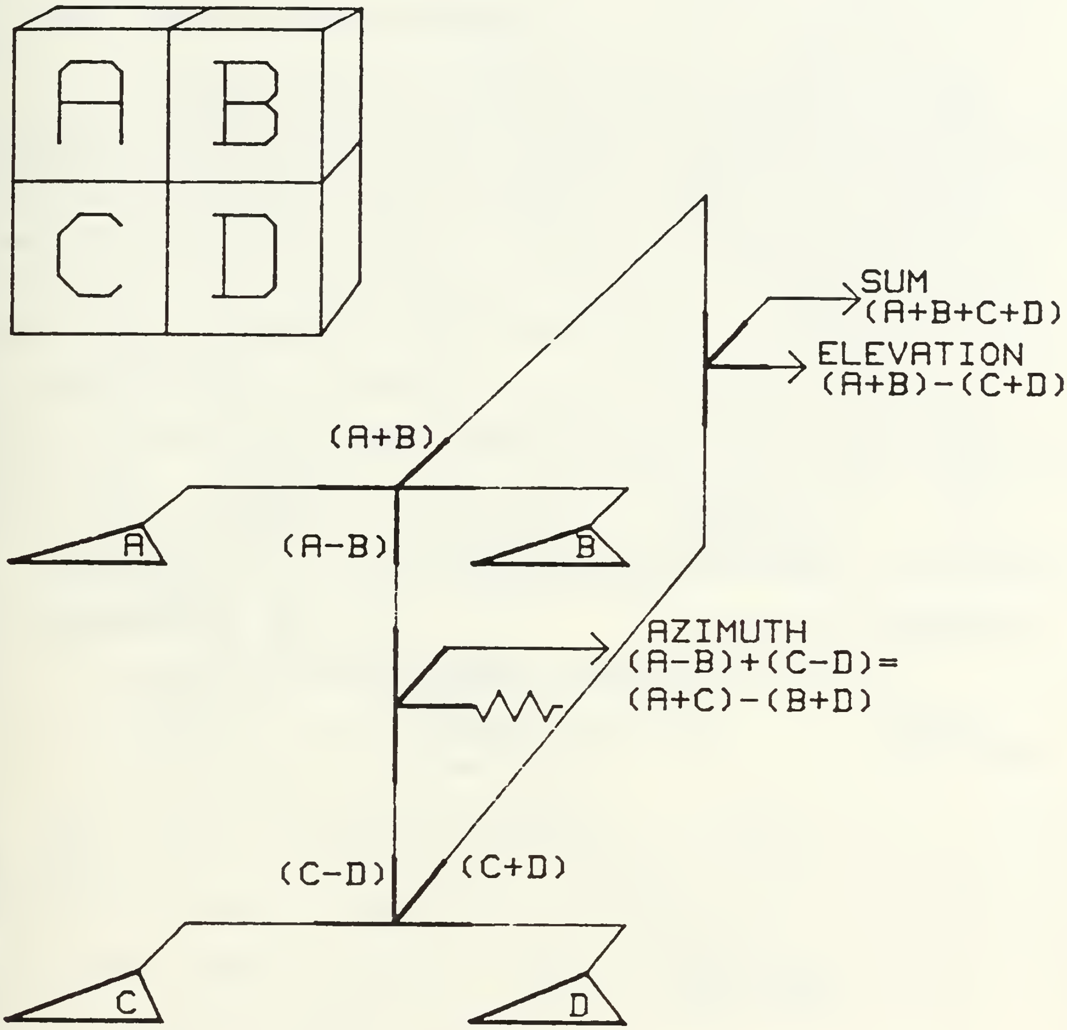

Square Monopulse Feed, with four Horns, and four Magic-Tees. The Sum Port is connected to the Transmit/Receive Device. The Difference Ports provide inputs to the Target Tracking Circuits.

Figure 2.6 Square Monopulse Feed.

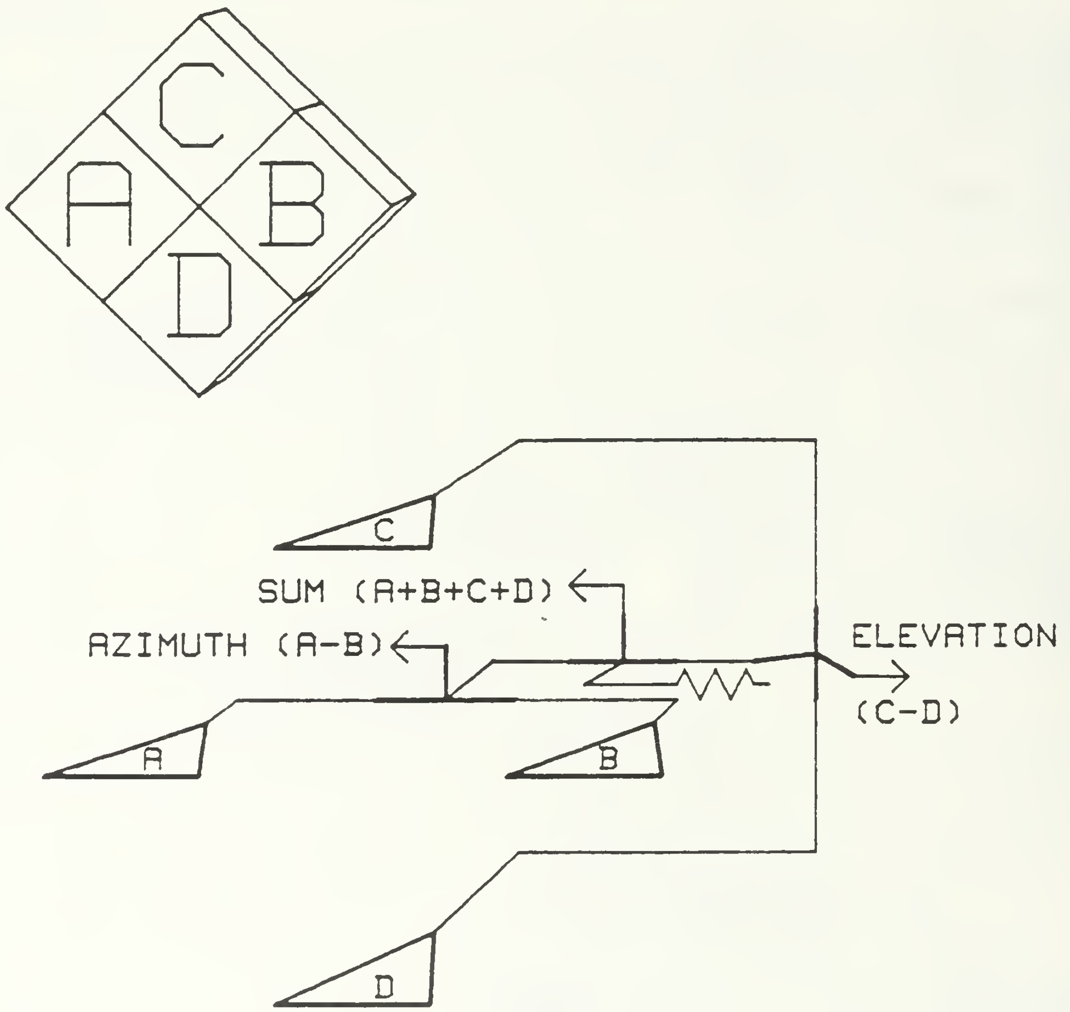

Figure 2.7 Diamond Shaped Monopulse Feed.

III. EXPERIMENT

A. NEAR-FIELD ANTENNA TESTING

For the near-field antenna testing, the first thing required is some sort of mechanism to hold the test antenna in a fixed position and to position and move the measurement probe precisely in steps, parallel to the antenna aperture plane. The test-bench made for this purpose is shown in Figure 3.1. This test-bench was made mostly of wood, except the slotted line , which was used for positioning the measurement probe. During measurement, the test-bench was completely covered with echosorb to avoid any reflection from nearby objects / instruments.

The following test equipment was used to complete the near-field test set-up.

1. HP 9845B Computer with 11863E software.
2. HP 8409C Vector Network Analyzer.
3. Designed Test-Bench.

The complete set-up is shown in Figure 3.2. The most important piece in the set-up is the network analyzer. The network analyzer measures the reflected and / or transmitted power and displays it as the S-parameters of a 2-port network. This equipment is controled by the HP 9845B computer using 11863E software.

The finline horn antenna shown in Figure 1.3 was fixed on the test bench as shown in Figure 3.1, such that its E-plane was parallel to the ground and to the S-band slotline used for probe positioning. A very small loop antenna was used as a measurement probe, which was considered the best possible choice. The antenna was connected to the network analyzer unknown port and the measurement probe was

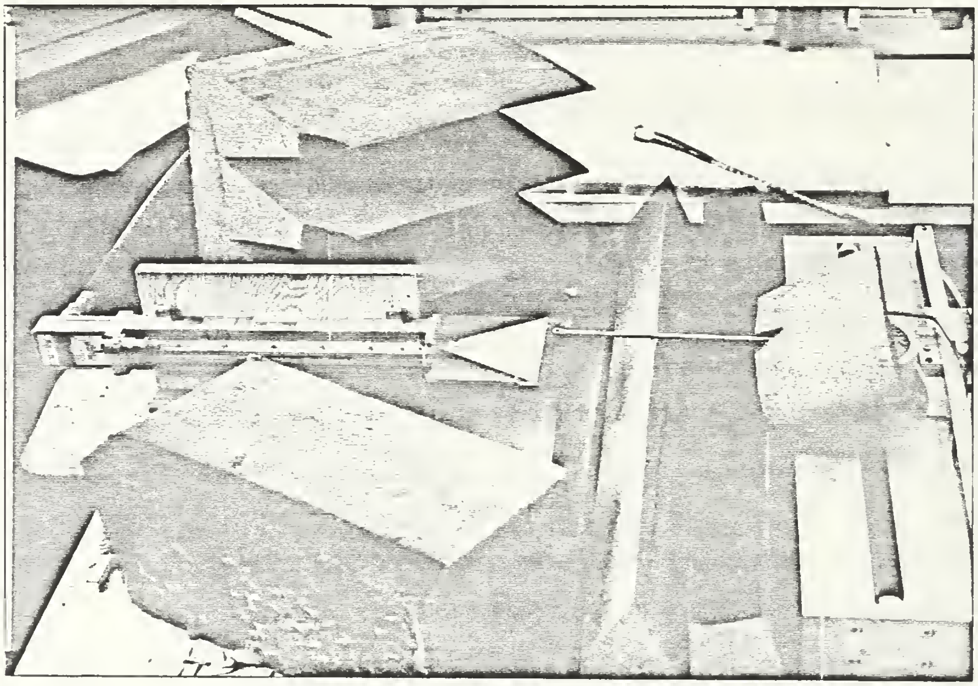

Figure 3.1 Near-Field Measurement Test-Bench.

connected to the transmission port as shown in Figure 3.2. The system was calibrated to measure S21, the transmission coefficient at the particular probe position.

For near-field measurement, the number of measurements, step size for measurement and the separation distance between the test antenna and measurement plane are very important. When transforming from near-field measurements to the far-field pattern, the number of measured samples should be a power of 2 and if the number of samples is not a power of 2 , it should be padded up with zero's to make the total samples equal to the required number. The measurements were made at 10.0 GHz, which gives the wavelength of 30 mm. In our set-up the size of the probe was quite small and we

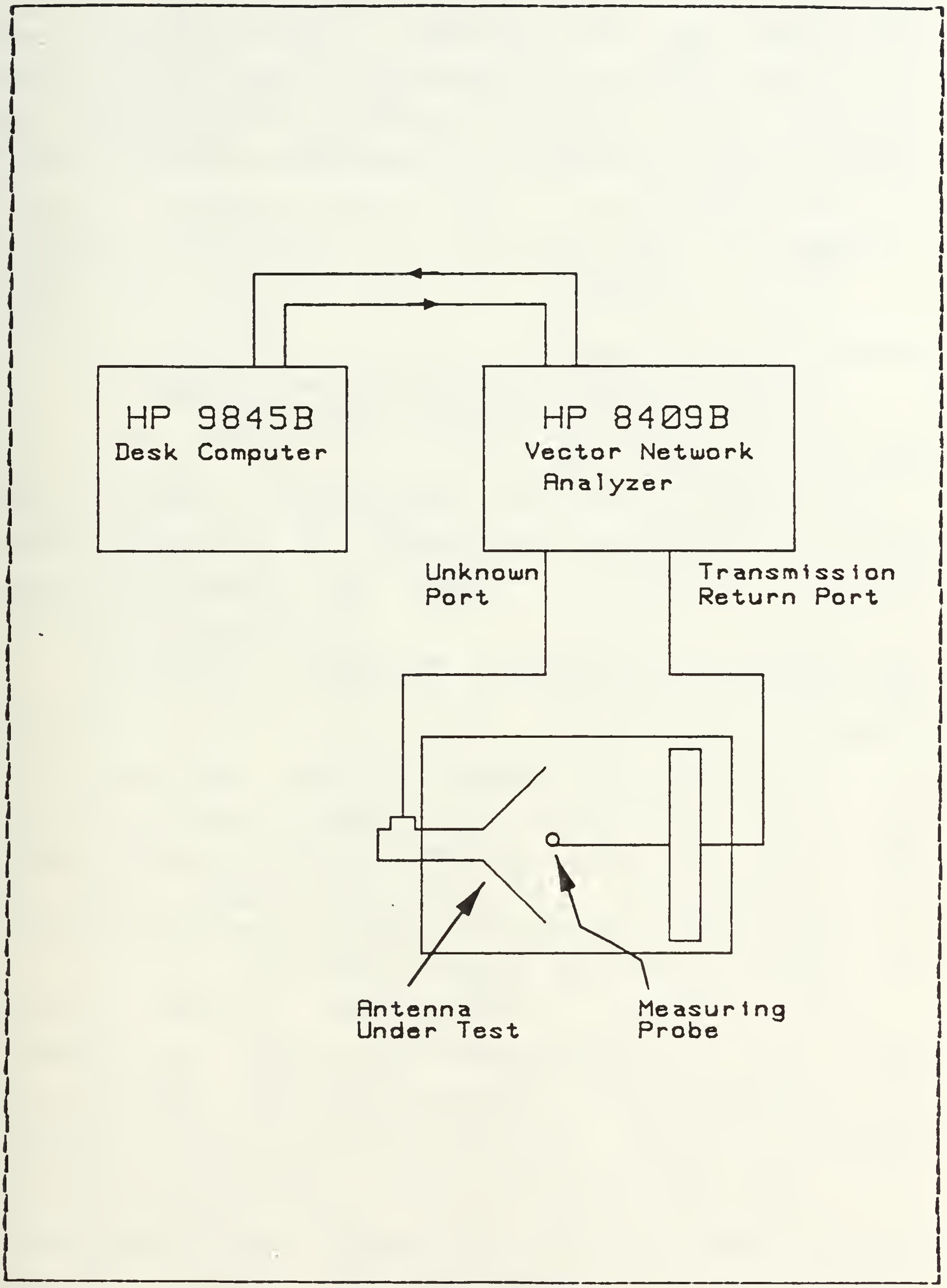

Figure 3.2 Near-Field Measurement Set-up.

decided to chose a separation distance of 5 mm, which was much smaller than the wavelength. When N discrete near-field measurements are transformed to obtain the far-field pattern, it gives N discrete points of the far-field, and these points are converted to far-field pattern with the following equation,

$$\frac{\mathrm{Sin}(Q)}{\lambda} = \frac{n}{N*SS} \qquad \text{(eqn 3.1)}$$

where Q is the beam angle,

N is total number of near-field measurements,

n is the far-field discrete point number,

and SS is the step size.

The visible limits for any far-field pattern are $\pm$ 90 deg., if we want far-field pattern up to visible limits , then n = N / 2 and Q = 90 deg., if we substitute these in Equation 3.1, we get SS $\leqslant$ λ/ 2. The test antenna used for near-field measurements had an aperture of 100 mm, we elected to use 5 mm step size in order to have enough measurements to transform.

The slotted line used for probe positioning was accurately positioned parallel to the antenna aperture. 16 measurements were taken on either side of the antenna center with a step size of 5 mm apart, which gave a total scan plane of 160 mm. Substituting these values in the Equation 2.1, gives the far-field limits of $\pm$80.2 deg.

During near-field antenna testing, to avoid any probe pattern and / or probe polarization error, we decided to take the same measurements by turning the probe at four different positions, two in the co-polarization plane and two in the cross-polarization plane. Throughout this thesis "loop 0 deg." is the probe in the co-polarization plane and "loop 180 deg." is also the probe in the co-polarization plane but 180 deg. shifted from "loop 0 deg." measurement position. Similarly the "loop 90 deg." is the loop in the cross-polarization plane and "loop -90 deg." is also the probe in the cross-polarization but 180 deg. shifted from the "loop 90 deg." measurement position. "Loop 0 deg." and "loop 180 deg." measurements are vectorally added to compensate for any probe pattern error. "Loop 90 deg." and "loop -90 deg." measurements are vectorally added to the "loop 0 deg." and "loop 180 deg." to compensate for any probe polarization error.

The near-field data (phase and amplitude) from each of the four scans was then input to a program written for IBM main frame computer, which calculates the resultant from the measured data. It also normalizes the phase and magnitude with respect to the highest value, and performs the fast Fourier transform on the resultant in order to obtain the far-field pattern. The listing of the computer program is included as Appendix C.

The normalized magnitude of measured and resultant field is shown in Figure 3.3 and the phase of the measured and resultant field is shown in Figure 3.4. From Figure 3.3 it can be seen that resultant field is mainly function of the field in the co-polarization plane and the cross-polarization field contributes negligibly to the resultant, therefore for the calculation of the resultant field, the cross-polarization measurements need not be considered. If we carefully visualize the magnitude of the "loop 0 deg." and "loop 180 deg." measurements in Figure 3.3, it can be seen that the "loop 0 deg." measurement are mirror image of the "loop 180 deg." measurements, but their peaks are not aligned and are not symmetrical about origin. It can also be seen from Figure 3.4, that there is a phase shift between the measurements. Since the test antenna is symmetrical and we expect to have symmetrical field distribution about the origin, it will be more reasonable to take only one measurement in the co-polarization plane and then add the mirror image of the same measurement by aligning the peaks of the magnitude. This procedure will be more accurate and will eliminate any probe pattern error. The normalized magnitude of measured and resultant field obtained with this procedure is shown in Figure 3.5. The measured, resultant and theoretical phase of an electromagnetic horn as explained by Jordan and Balmain [Ref. 15] is shown in Figure 3.6.

B. OBSERVATION OF NEAR FIELD MEASUREMENT

It was observed during the near-field measurement that a slight movement on the top or bottom of the antenna greatly changes the amplitude of the field, which clearly shows the fact that field was also radiating from the top and bottom of the dielectric.

Comparing the resultant phase with the theoretical phase shown in the Figure 3.6, it can be seen that theoretical phase shifts parabolically to the sides, whereas the resultant measured phase only approximates this shape. The phase deviations across the aperture contribute to loss of main beam gain and an increase in sidelobe levels.

Fourier transform of the near-field measurements was converted to a far-field pattern using the Equation 3.1. Far-field pattern was not very accurate because it was was being predicted with only 11 points, therefore it did not have the resolution.

C. REDESIGN OF FINLINE HORN

In this section, we will improve upon the design of the finline horn antenna and discuss the different parameters which can effect the performance of the finline horn. As a first step to stop the radiation from the top and bottom of

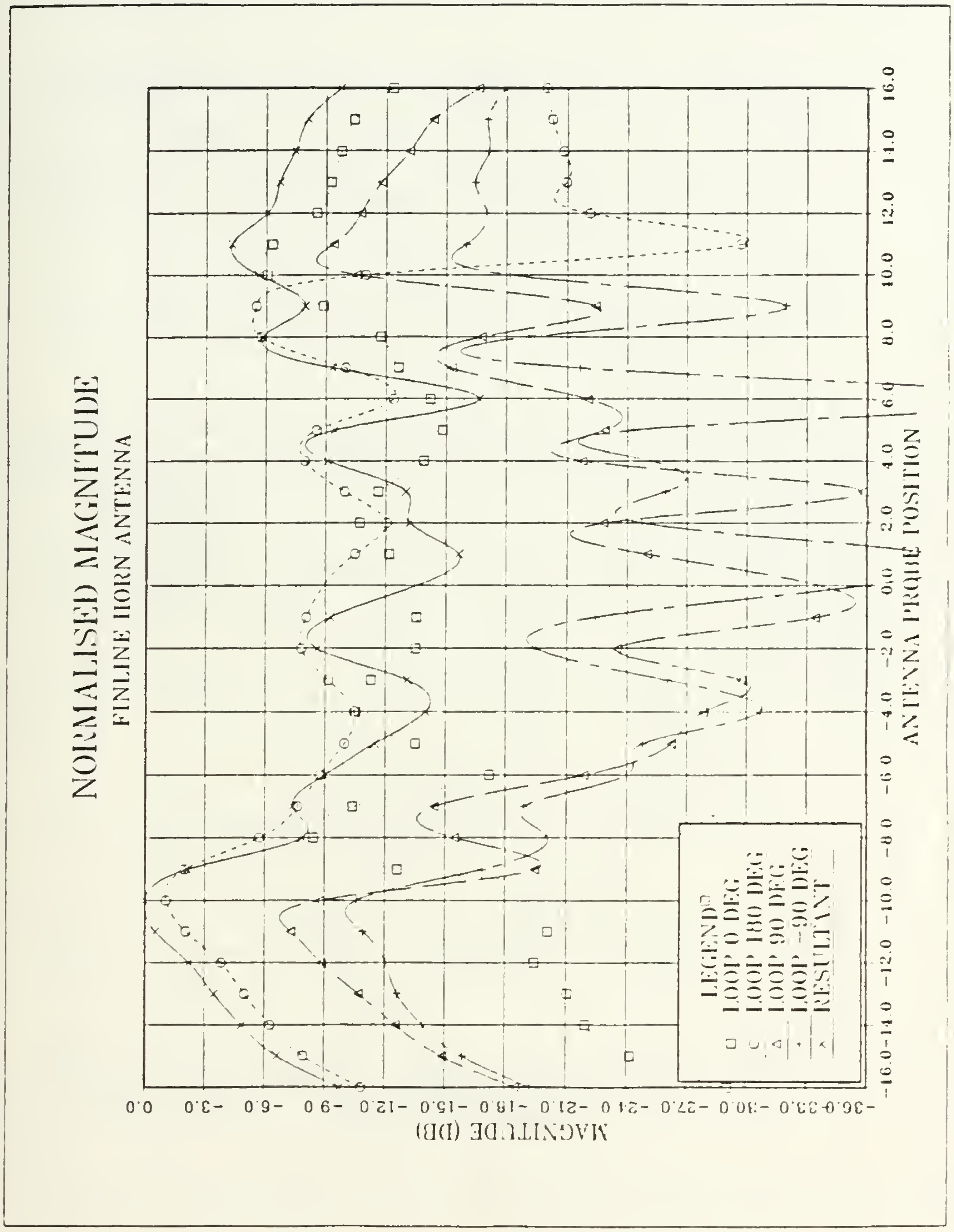

Figure 3.3 Near-Field Normalized Magnitude.

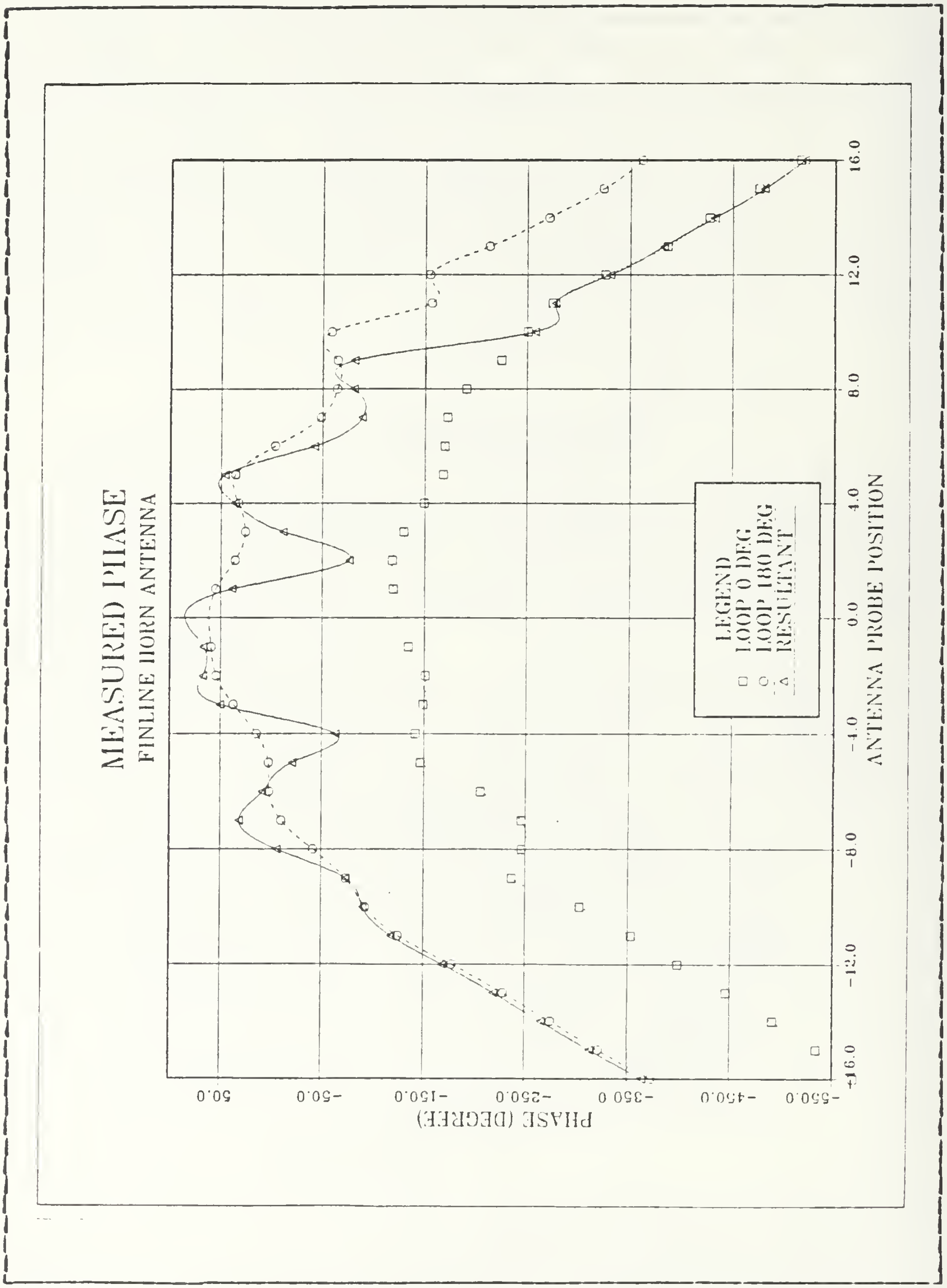

Figure 3.4 Near-Field Measured Phase.

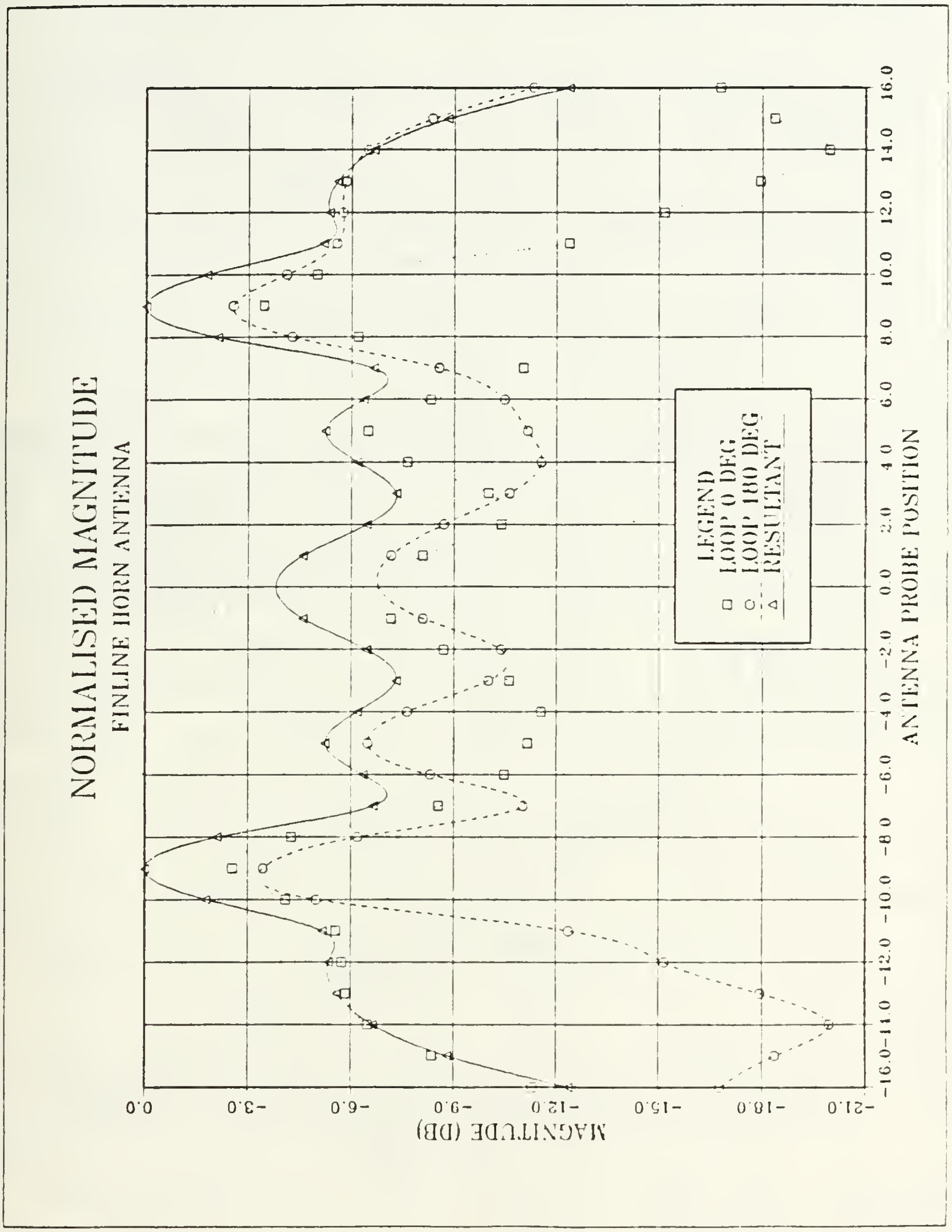

Figure 3.5 Modified Near-Field Normalized Magnitude.

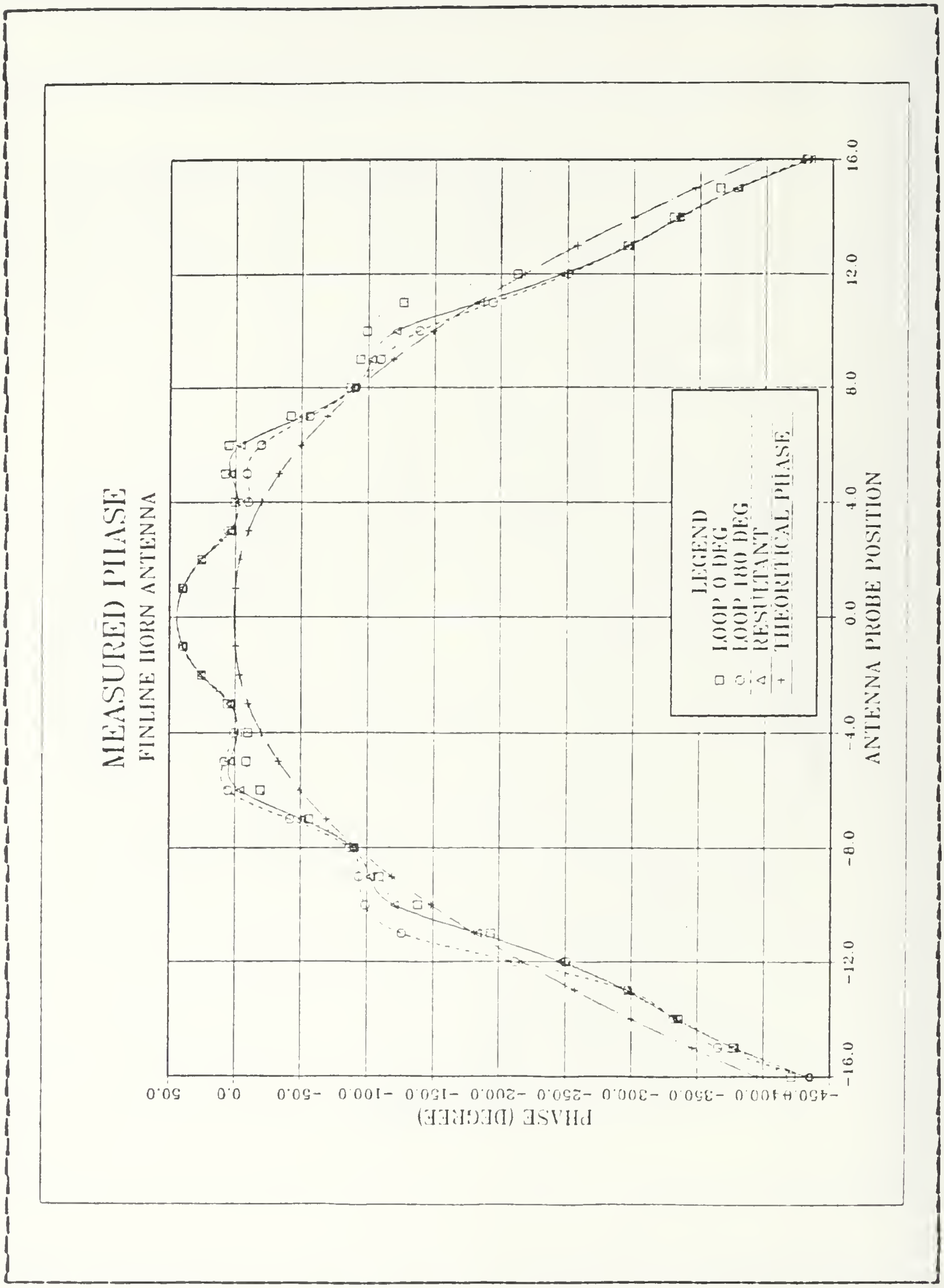

Figure 3.6 Modified Near-Field Phase.

the antenna through the dielectric, we decided to make the metallic flared strip throughout of uniform width. The strip width can be made $\lambda/4$, so that the open from the edge of the fins should reflect back as a short or it can be made $\lambda/2$ in which case we put a copper tape on the outer edge of the fins so that the short at the outer edge reflects back as a short at the fins inner edge.

The new design of finline horn antenna with some of the variable parameters is shown in Figure 3.7. In addition to the parameters shown in Figure 3.7, the dielectric constant of the material and the maximum phase deviation in wavelengths, (S), also influences the far-field radiation pattern. For the initial design, we selected $Er = 2.54$. With this dielectric constant it was not possible to obtain a fin height of $\lambda/2$, as explained in preceding section, therefore we had choice of selecting the different slot width and to find the optimum size of slot from experimental results. The slot was matched to the waveguide by a taper design.

A computer program was written on HP 9845B computer, which draws the outline of finline horn antennas with the specified parameters and uniform phase front on a HP 9872C plotter. This drawing can then further be used for etching of the horn antenna on the substrate. The listing of the program is included as Appendix B. A finline horn antenna with test fixture is shown in Figure 3.8.

The technique of optimization by trial and error was used to find the best design of the finline horn antenna, The different designs of finline horns fabricated and tested are listed in table I with their parameters and some of the finline horn antennas tested are shown in Figure 3.9.

A Microline 56X1 regular standard gain horn was used as a reference, to compare the shape of the radiation pattern and calculate the gain of the finline horns. Most of our radiation patterns were taken at 10.0 GHz, the Microline 56X1 had a gain of 16.2 dB at this frequency.

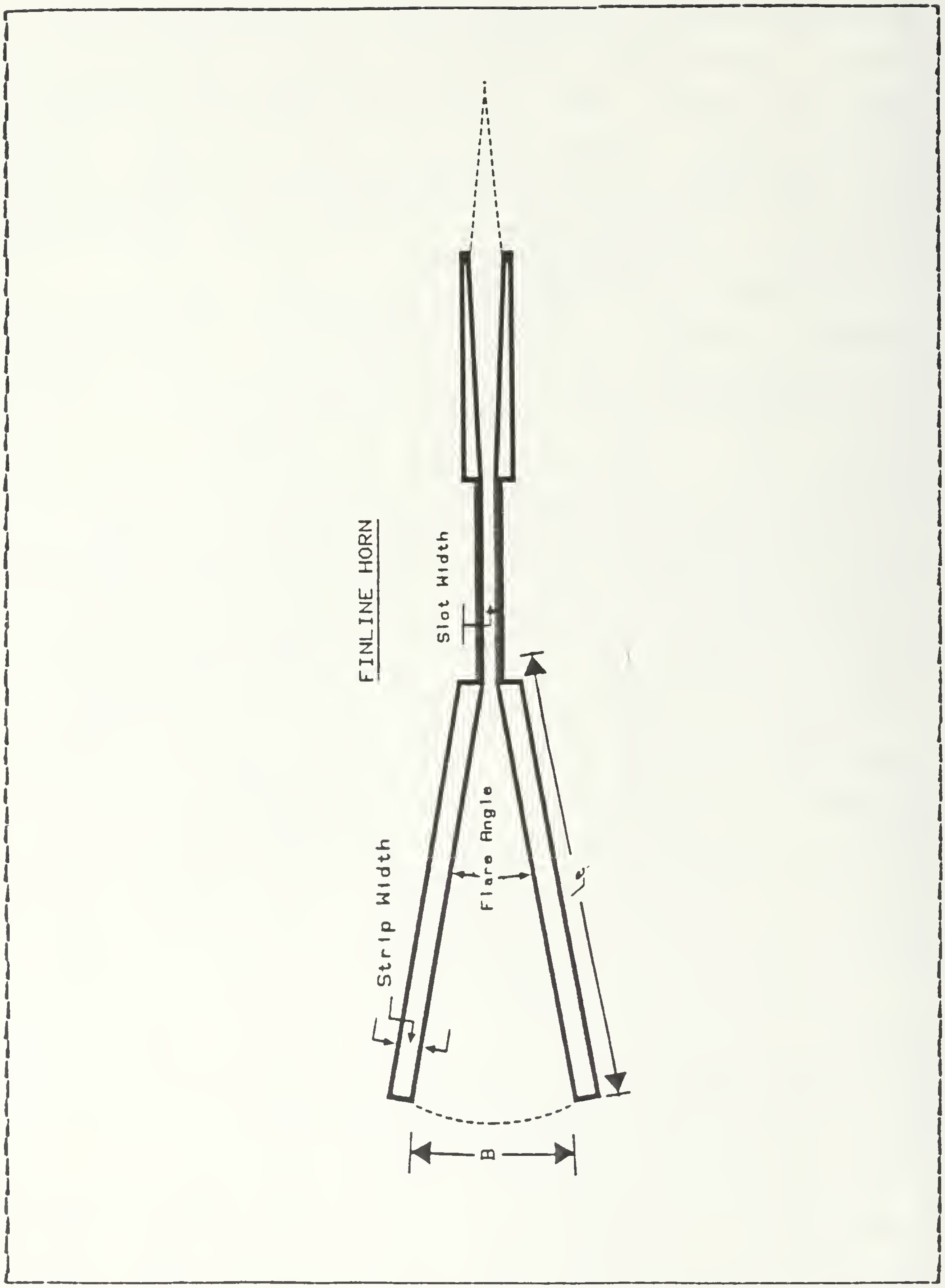

Figure 3.7   New Design of Finline Horn Antenna.

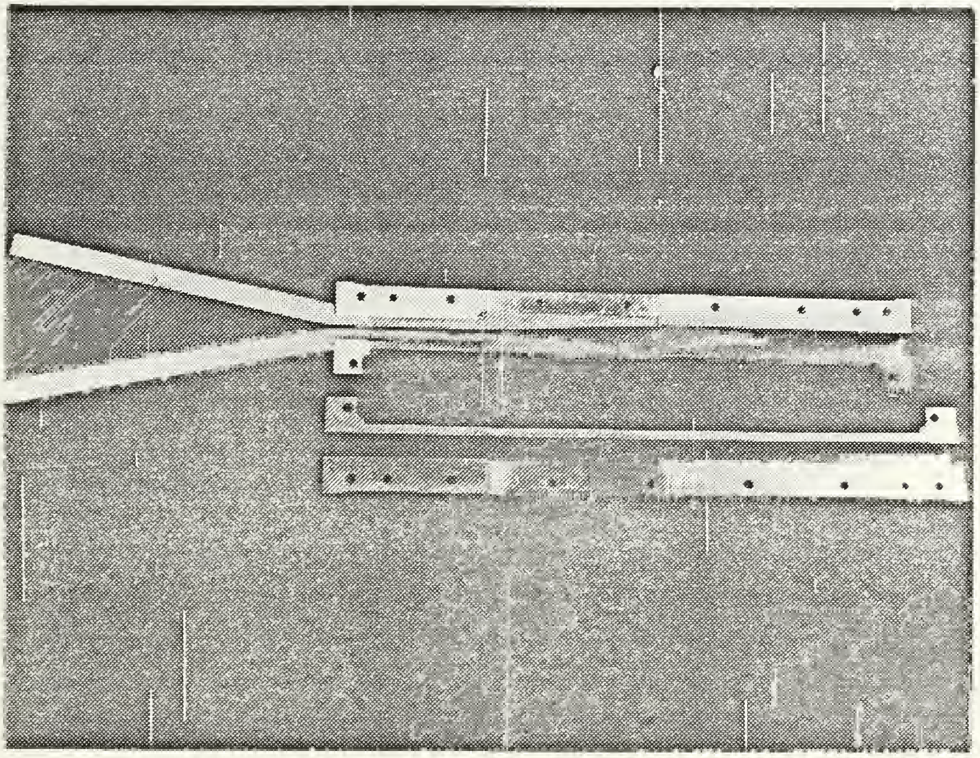

Figure 3.8   Finline Horn Antenna with Test Fixture.

D. RESULTS FOR FINLINE HORN ANTENNAS

In this section, we will discuss the results of the far-field radiation patterns obtained from the different designs of finline horn antennas and to find out the effect of different parameters over the performance of the finline horn antenna.

Before considering the radiation pattern, it is important to mention a few possible factors which could contribute to the asymmetry of the measured pattern.

The layout of the radiation chamber is shown in Figure 3.10. It can be seen that the chamber is not symmetrical and particularly, at +36 degree beam, the test antenna faces a sharp corner and at -36 degree beam, the test antenna faces

TABLE I

DIFFERENT DESIGN OF FINLINE HORN ANTENNAS

Finline Horn	Le=N* d N	Le (mm)	B (mm)	Flare Angle (deg)	Slot Width (mm)	Strip Width	S	Er
A	5.5	103.5	64.0	36.20	2.50	λ/4	0.26	2.54
B	5.8	110.1	88.0	47.20	2.50	λ/4	0.47	2.54
C	5.0	94.1	72.0	45.00	2.50	λ/4	0.37	2.54
D	5.0	94.1	72.0	45.00	2.50	λ/4	0.37	2.54
E	5.0	94.1	72.0	45.00	2.50	λ/2	0.37	2.54
F	8.0	150.6	47.6	18.20	2.50	λ/2	0.10	2.54
G	10.0	188.2	53.0	16.20	2.50	λ/2	0.10	2.54
H1	8.0	150.6	47.6	18.20	1.60	λ/2	0.10	2.54
H2	8.0	150.6	53.3	20.20	1.60	λ/2	0.12	2.54
H3	8.0	150.6	58.5	22.20	1.60	λ/2	0.15	2.54
I	8.0	75.2	23.8	18.20	0.50	λ/2	0.10	10.20
J	17.4	150.6	53.3	20.20	1.60	λ/2	0.12	12.00

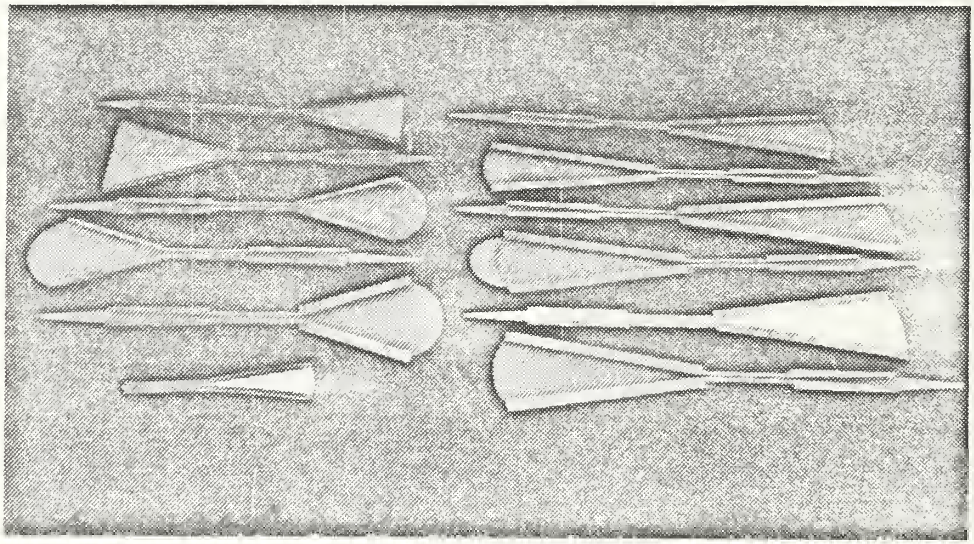

Figure 3.9 Some of the Finline Horn Antennas Tested.

a straight wall. Therefore at this angle, there will be asymmetry in the measured radiation pattern. Secondly the absorber used to avoid reflections from the chamber walls is of very poor quality and when the test antenna is facing toward the side walls, it receives a high reflection which results in false side lobes.

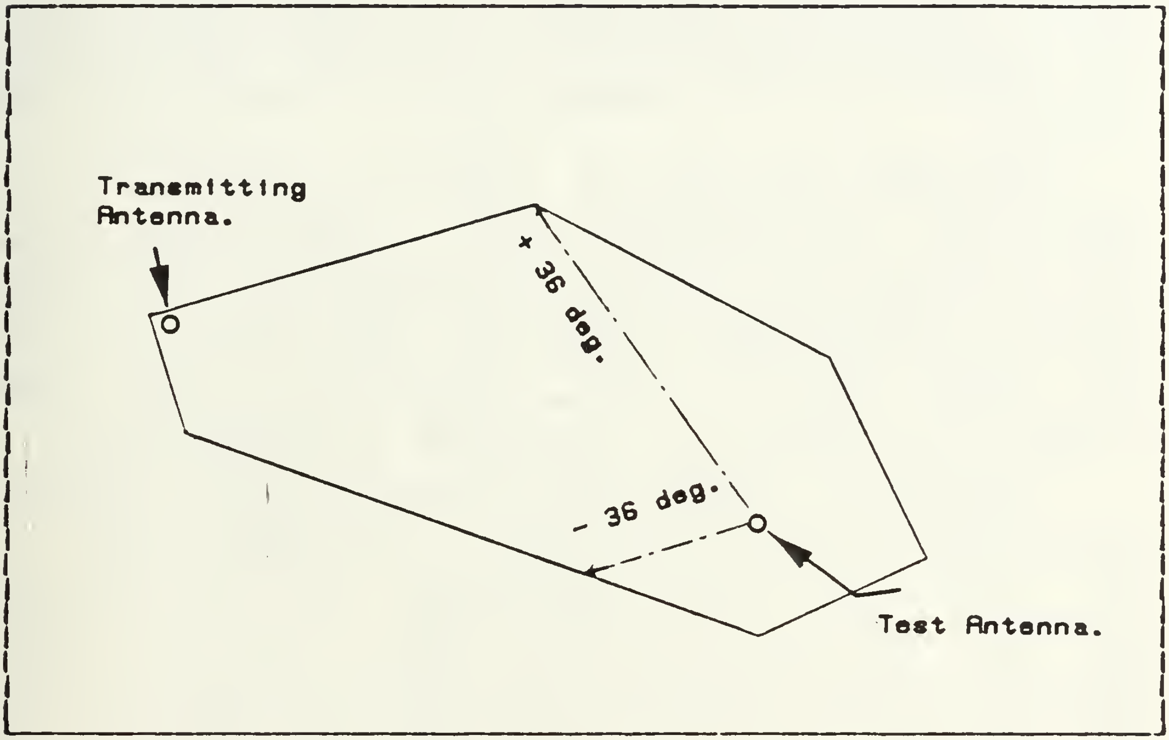

Figure 3.10 Layout of Radiation Chamber.

The X-band slotted line used as a shield for the feed to the finline horn antennas is also not symmetrical. Therefore, it might contribute to some extent to the asymmetry of the measured radiation patterns of the finline horn antennas.

The far-field radiation patterns of finline horn antennas and the return loss of some of the antennas are included in Appendix A.

Figure A.1 shows the E-plane radiation pattern of the finline horn "A" with uniform phase design. It had a gain of 12.2 dB and E-plane beam width of 22.0 degrees but it had high shoulders. Figure A.2 shows the E-plane radiation pattern of finline horn "A" without uniform phase design. It had a gain of 10.2 dB and E-plane beam width of 24.0 degrees. It can be seen from these two Figures that the uniform phase design increases the gain by several dBs and narrows down the beam in E-plane. The amount of increase in gain depends upon the radiating aperture and is not a fixed number.

The Figure A.3 shows the radiation pattern of finline antenna "B", the far-field pattern of finline horn antenna "B" had very high side lobes as compared to the radiation pattern of finline horn antenna "A". This is due to the fact that finline horn "B" had a large aperture and a higher value of S as compared to the finline horn antenna "A".

The radiation pattern of finline horn "C" is shown in Figure A.4, its sidelobes are also quite high as compared to the finline horn "A". The finline horn "C" and "D" had same parameters except that the finline horn "D" had a wide feed line slot width as compared to the finline horn "C". It can be seen from the radiation pattern shown in Figure A.5, that the side lobes are even higher then the main beam. By inserting a piece of echosorb in the opening of the wave-guide feed the sidelobes can be reduced as shown in Figure A.6. This indicates that wide feed line slots cause pattern degradation due to secondary radiation from the end of the feed lineshield. By inserting the echosorb in the mouth of the waveguide, the radiation from this source was stopped and the radiation pattern achieved with this configuration was determined only by the finline horn antenna. But the finline horn "C" still had a better pattern as compared to the finline horn "D".

The finline horn "E" had the same parameters as finline horn "D" except that the horn "D" had a flare strip width of $\lambda/4$ and the horn "E" had a strip width of $\lambda/2$ and copper tape on the outer edge to create an electrical short. The finline horn "E" also had a wide slot width. The radiation patterns of finline horn "E" with and without the echosorb in the waveguide are shown in Figures A.7 and A.8 respectively. Comparing the patterns of finline horn "D" and "E", it can be seen that finline horn "E" had better radiation pattern as compared to the finline horn "D".

Summarizing the results of the far-field patterns of finline horns A,B,C,D and E, for lower side lobes, a lower value of S is desired, of the order of 0.1 or less. A slot width of 2.5mm gives better results as compared to a slot width of 5.0mm because the field concentrates in the slot. A flare strip of $\lambda/2$ works better than a flare strip of $\lambda/4$ because it provides a positive short at the outer edge and reduced radiation leakage from the edges of the horn.

The finline horn "F" was made with the optimum parameters obtained from the preceding results, with S=0.1, slot width of 2.5mm and flare strip width of $\lambda/2$ with copper tape on the outer edge and flare length of 150.6mm ($Le=8*\lambda d$), which gives a radiating aperture of 47.6mm. The E-plane and H-plane radiation patterns are shown in Figures A.9 and A.10 respectively. It can be seen from these Figures that the finline horn "F" had a very clear radiation pattern with a well defined main beam, gain of 10.7 dB and E-plane beam width of 26.0 degrees. H-plane beam width of 36.0 degrees. Side lobes were approximatly 13 dB below the main beam in the E-plane and 9-10 dB below the main beam in the H-plane.

To further improve the gain of a finline horn , we increased the flare length to 188.2mm ($Le=10*\lambda d$) to achieve a wider aperture while keeping the other parameters the same as for finline horn "F". The E-plane and H-plane radiation patterns of finline horn "G" are shown in Figures A.11 and A.12 respectively. It can be seen from Figure A.12 that it had gain of 13.0dB in the H-plane but only 11.0 dB in the E-plane. This discrepancy might be due to the fact that the finline antenna in the E-plane might not be pointing exactly at the transmitting antenna center and may be tilted down due to its extra length. The finline horn "G" had a beam width of 22.0 degrees in the E-plane and 36.0 degree in the H-plane. We were able to obtain the higher gain by increasing the width of the radiating aperture, but with the available dielectric material and under these laboratory conditions, it was not possible to make large antennas.

Next we considered improving the gain by further reducing the slot width. The finline horn "H1" had the same parameters of finline horn "F" but the slot width was reduced to 1.6mm. The E-plane and H-plane radiation patterns of finline horn "H1" are shown in Figures A.13 and A.14 respectively. The finline horn "H1" had a gain of 12.2 dB and beamwidths of 25 deg. and 40 deg. in the E and H-planes, respectively. The side lobes at 36 deg. were approximatly 9 dB lower than the main beam. It can be seen from Figure A.13 that E-plane side lobes are higher on one side as compared to the other side. This is probably due to the shape of the radiation chamber and multi path reflections from the corners of the chamber. The finline horn "H1" had 1.5dB higher gain as compared to the finline horn "F". This shows, that a slot width of 1.6mm gives better results as compared to a slot width of 2.5mm. Therefore, for other experiments we used a slot width of 1.6mm.

The finline horn "H1" had a flare angle of 18.2 degrees. We made two more antennas with the same parameters as finline horn "H1" but with different flare angles. The finline horn "H2" had a flare angle of 20.2 deg. and finline horn "H3" had a flare angle of 22.2 deg. The finline horn

"H2" had a gain of 13.3 dB. Beam widths were 23.0 deg. and 36.0 deg. in the E-plane and the H-plane, respectively. The E-plane side lobes were 12.0 dB lower than the main beam. The radiation pattern of horn"H2" in the E-plane and in the H-plane are shown in Figures A.15 and A.16 respectively. The finline horn "H3" had a gain of 12.0 dB and the beam widths were 22.0 deg. and 40.0 deg. in the E-plane and the H-plane respectively. The sidelobes were 10.0 - 12.0 dB lower than the main beam. The radiation patterns of horn"H3" in the E-plane and the H-plane are shown in Figures A.18 and A.19 respectively.

The gain of finline horn antennas "H1","H2" and "H3" were measured for a frequency range of 8.2 GHz to 12.4 GHz and are shown in Figure 3.11. The reflected power of finline horn antennas "H1","H2" and "H3" were measured on the vector network analyzer from 8.0 GHz to 12.4 GHz. The reflected power vs frequency of finline antennas "H1", "H2" and "H3" is shown in Figures A.24,A.25 and A.26 respectively. It can be seen from Figure 3.11 that finline horn "H1" and "H2" had a steady gain over a band of frequency but the finline horn "H3" had a very oscillating gain. The finline horn antenna "H1" had a gain of 12.75$\pm$0.25 dB over a band of 9.8 GHz to 11.6 GHz with a VSWR of 1.67. The finline horn antenna "H2" had a gain of 14.00$\pm$ 0.75 dB over a band of 9.8 GHz to 12.2 GHz with a VSWR of 1.43.

Up to this point all the finline horns were designed for a uniform phase front. If we extend the dielectric further, we can make a converging lens. In order to see the effect of this extra lens beyond the lens already extended for the uniform phase front, we extended the dielectric of finline horn "H2" in a half circle shape and measured the gain for a frequency range of 8.2 GHz to 12.4 GHz. The E-plan radiation pattern of finline horn "H2" with converging lens is shown in Figure A.17. It can be seen from the radiation pattern

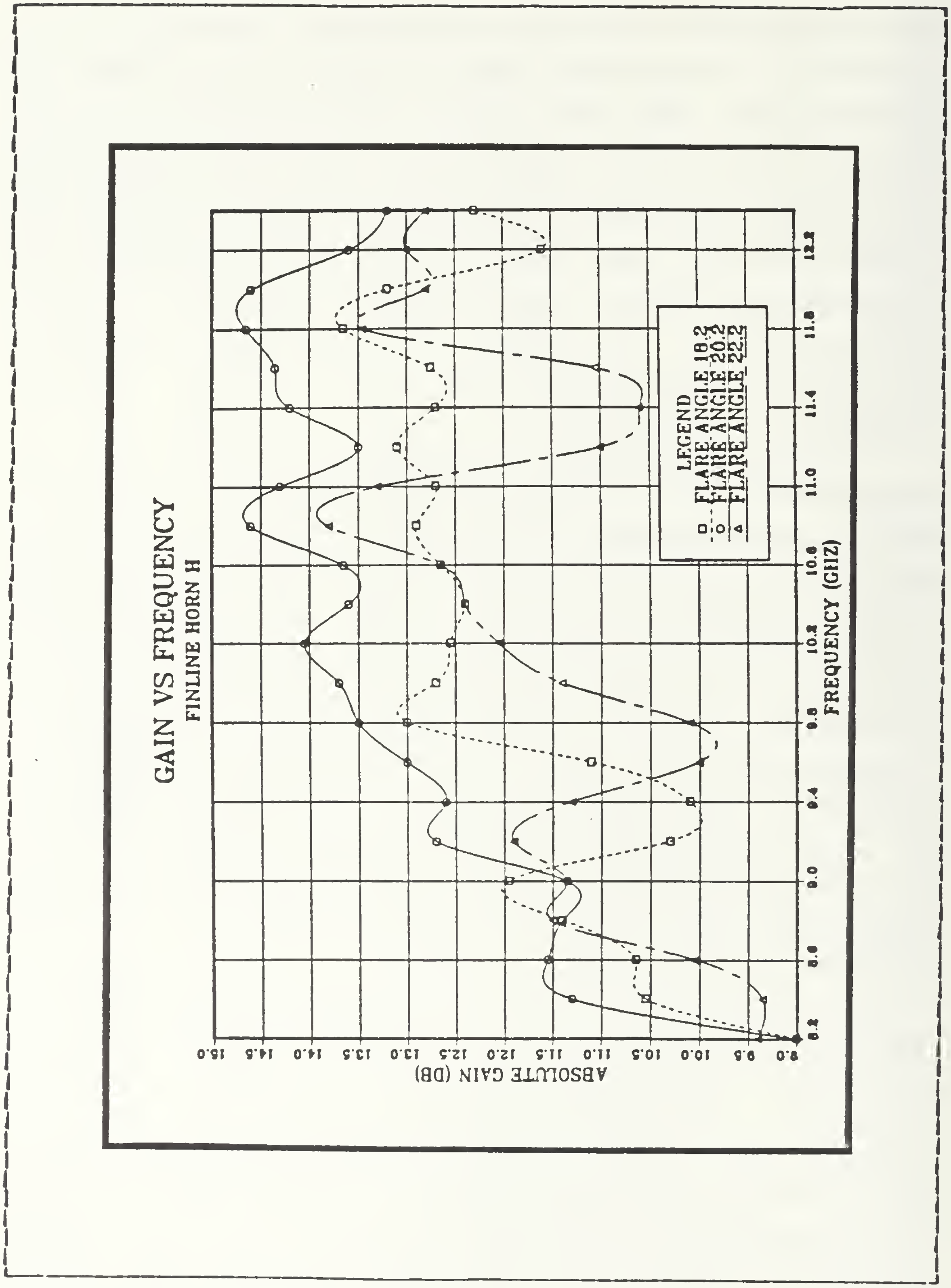

Figure 3.11 Gain of Finline Horn H1, H2, and H3.

that it had a gain of 13.0 dB , 20.0 deg. beam width in the E-plane and the side lobes were 12.0 db lower than the main beam. The gain of finline horn "H2" with uniform phase lens and "H2" with converging lens is shown in Figure 3.12. It can be seen that finline horn "H2" with uniform phase lens had an overall higher gain as compared to the finline horn "H2" with converging lens.

In the preceding paragraphs, we have considered the effect of the different parameters like "S", slot width, strip width, lens effect, flare length(Le) and flare angle. In the following paragraphs we will consider the effect of the dielectric constant (Er).

We made a finline horn "I" with Er=10.2, the slot was transitioned fron the coaxial cable and the width of the slot was match to the impedance of the coaxial cable. The parameters are shown in Table I. The E-plane and the H-plane radiation patterns are shown in Figures A.20 and A.21 respectively. This horn had a gain of 4.0 dB. The beam widths in the E-plane and the H-plane were 36.0 deg. and 96.0 deg. respectively. The side lobes were 14.0 dB lower than the main beam in the E-plane. This horn was used for the design of the monopulse comparator.

In order to see the effect of dielectric constant (Er) over a wide radiating aperture, we made the finline horn "J" with the same dimensions as finline horn "H2" , but on an Er=12.0 substrate. The radiation patterns of this horn in the E and H-planes are shown in Figures A.22 and A.23, respectively. The reflected power is shown in the Figure A.27. It had a gain of 4.6 dB ,28.0 deg. and 100 deg. beam widths in the E and H-planes respectively and the E-plane side lobes were 16 dB down. It had a VSWR of 1.67 over the same frequency range as finline horn "H2".

It can also be seen that the main beam pattern of finline horn "J" was not smooth, this was probably due to

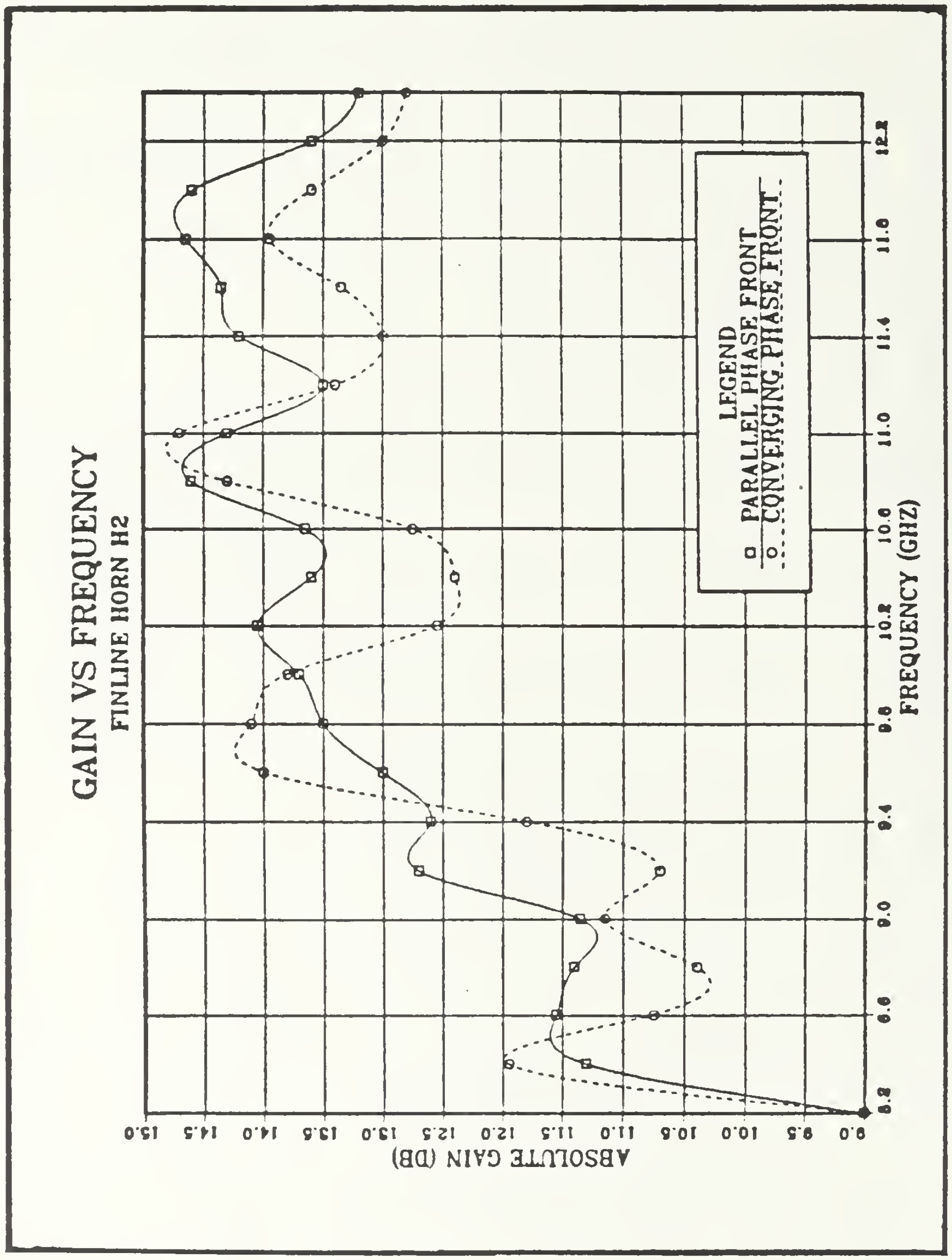

Figure 3.12 Gain of Finline Horn H2 with Different Lens.

the fact that the wavelength in dielectric for this horn is much smaller as compared to the finline horn "H2" made on a lower Er material. Therefore due to the shorter wavelength the slight rough edges on the antenna will cause phase distortion.

In summary, the higher dielectric constant reduces the overall gain of the antenna, does not change the beam width in E-plane much, but increases the beam width in H-plane by a large amount.

Before concluding the results of the finline horn antennas of different designs, we would like to derive an approximate gain equation from these results.

The finline horn "H1" had a aperture of 47.6mm, gain of 12.2dB at 10.0 GHz and was made with Er=2.54, substituting these values in Equation 2.5 gives

$$12.2\text{dB} = C1 * \frac{47.6}{30.0 * (2.54)^{C_2}} \qquad \text{(eqn 3.2)}$$

Finline horn "I" had a aperture of 23.8mm, gain of 4.0 dB at 10.3 GHz and was made with Er=10.2. Substituting, these values in Equation 2.5 gives

$$4.0\text{dB} = C1 * \frac{23.8}{29.13 * (10.2)^{C_2}} \qquad \text{(eqn 3.3)}$$

Simultaneously solving the Equations 3.2 and 3.3 gives the value of constants C1= 23.77 and C2= 0.88, substituting these values in Equation 2.5, gives an approximate gain equation for finline horn antennas,

$$\text{Gain} = (23.77) * \frac{B}{\lambda * (E_r)^{0.88}} . \qquad \text{(eqn 3.4)}$$

The calculated gain from Equation 3.4 and the measured gain are shown in Table II.

TABLE II

CALCULATED AND MEASURED GAIN

Finline Horn	Measured Gain	Calculated Gain
F	10.7 dB	12.2 dB
G	12.7 dB	13.0 dB
H1	12.2 dB	12.2 dB
H2	13.3 dB	12.7 dB
H3	12.0 dB	13.1 dB
I	4.0 dB	4.0 dB
J	4.6 dB	6.7 dB

It can be seen from Table II, that the calculated gain is close to the measured gain but we do not consider that the value of constants are exact , because the finline horn antennas used for the derivation were being optimized by the experimental results and only two finline horns were tested on different dielectric constant substrate. However, it can be seen that the theoretical aspect explained in Chapter 2 works and the exact gain equation can be derived by the optimum designed finline horn antenna tested in an ideal conditions and with different type of substrate. In a similar way, the equation for beam widths can also be derived.

The summary of all the finline horns tested is as follows.

The gain of the finline horn is directly proportional to the radiating aperture in the E-plane and decreases with increasing value of dielectric constant, Er. The dielectric constant controls the beam width in the H-plane and the beam width in the E-plane is mostly controlled by the aperture size. The E-plane beamwidth has very little dependence on dielectric constant.

The shape of the radiation pattern mostly depends upon the phase deviation in the E-plane (S) and the phase deviation in the H-plane (T). For a neat radiation pattern with clear main beam and low side lobes in the E-plane the valve of "S" needs to be less than 0.1 and for a neat radiation pattern in the H-plane the value of T also needs to be low. However, a high value T does not distort the H-plane pattern but will give a wide beamwidth.

The slot width needs to be narrow. As we saw for Er=2.54, a slot width of 1.6mm gave nice results. A further reduction in the slot width might improve the gain slightly.

The width of the flare strip, can be $\lambda/4$ or $\lambda/2$ with copper tape on the outer edge. However, in the later experiments, we concentrated on the $\lambda/2$ configuration, because it seems to reduce the field radiated from the top and bottom edges of the antenna through the dielectric.

The extended shape of dielectric to produce a uniform phase front at an imaginary plane increases the gain but the use of a converging lens decreased the overall gain of the one finline horn antenna which was tested.

IV. FINLINE MONOPULSE COMPARATOR

This part of thesis was jointly done by the author and Rowley [Ref. 16], who was working on the finline magic-tee.

A. DESIGN OF MONOPULSE COMPARATOR

Two finline horns joined with a finline magic-tee made on a single substrate can form a single channel of monopulse comparator.

Port 1 and port 2 of the finline magic-tee [Ref. 16] were flared to a radiating aperture to make a finline horn on either port. The finline horns had the same physical dimensions as finline horn antenna "I" previously described. The layout of the two finline horn antennas joined with a finline magic-tee is shown in Figure 4.2. The monopulse comparator with fixture is shown in Figure 4.1. The outputs from the sum and difference ports were fed through microstrip to coaxial cable as explained by Rowley [Ref. 16] and as shown in Figure 4.2. The comparator was etched on a dielectric constant of 10.2 substrate with a thickness of 0.03125 inches. The comparator was designed at 10.3 GHz center frequency, because at this frequency the fin's height was made $\lambda/2$, so that the short from the waveguide wall would reflect back as a short at the inner edge of the slot. The width of the slot was matched to the microstrip and subsequently to the co-axial cable impedance.

The parameters of individual finline horn antennas are determined by the gain, beamwidth and sidelobe requirements. The distance between the horns is also very important because the final shape of the pattern can be controlled by the distance between the individual elements. For the sum

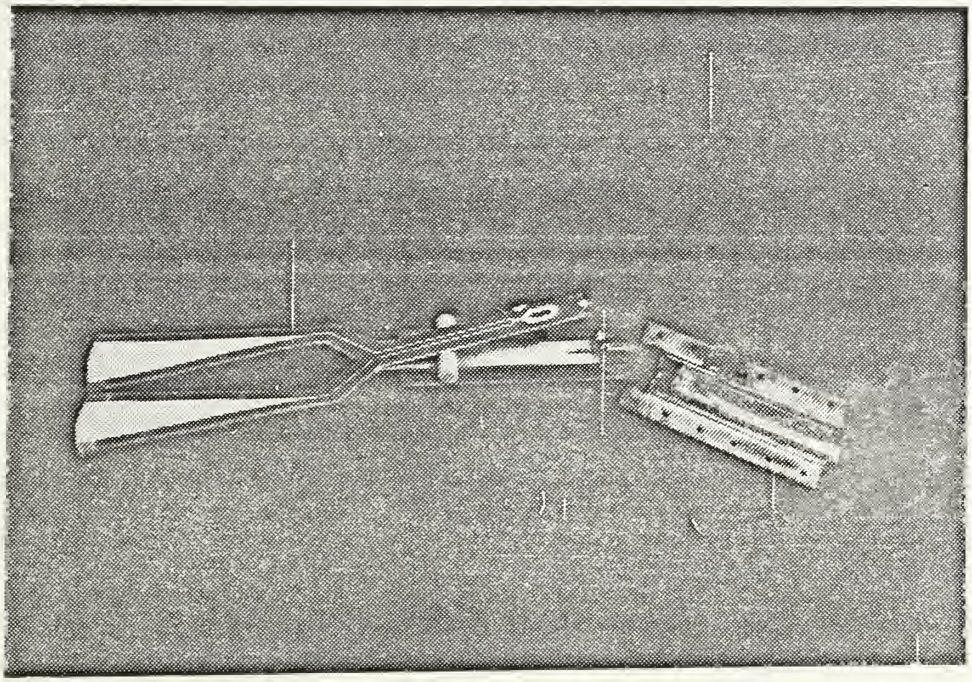

Figure 4.1 Picture of Monopulse Comparator with Fixture.

pattern the element pattern is multiplied by the normalised cosine function and for the difference pattern the element pattern is multiplied by the normalised sine function. The distance between the nulls of the sine or cosine function depends upon the distance betweens the element in wavelengths. For this design the distance between the horns was arbitrarily chosen.

B. PERFORMANCE OF MONOPULSE COMPARATOR

The microline 56X1 standard gain horn antenna was used for reference patterns. The E-plane sum pattern is shown in Figure 4.3, it had a gain of 8.0dB and beam width of 24.0 degrees. From here, it can be calculated that the element pattern had a gain of 5.0dB, which is 1.0dB higher than the measured gain of the finline horn antenna "I". The E-plane

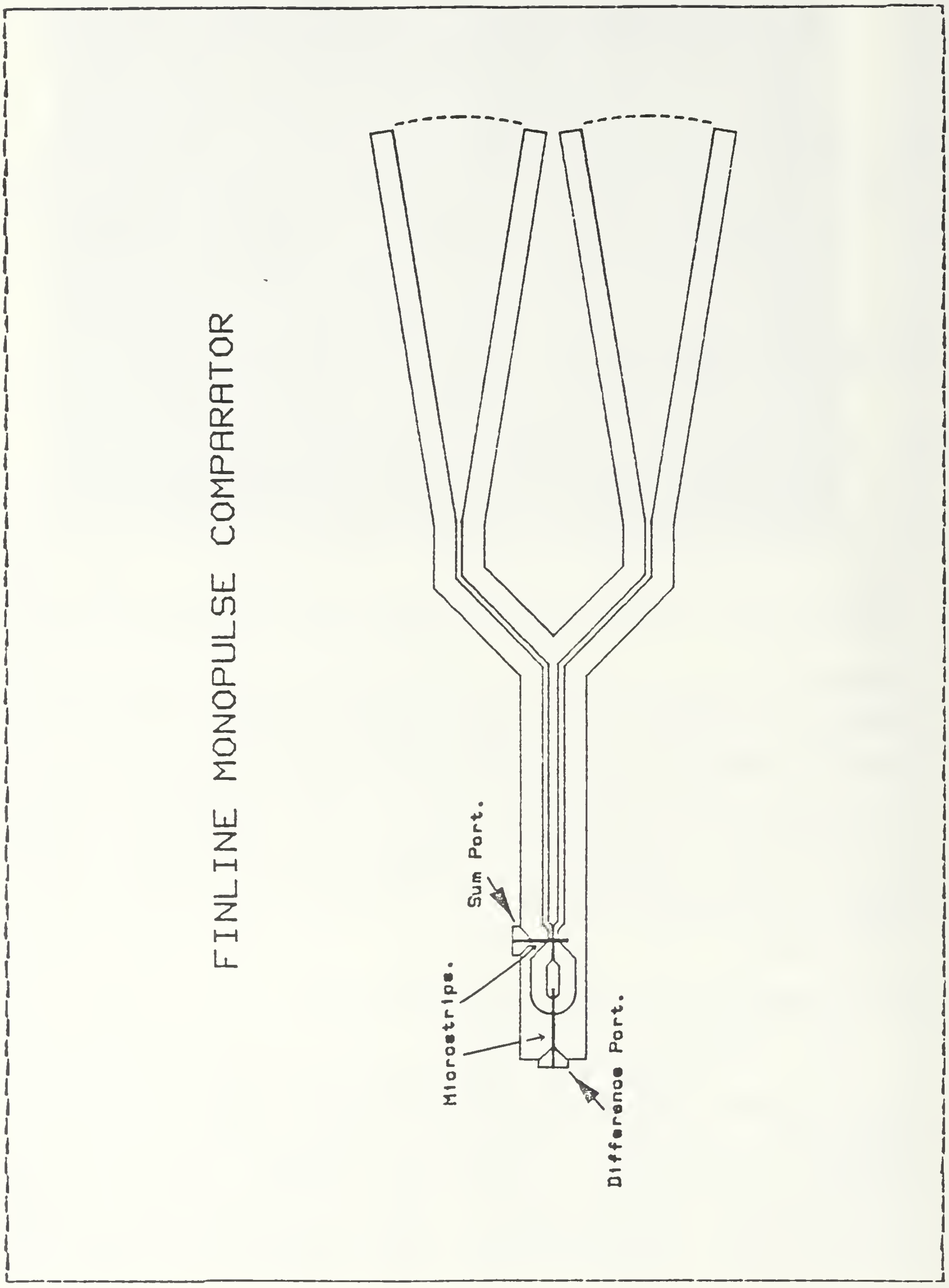

Figure 4.2 Layout of Monopulse Comparator.

difference pattern is shown in Figure 4.4, it shows a nice null at the center. The E-plane sum and difference patterns are shown togather in Figure 4.5. The amplified sum and difference patterns are shown in the Figure 4.6, which shows that the null depth in the difference pattern was greater than 40 dB from the peak of the sum pattern. The H-plane radiation patterns are shown in Figures 4.7, 4.8 and 4.9. In the H-plane the comparator had the same gain as in the E-plane. The sum pattern had a very wide beam width and there was almost no power in the difference pattern.

The sum and difference port reflected power is shown in Figures 4.10 and 4.11 respectively. It can be seen from these Figures that there was high reflected power on both ports. Most of the reflection was caused by the microstrip to coaxial cable transition because the dielectric used was very soft. The connectors center conductor were not making a stronge contact with the microstrips and were finally soldered for continuity. It can also be seen that it had less reflected power at the higher frequencies.

The two of these single plane comparators orthogonal to each other with one more magic-tee or two of these parallel to each other with two magic-tees can form a dual plane finline monopulse comparator system. This type of light weight, integrated monopulse feed system has great possibilities for military and space applications in future.

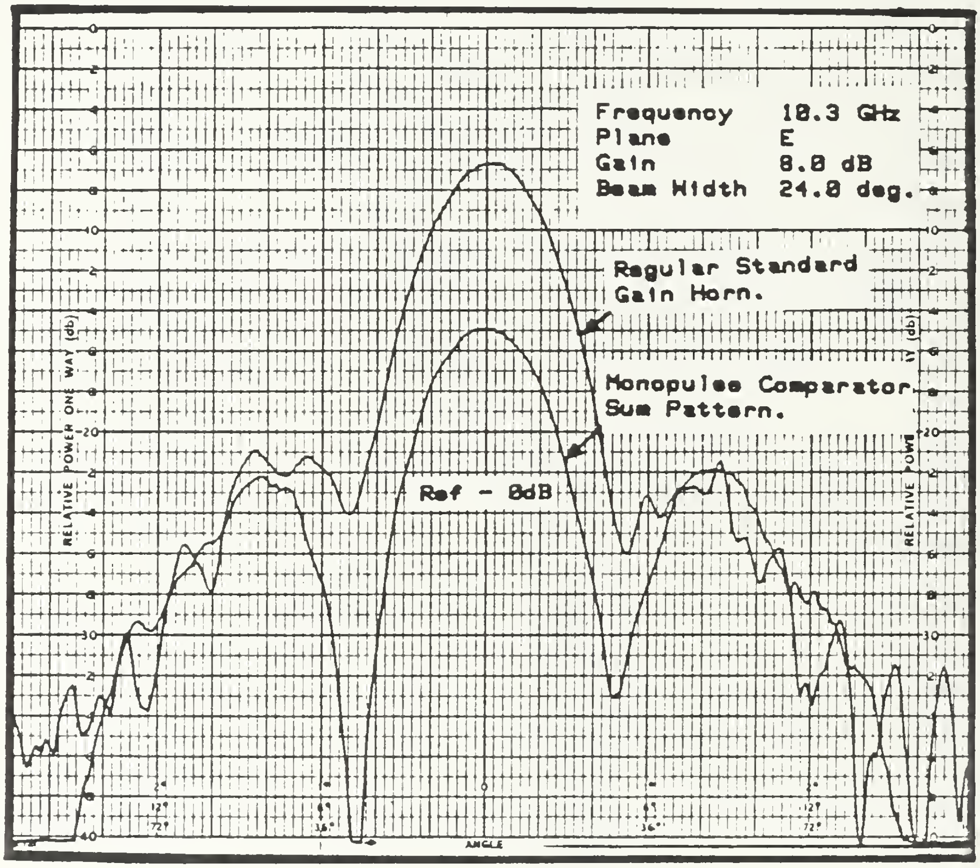

Figure 4.3 E-Plane Monopulse Comparator Sum Pattern.

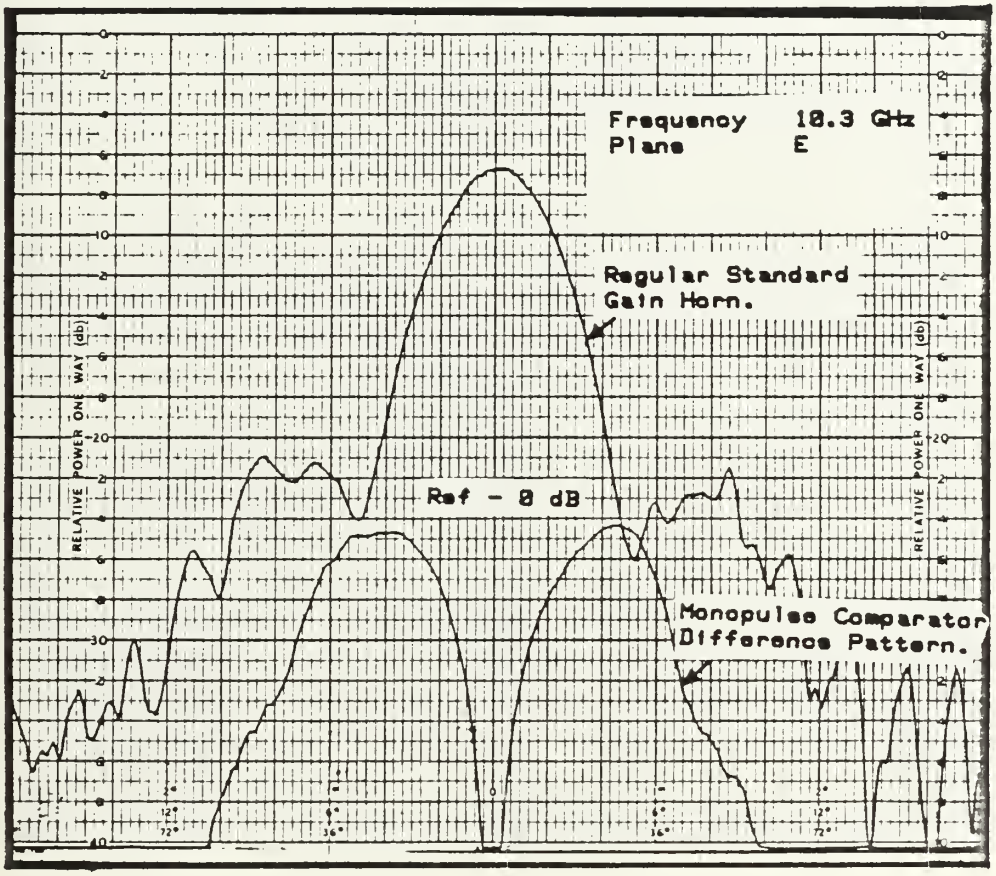

Figure 4.4 E-Plane Monopulse Comparator Difference Pattern.

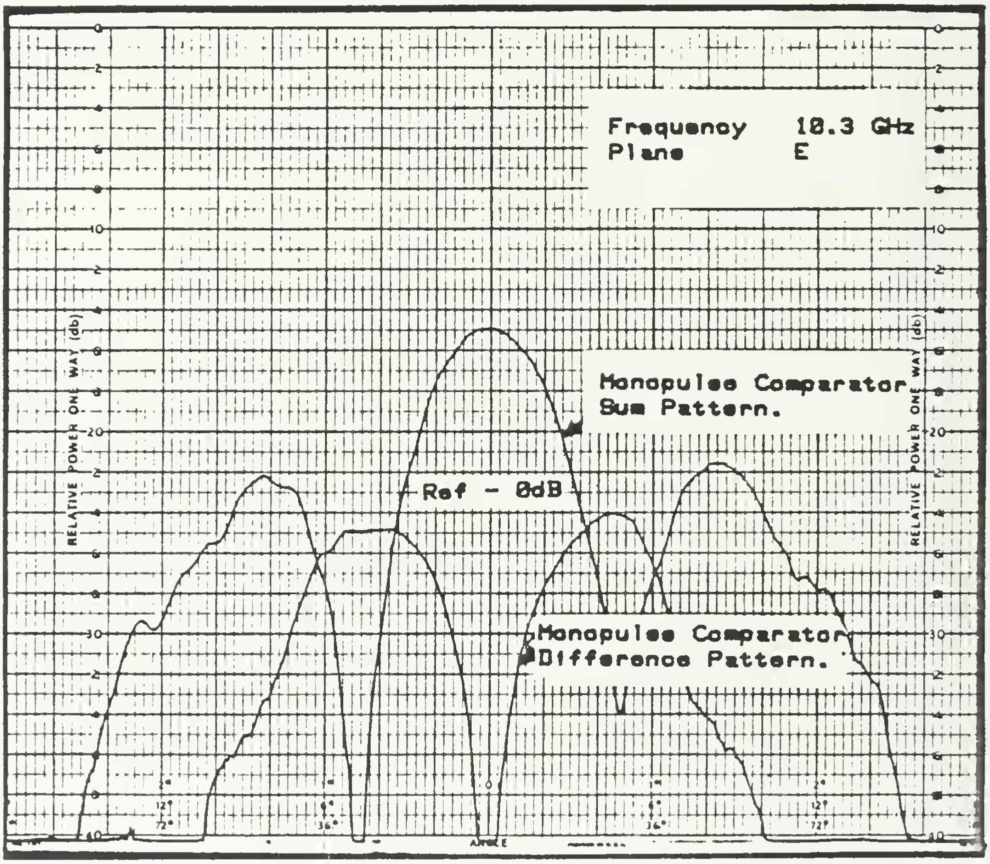

Figure 4.5 E-Plane Monopulse Comparator Sum and Difference Patterns.

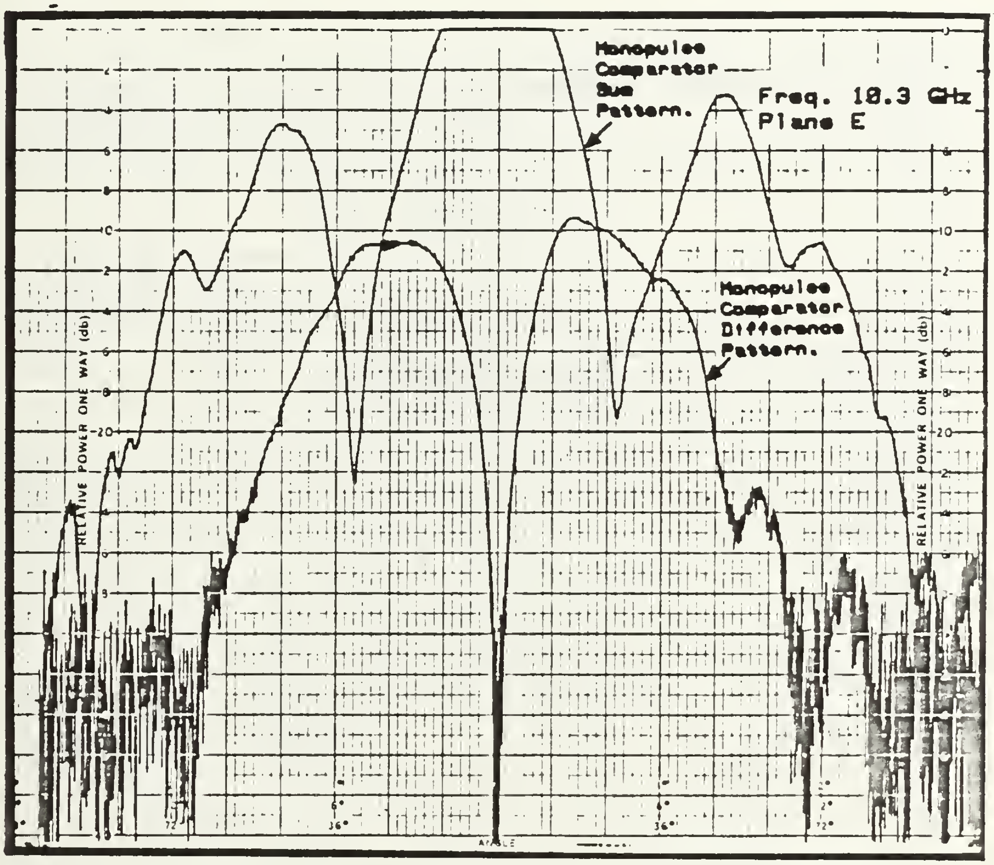

Figure 4.6 Amplified E-Plane Sum and Difference Patterns For Monopulse Comparator.

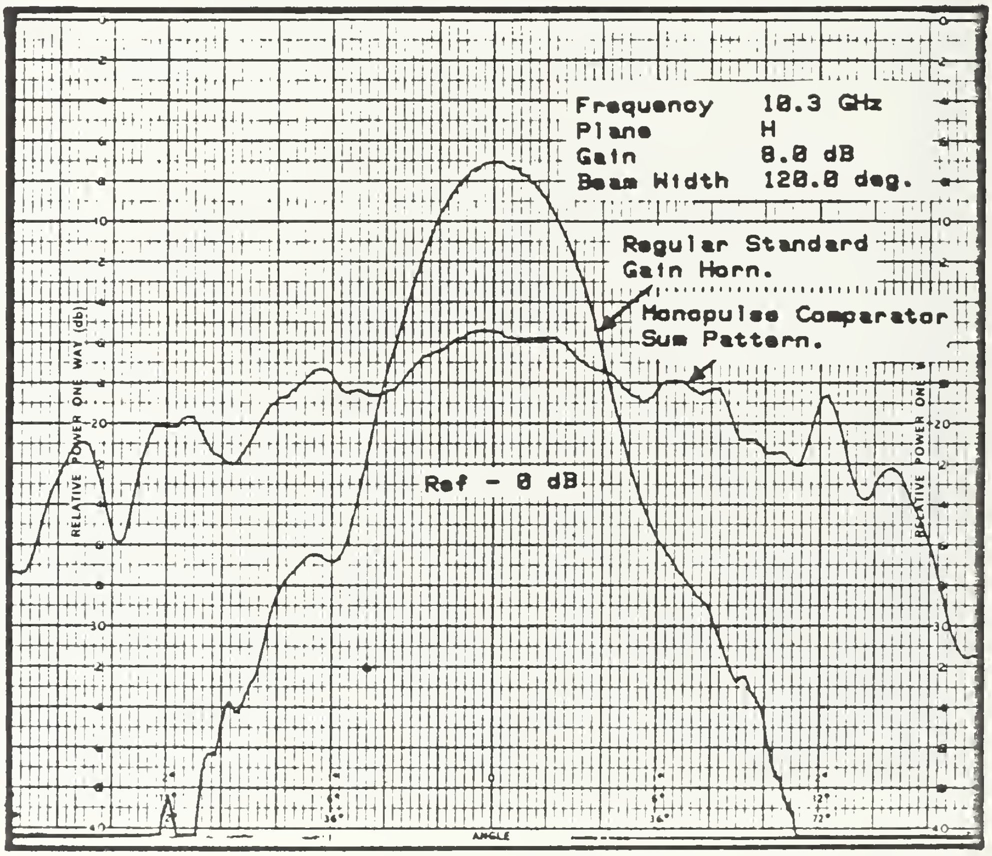

Figure 4.7 H-Plane Monopulse Comparator Sum Pattern.

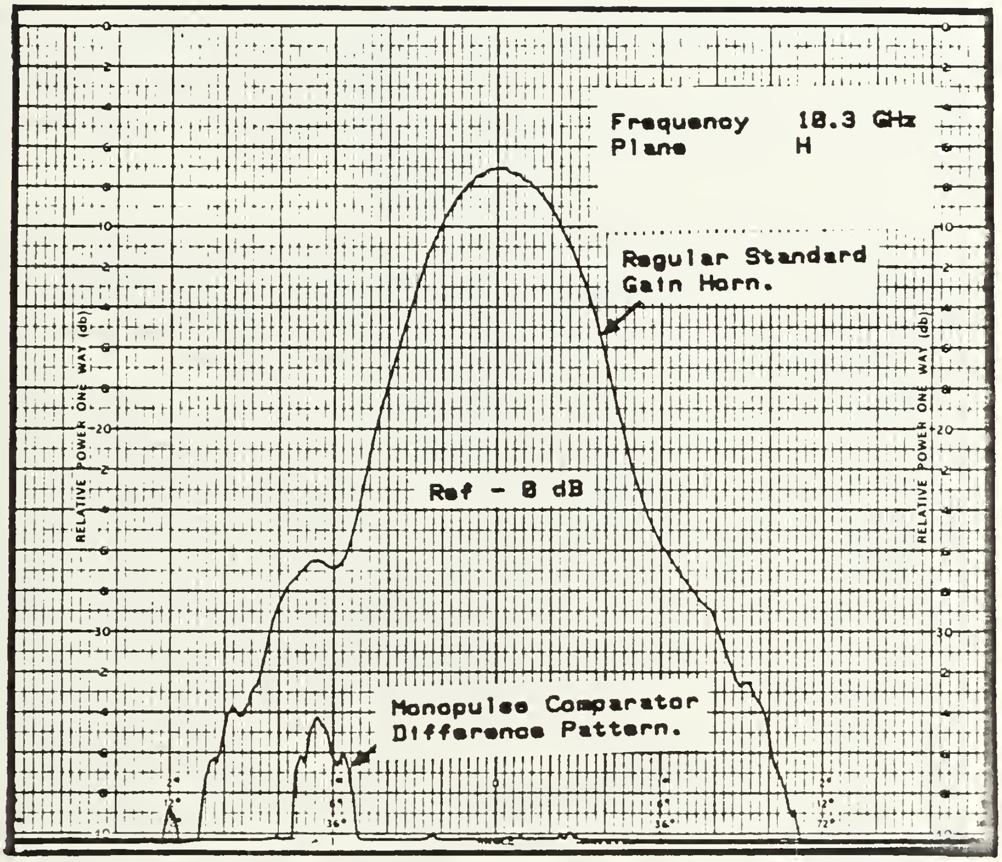

Figure 4.8 H-Plane Monopulse Comparator Difference Pattern.

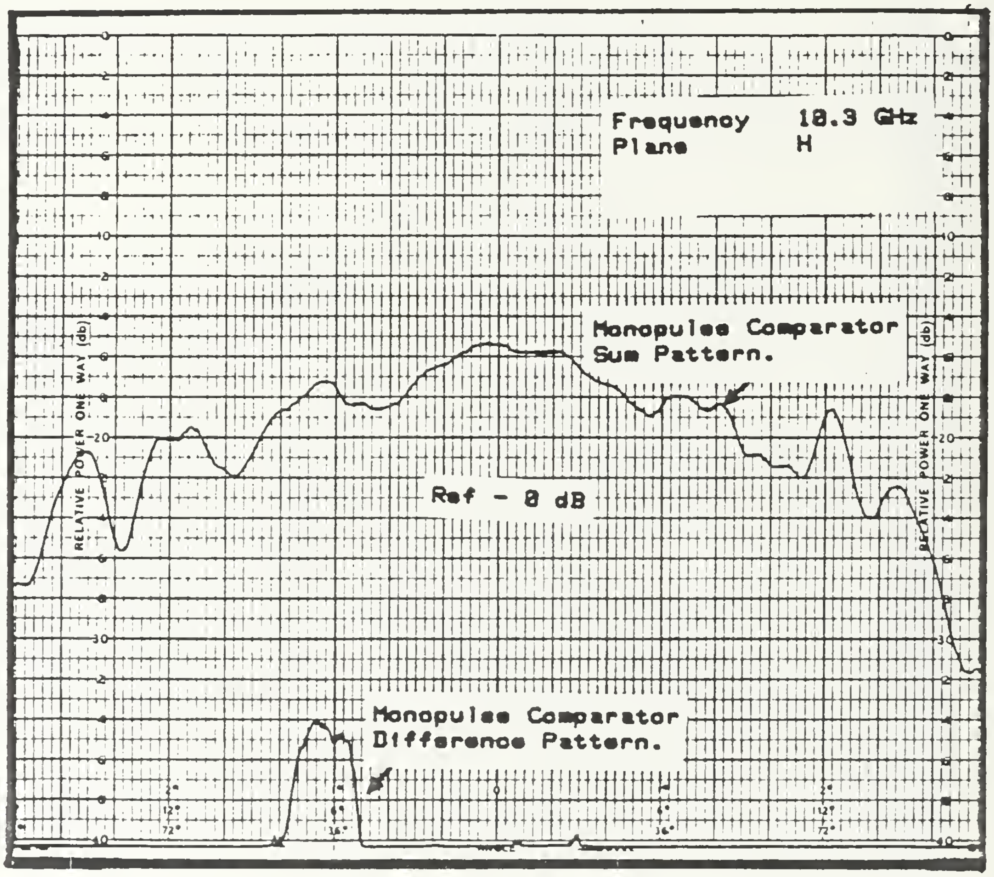

Figure 4.9 H-Plane Monopulse Comparator
Sum and Difference Patterns.

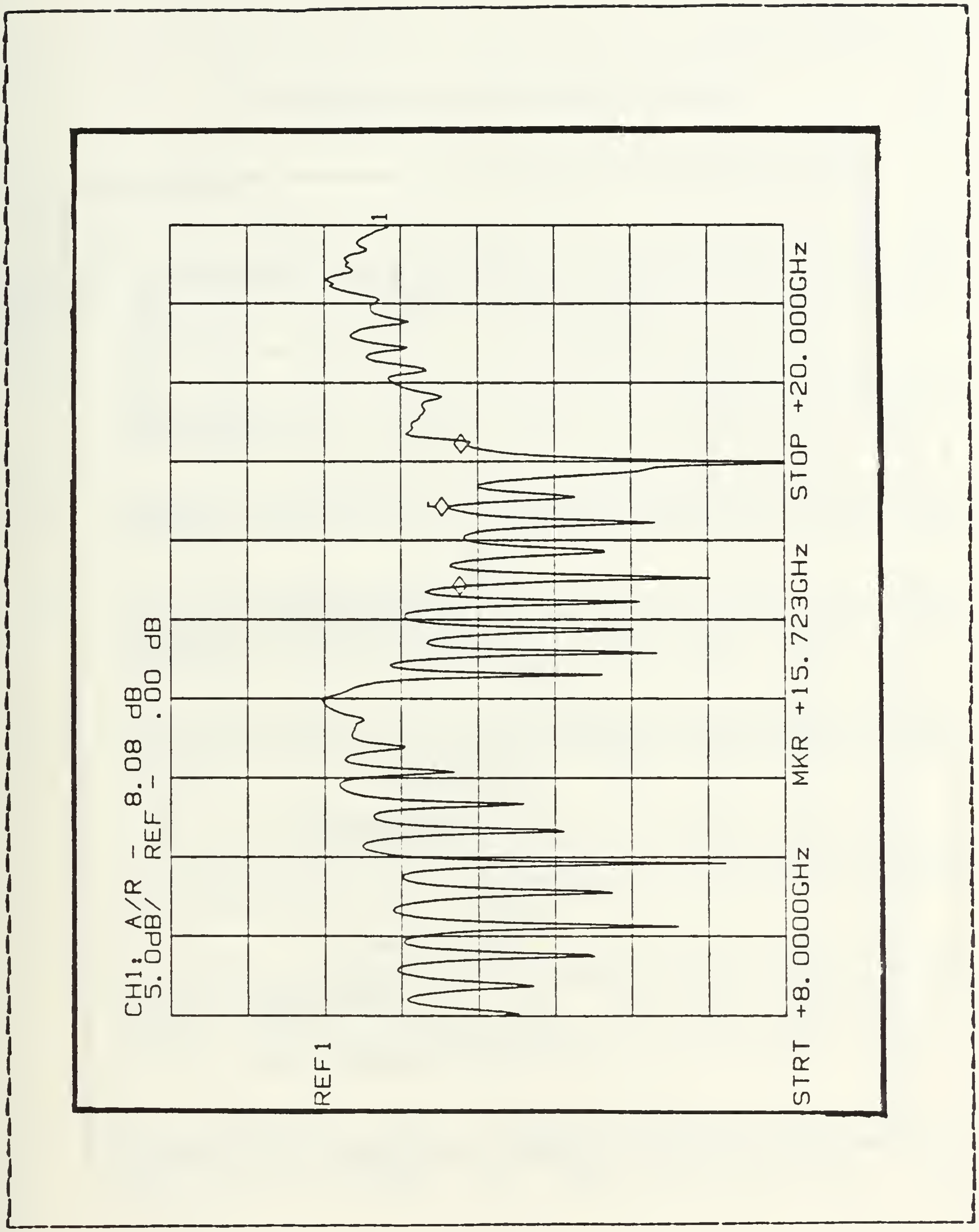

Figure 4.10 Monopulse Comparator Sum Port Reflected Power.

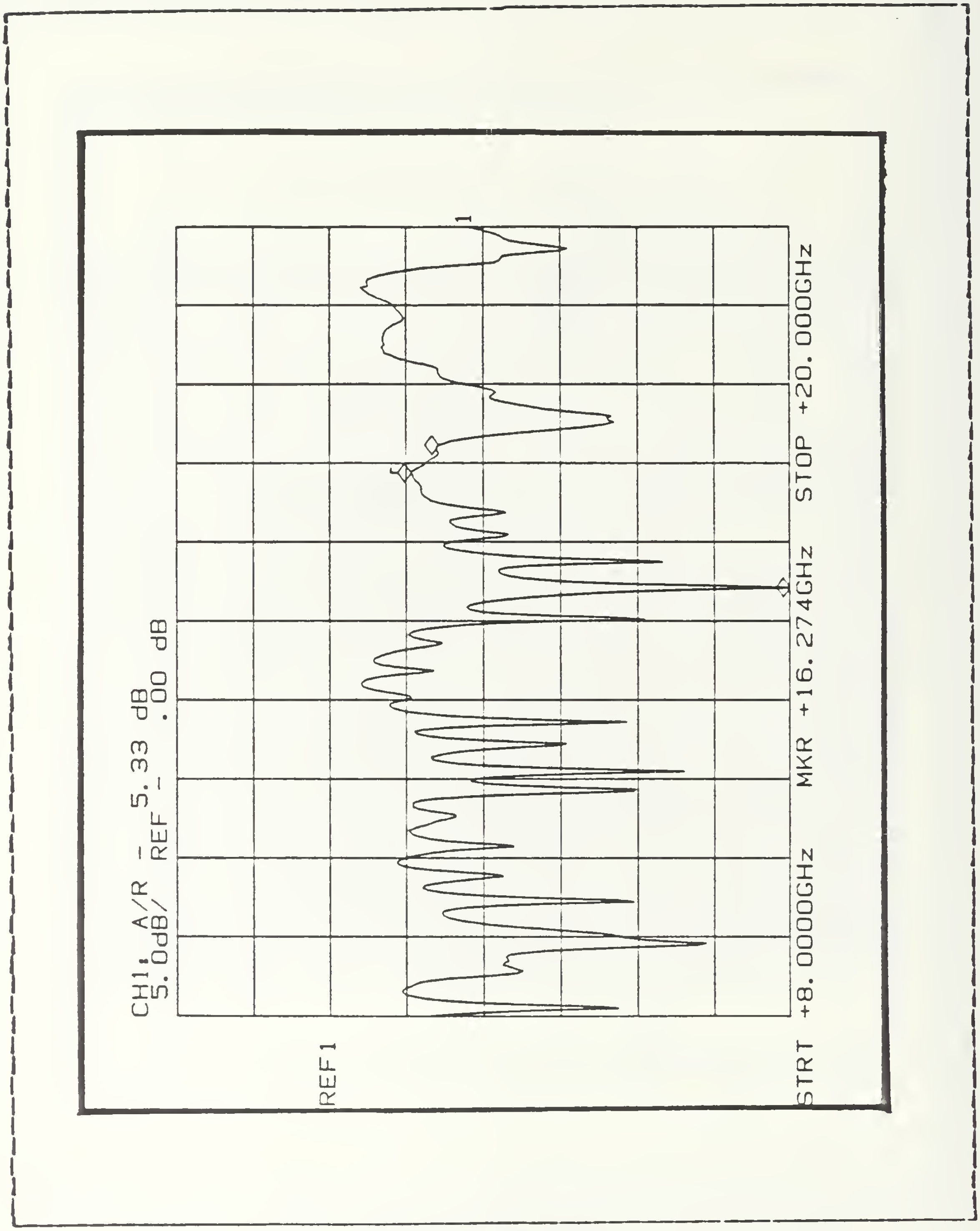

Figure 4.11 Monopulse Comparator Difference Port Reflected Power.

V. CONCLUSION AND RECOMMENDATION

A. CONCLUSIONS

This thesis mainly concentrated on the optimization of a finline horn antenna and showed its application in a monopulse comparator. A summary of the results is as follows:

1. The gain of the finline horn antenna is directly proportional to the size of the radiating aperture in the E-plane.

2. A higher dielectric constant decreases the gain of a finline horn antenna if other parameters are held constant.

3. The slot width need to be narrow to prevent secondary radiation from the end of the antenna feed line. For Er=2.54 a slot width of 1.6mm gave satisfactory results.

4. For the lower side lobes the maximum phase deviation in wavelengths, (S), needs to be lower than 1/8. This helps in calculating the flare angle and flare length.

5. The beam width in the E-plane is mainly controlled by the size of the radiating aperture and the beam width in the H-plane is controlled by the dielectric constant of the material.

6. A uniform phase front design increases the overall gain of the finline horn antenna. We also saw that further extension of the dielectric beyond the uniform phase front design in a half circle shape to form a converging lens, adversly affects the performance of the antenna.

7. An approximate gain equation for the finline horn antenna can be derived from the experimental results obtained for properly designed antennas with optimum gain and fabricated on different dielectric substrates.

8. Two finline horn antennas can be integrated with a finline magic-tee to form a monopulse comparator. Very nice sum and difference patterns were obtained.

B. RECOMMENDATIONS

In view of the different observations made during testing, follow up work is recommended as inicated below:

1. A better fixture for holding the finline horn antenna sould be designed for further experimentation.

2. The effect of different parameters on the performance on the finline horn antenna has been noted. However, the thickness of the dielectric was not considered. It might be intesting to see the effect of the dielectric thickness by testing the same horn fabricated on different dielectric thickness material but with the same dielectric constant.

3. The material used for the monopulse comparator was very thin and soft. For better results the comparator should be fabricated and tested using a hard material. A better fixture for the monopulse comparator is also required for any further testing.

4. It might be intersting to try making four finline horn antennas and four magic-tees on a single soft substrate and bending it in a U shape to form a dual plane finline monopulse system.

5. It might be intersting to measure near-field (phase and amplitude) of the optimized finline horn and compare with the regular horn antenna.

APPENDIX A
RADIATION PATTERNS

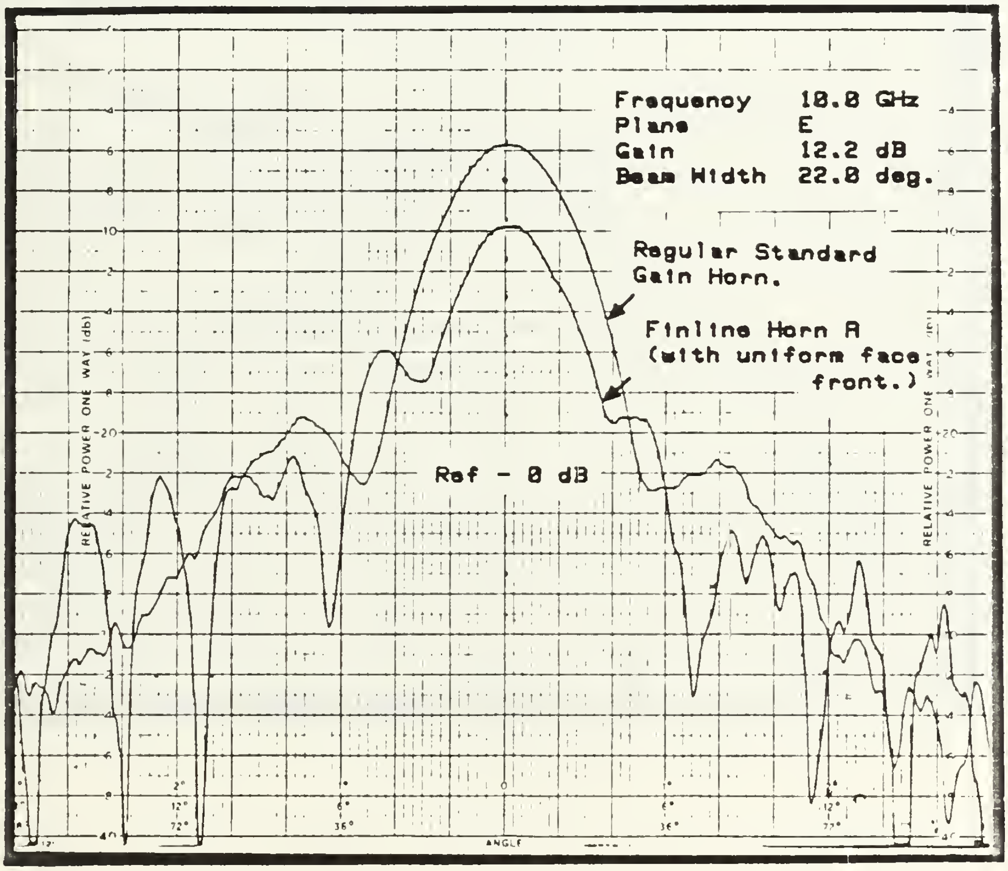

Figure A.1 E-Plane Radiation Pattern of Finline Horn "A".

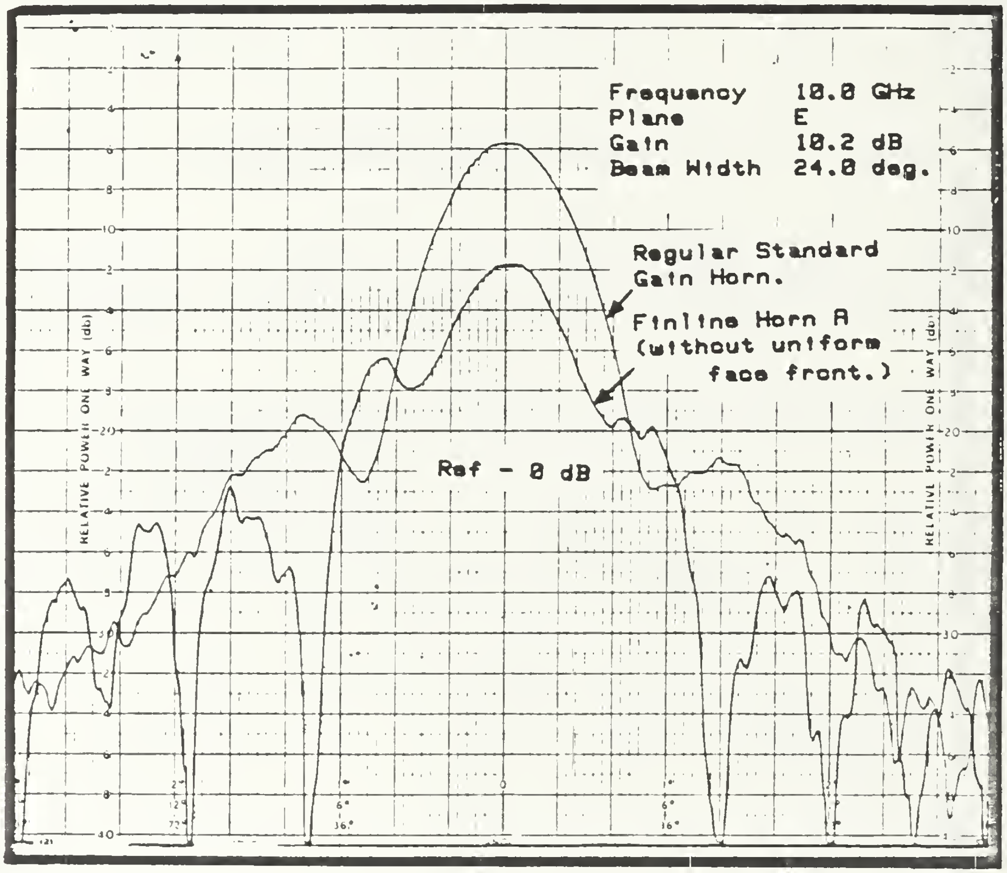

Figure A.2 E-Plane Radiation Pattern of Finline Horn "A".

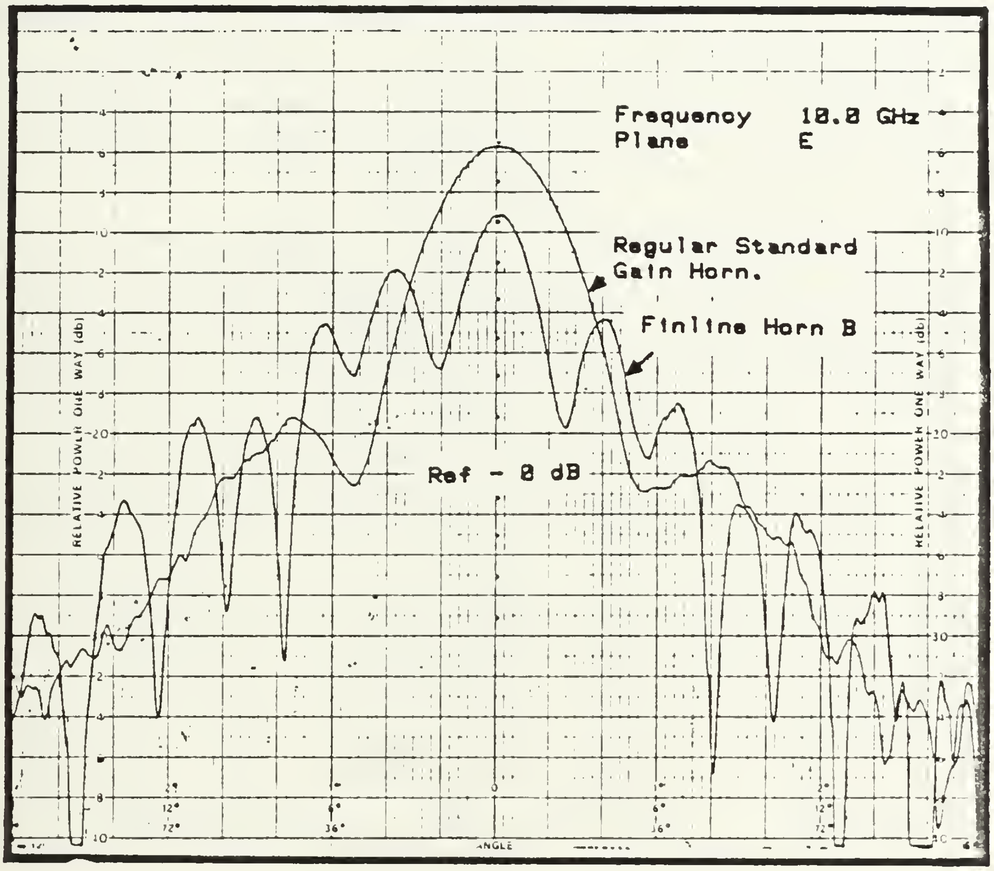

Figure A.3 E-Plane Radiation Pattern of Finline Horn "B".

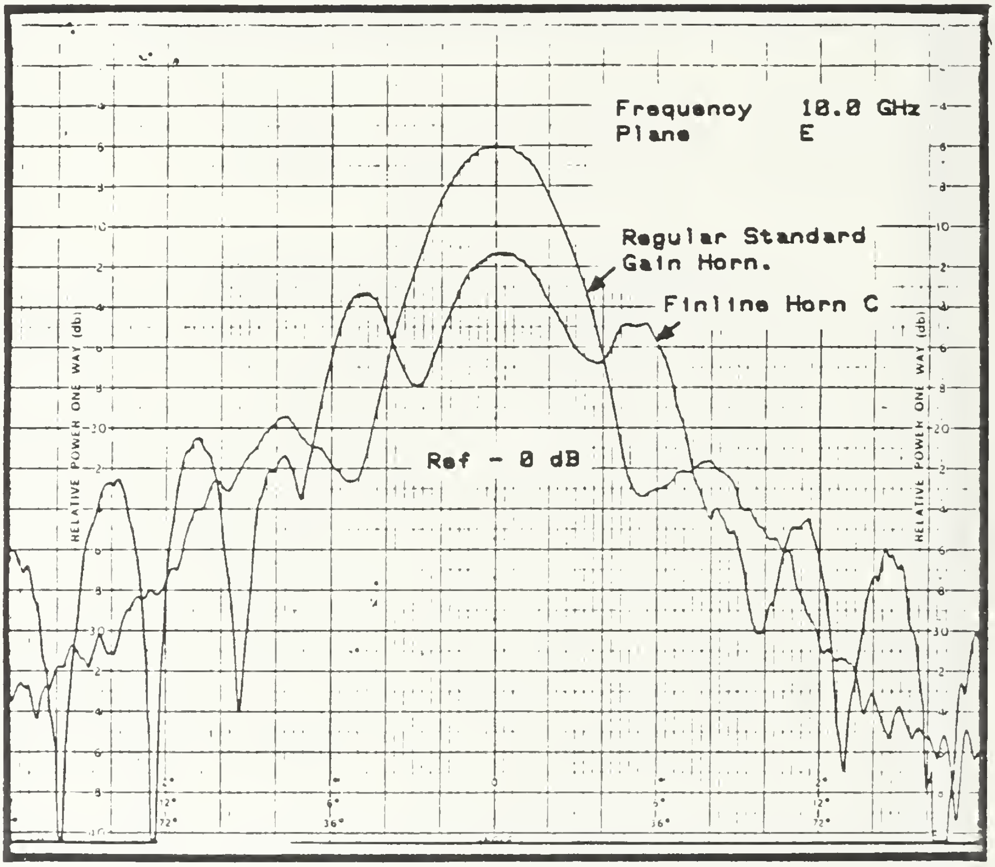

Figure A.4 E-Plane Radiation Pattern of Finline Horn "C".

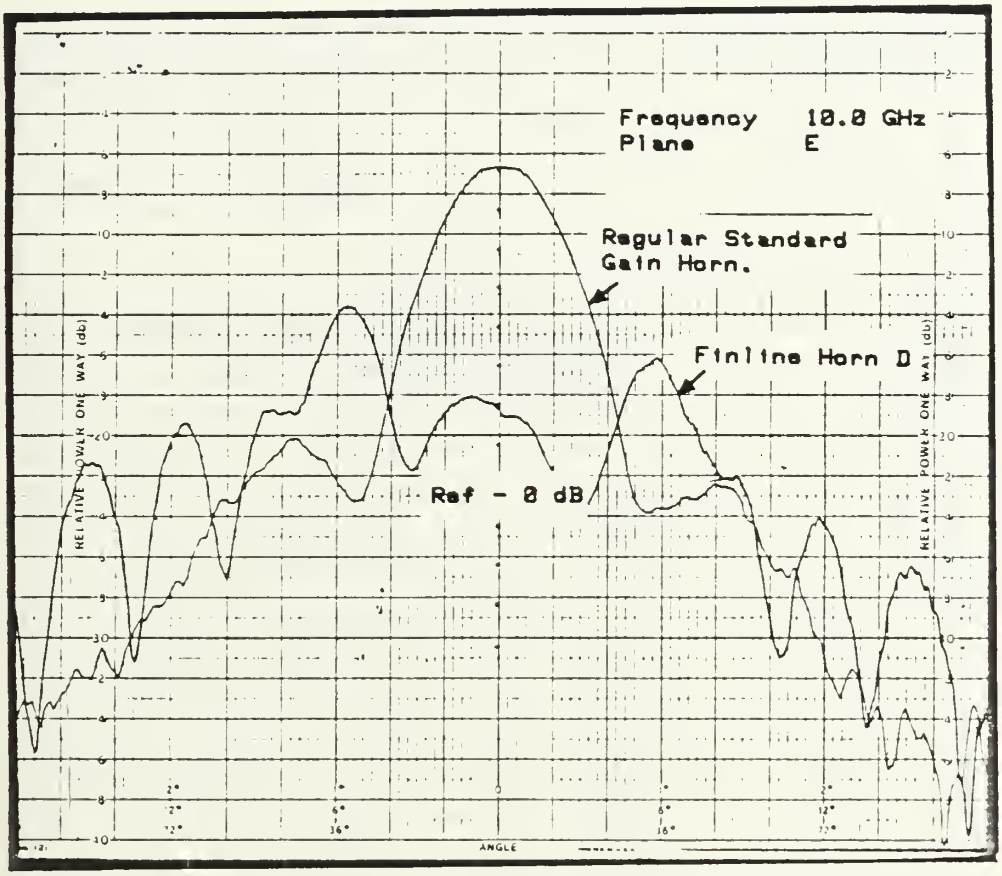

Figure A.5 E-Plane Radiation Pattern of Finline Horn "D".

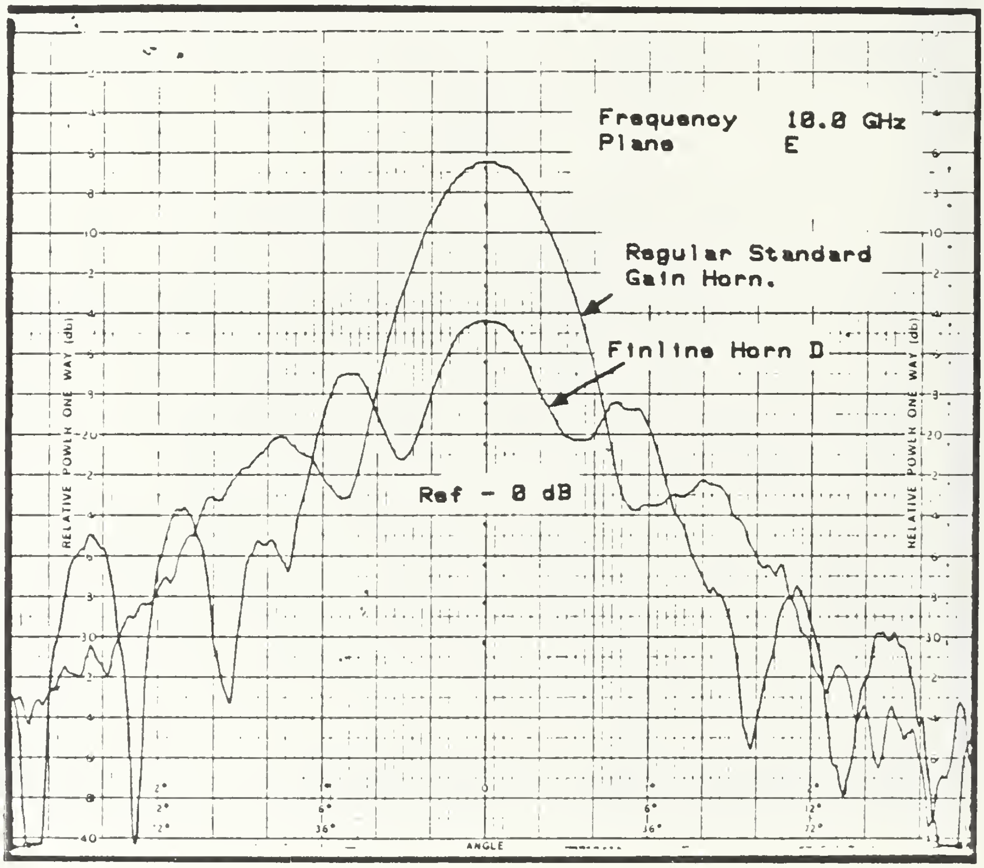

Figure A.6 E-Plane Radiation Pattern of Finline Horn "D" with Echosorb in the Feedline Opening.

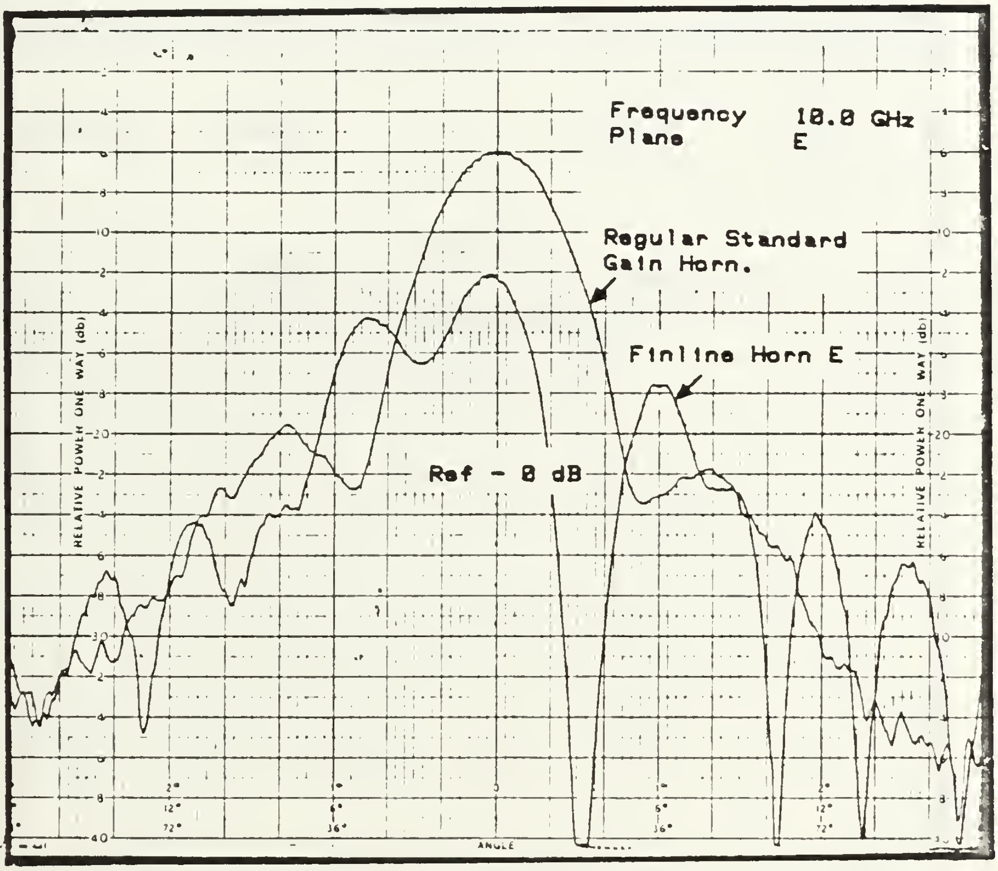

Figure A.7 E-Plane Radiation Pattern of Finline Horn "E".

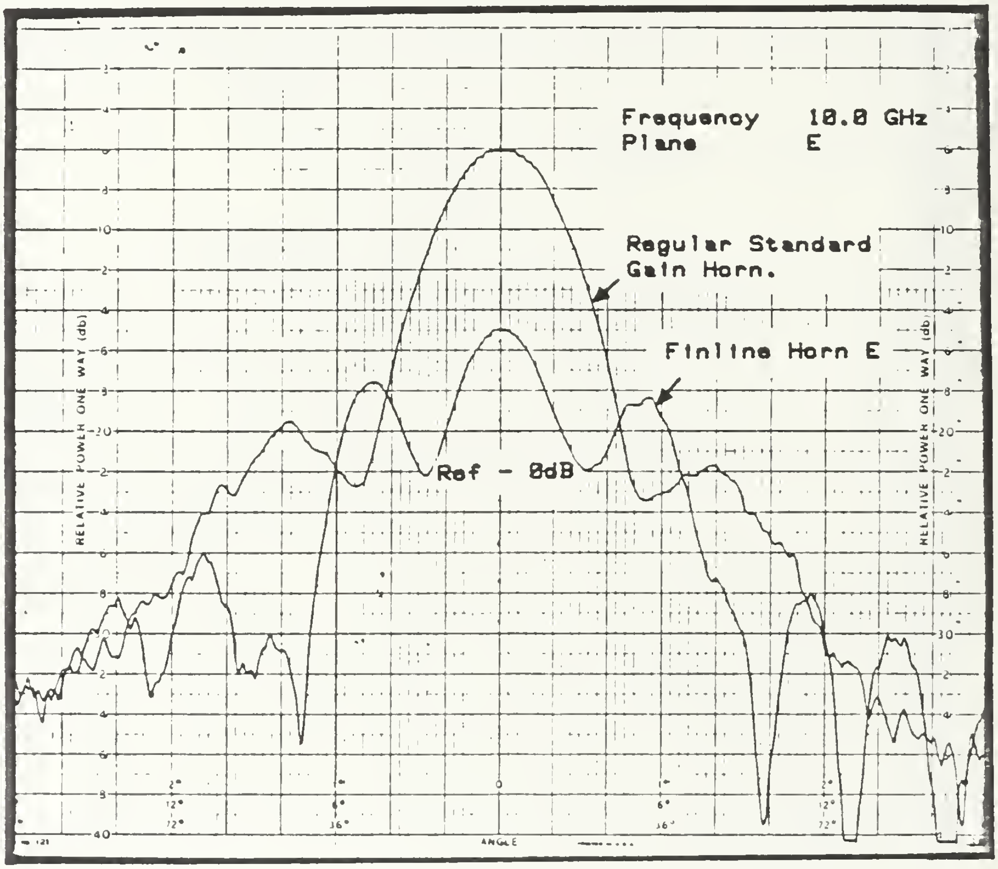

Figure A.8 E-Plane Radiation Pattern of Finline Horn "E" with Echosorb in the Feedline Opening.

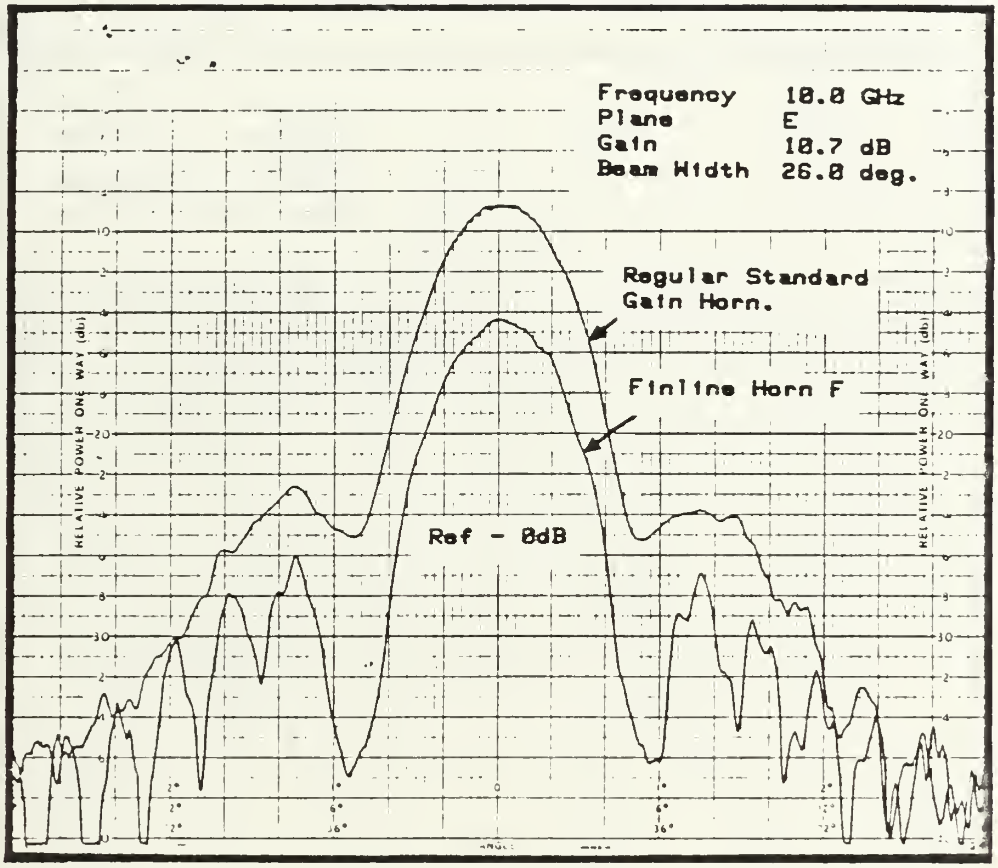

Figure A.9 E-Plane Radiation Pattern of Finline Horn "F".

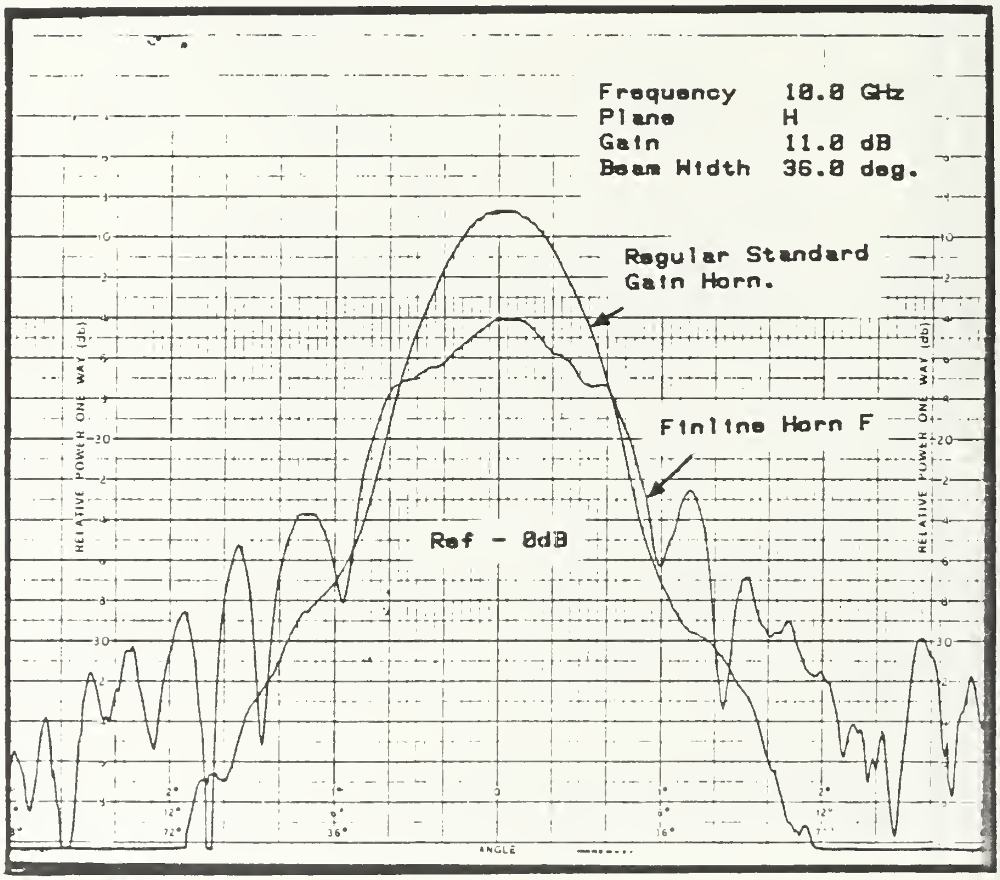

Figure A.10 H-Plane Radiation Pattern of Finline Horn "F".

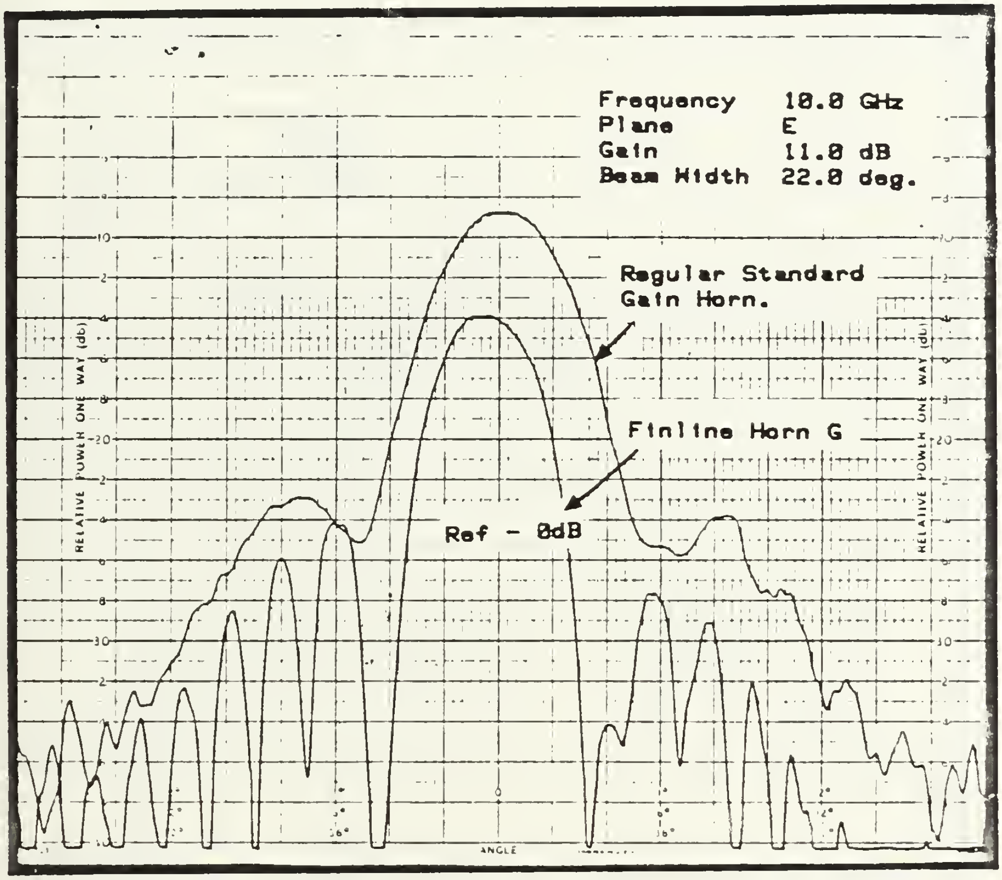

Figure A.11 E-Plane Radiation Pattern of Finline Horn "G".

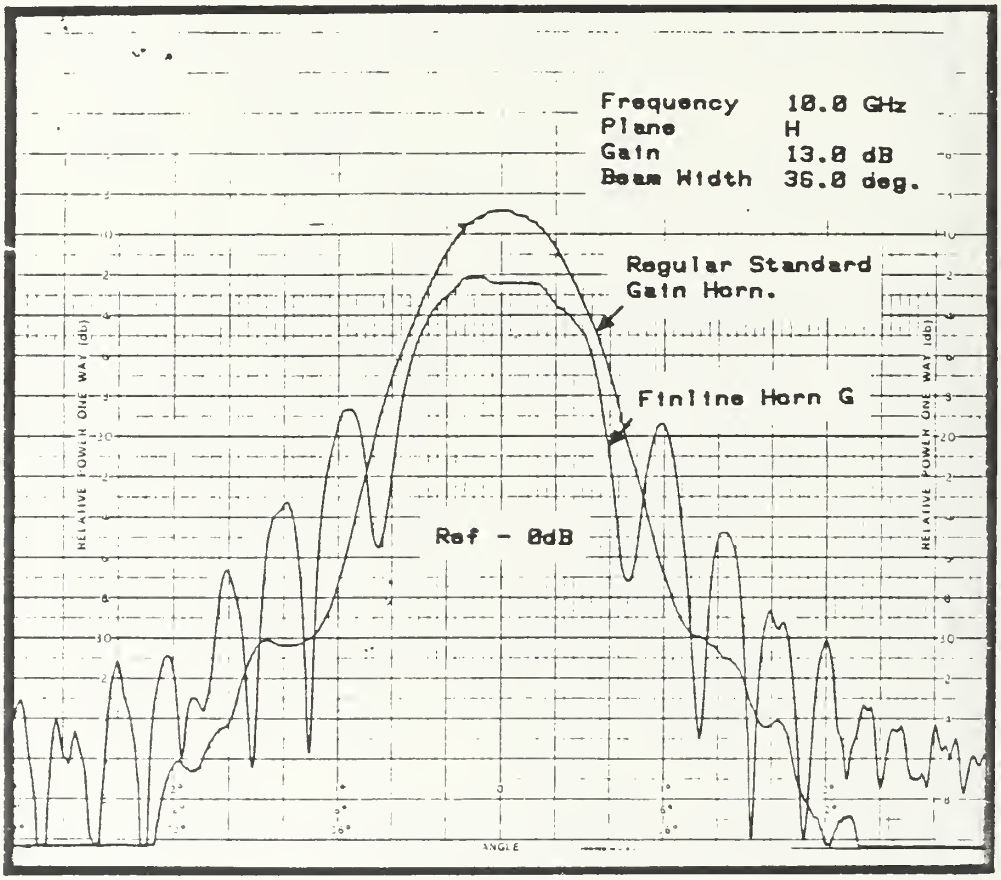

Figure A.12 H-Plane Radiation Pattern of Finline Horn "G".

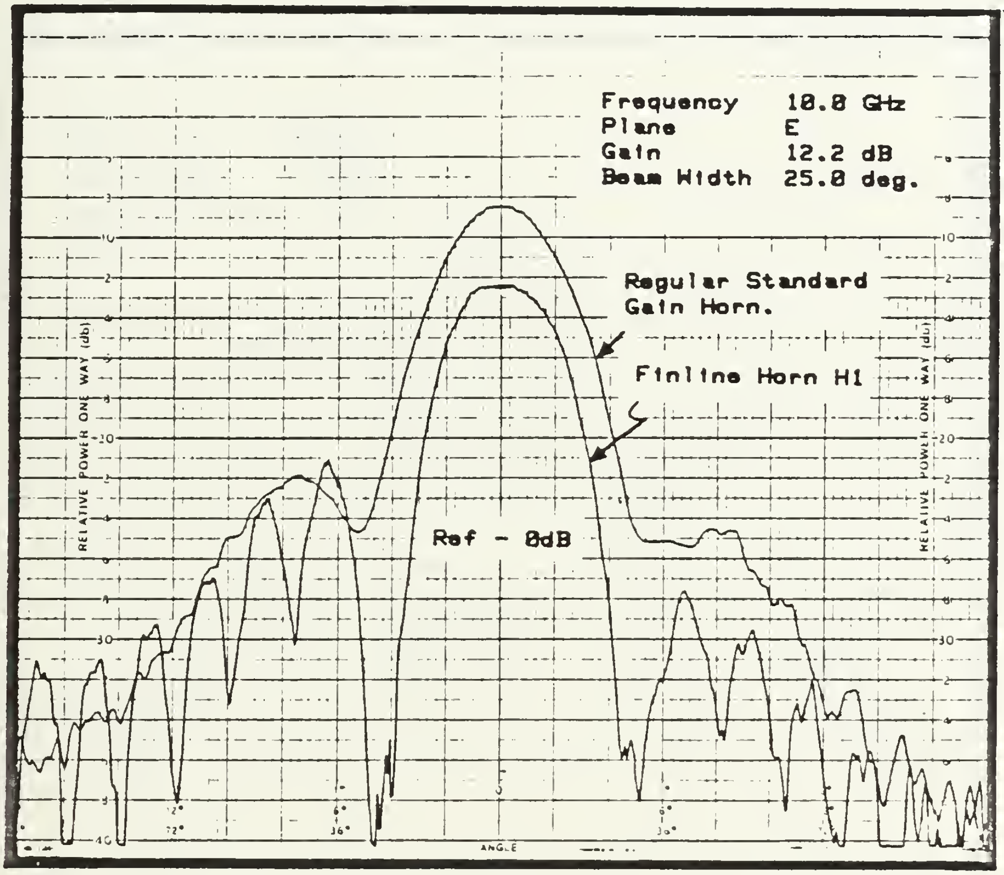

Figure A.13 E-Plane Radiation Pattern of Finline Horn "H1".

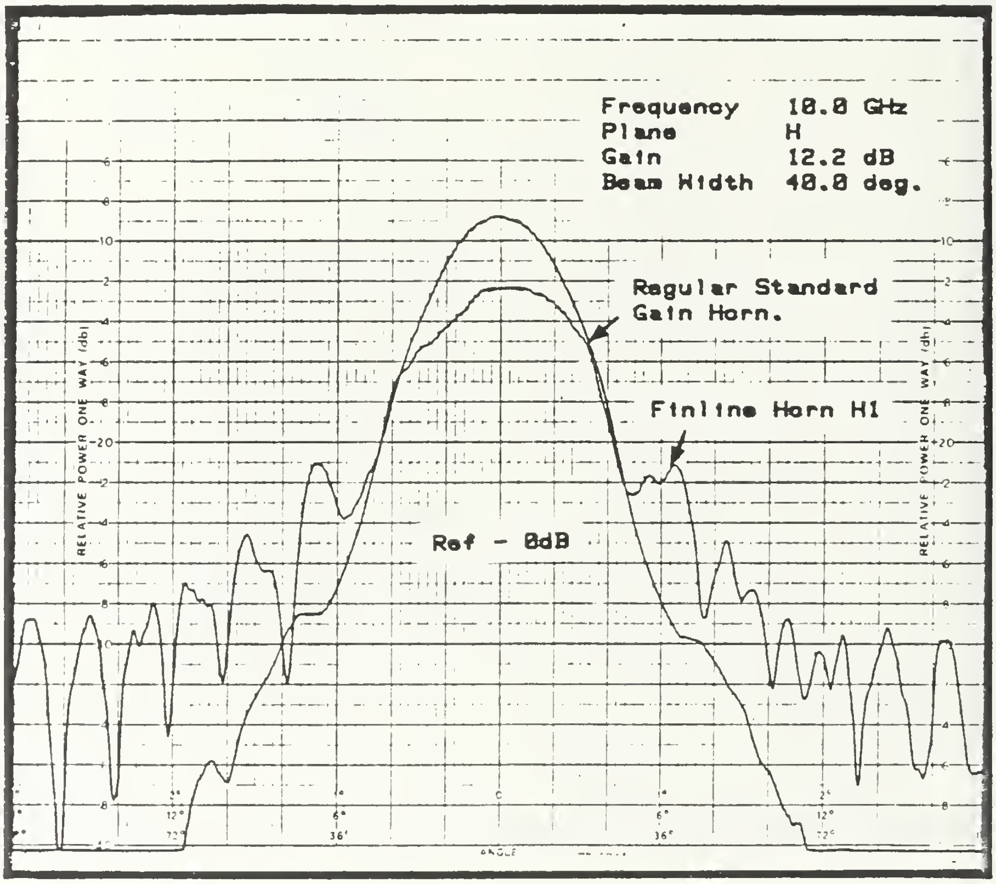

Figure A.14 H-Plane Radiation Pattern of Finline Horn "H1".

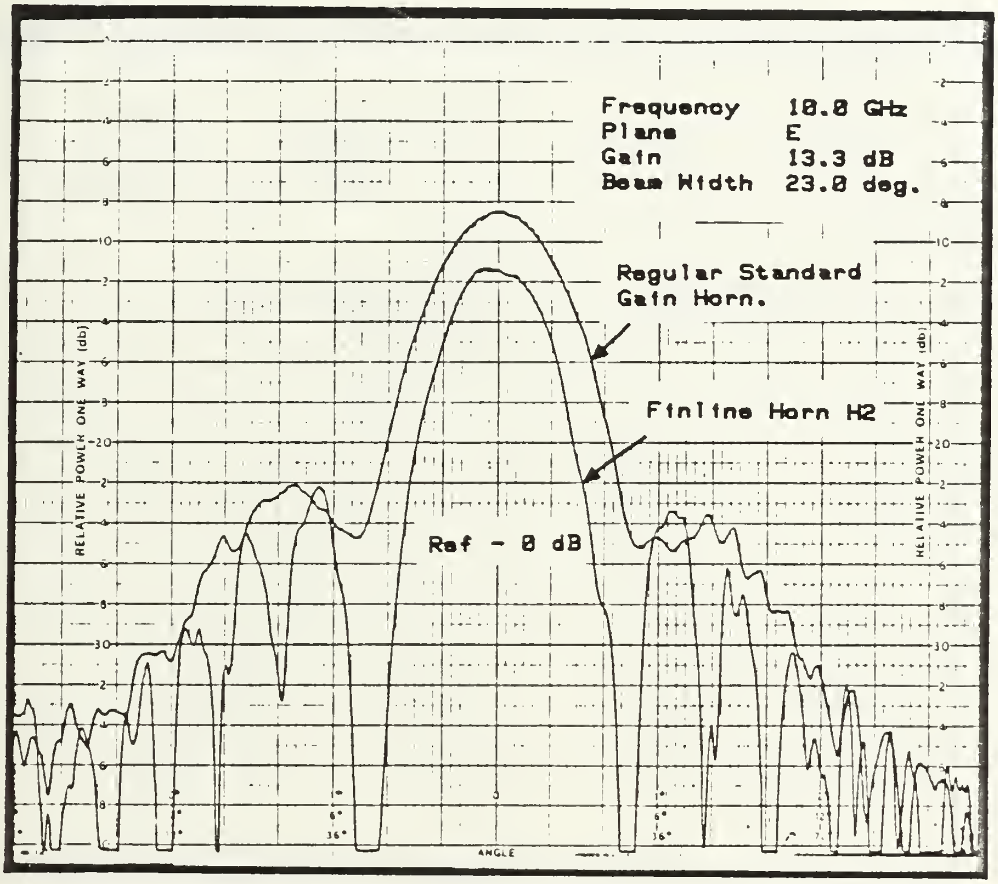

Figure A.15 E-Plane Radiation Pattern of Finline Horn "H2".

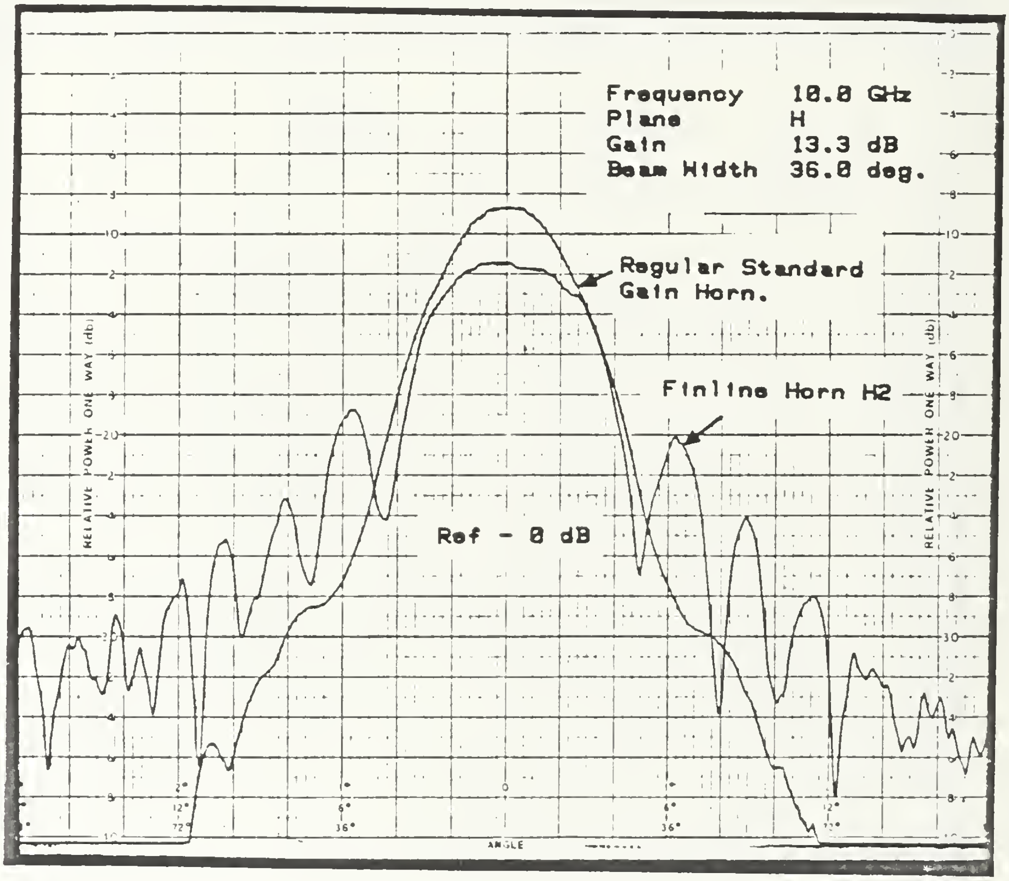

Figure A.16 H-Plane Radiation Pattern of Finline Horn "H2".

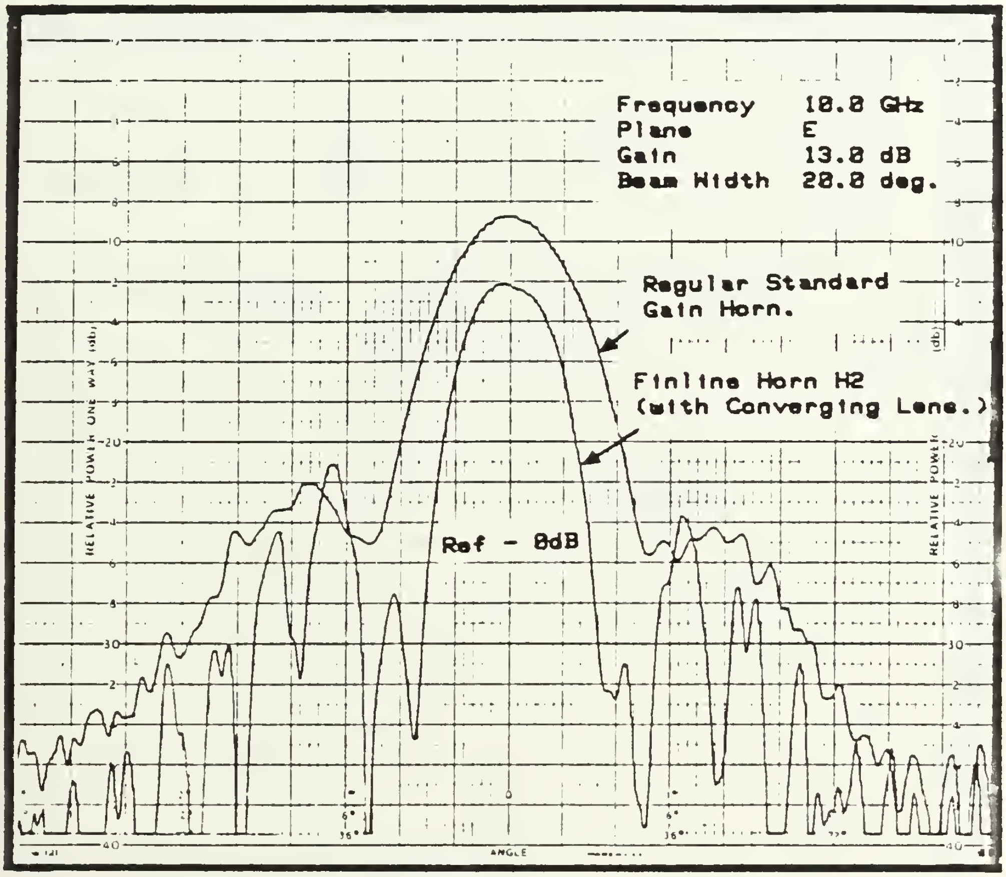

Figure A.17 E-Plane Radiation Pattern of Finline Horn "H2".

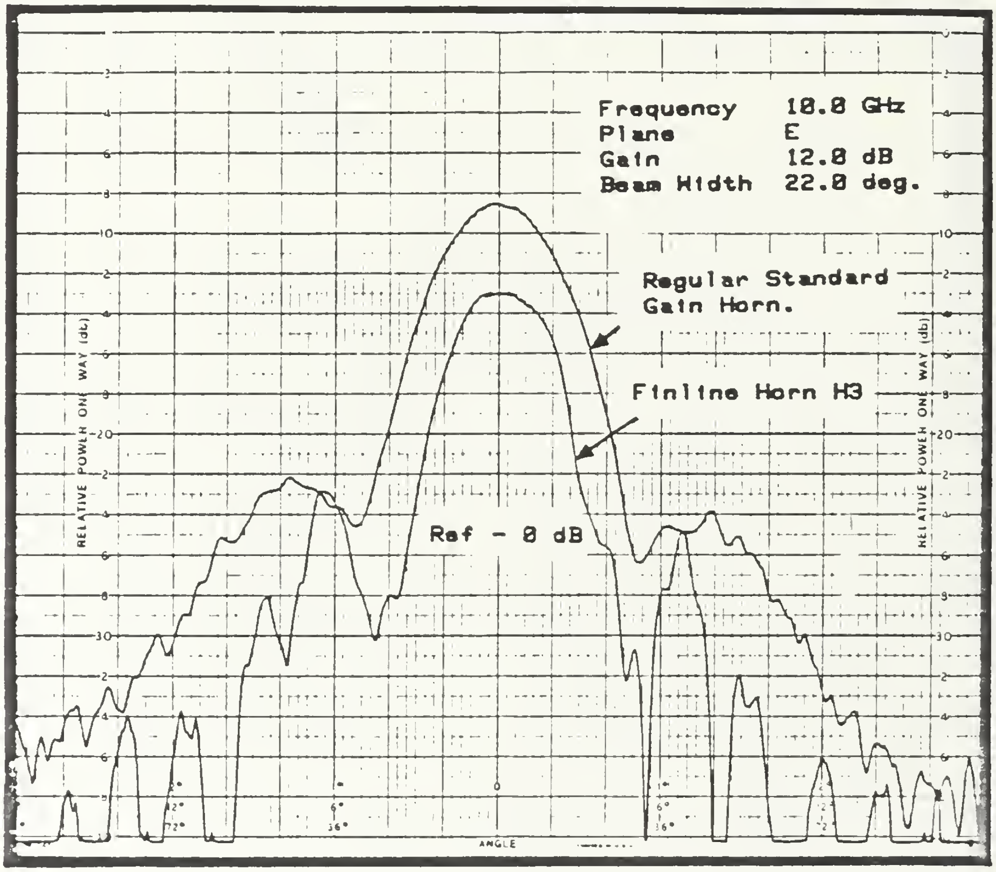

Figure A.18 E-Plane Radiation Pattern of Finline Horn "H3".

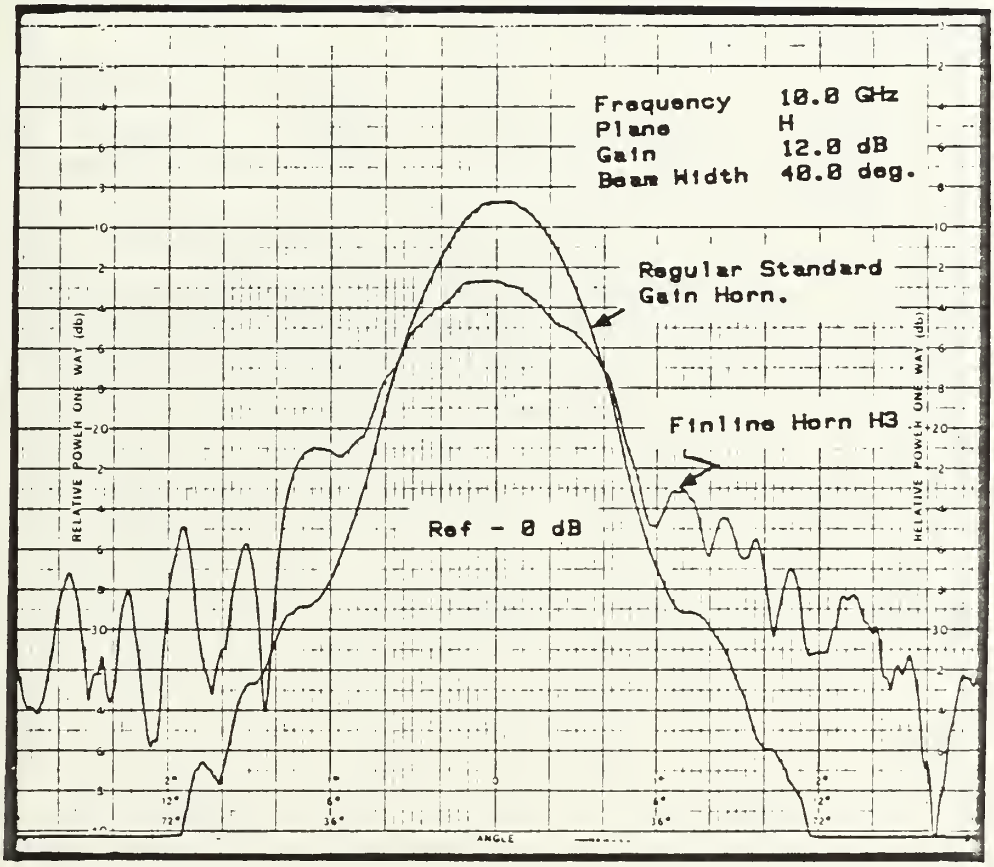

Figure A.19 H-Plane Radiation Pattern of Finline Horn "H3".

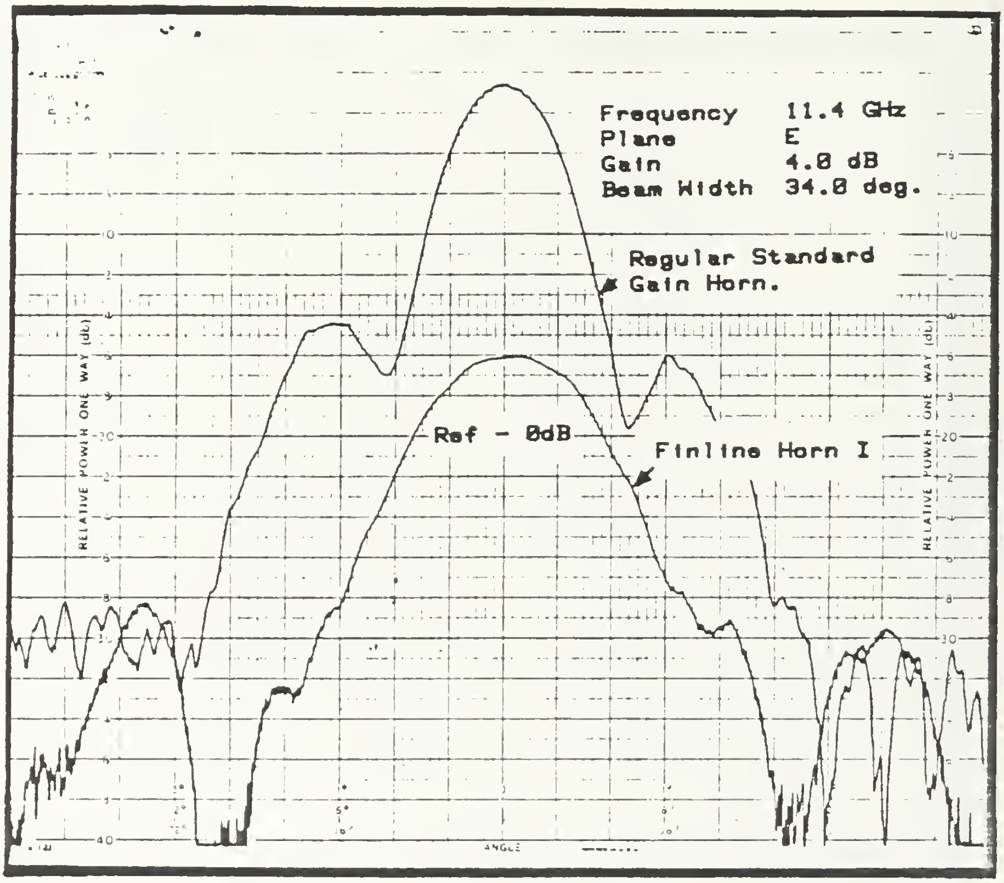

Figure A.20 E-Plane Radiation Pattern of Finline Horn "I".

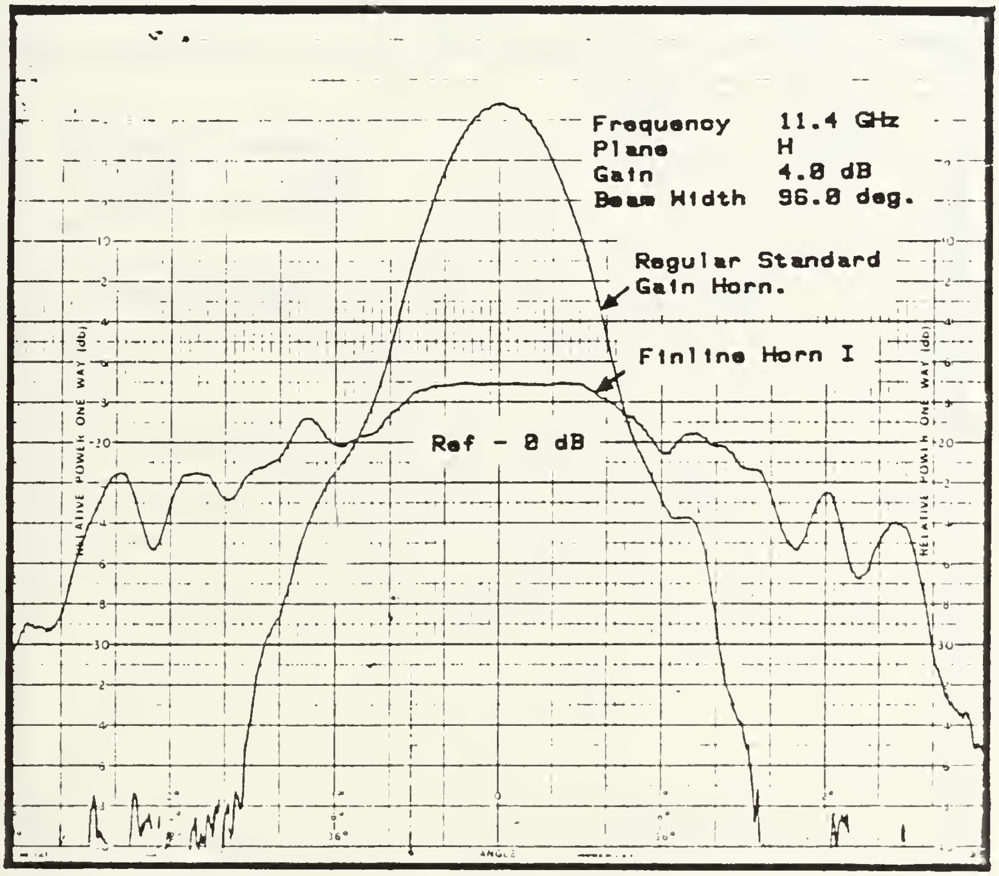

Figure A.21 H-Plane Radiation Pattern of Finline Horn "I".

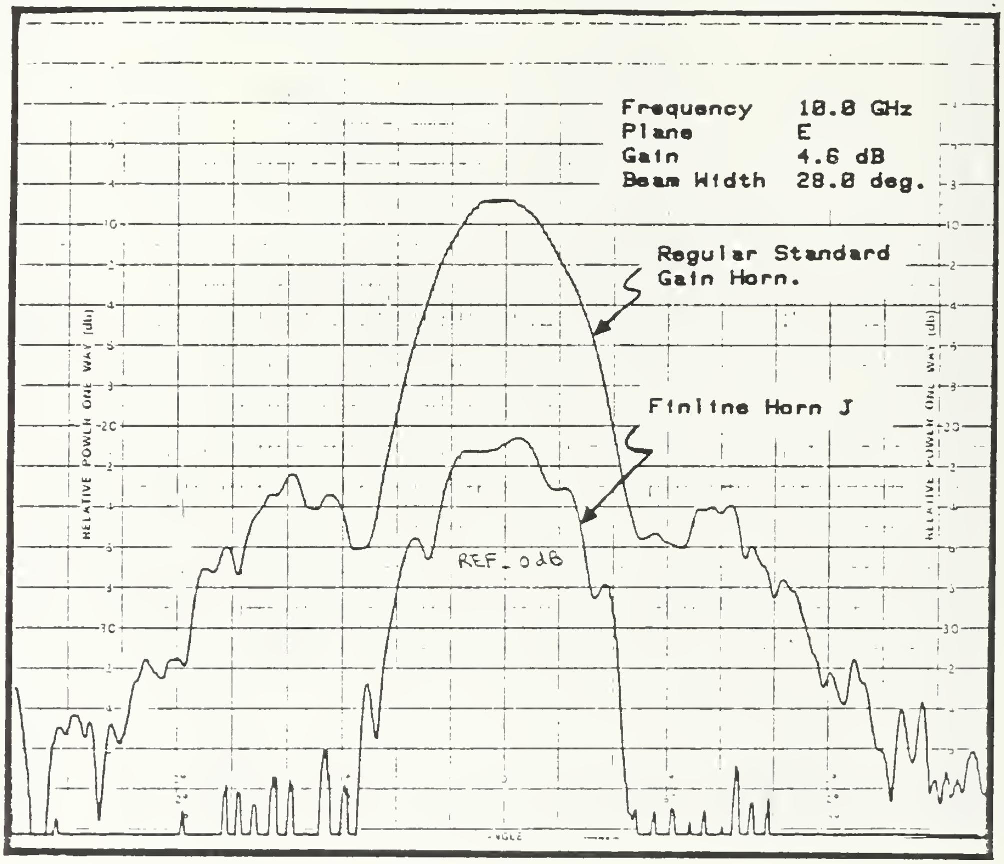

Figure A.22 E-Plane Radiation Pattern of Finline Horn "J".

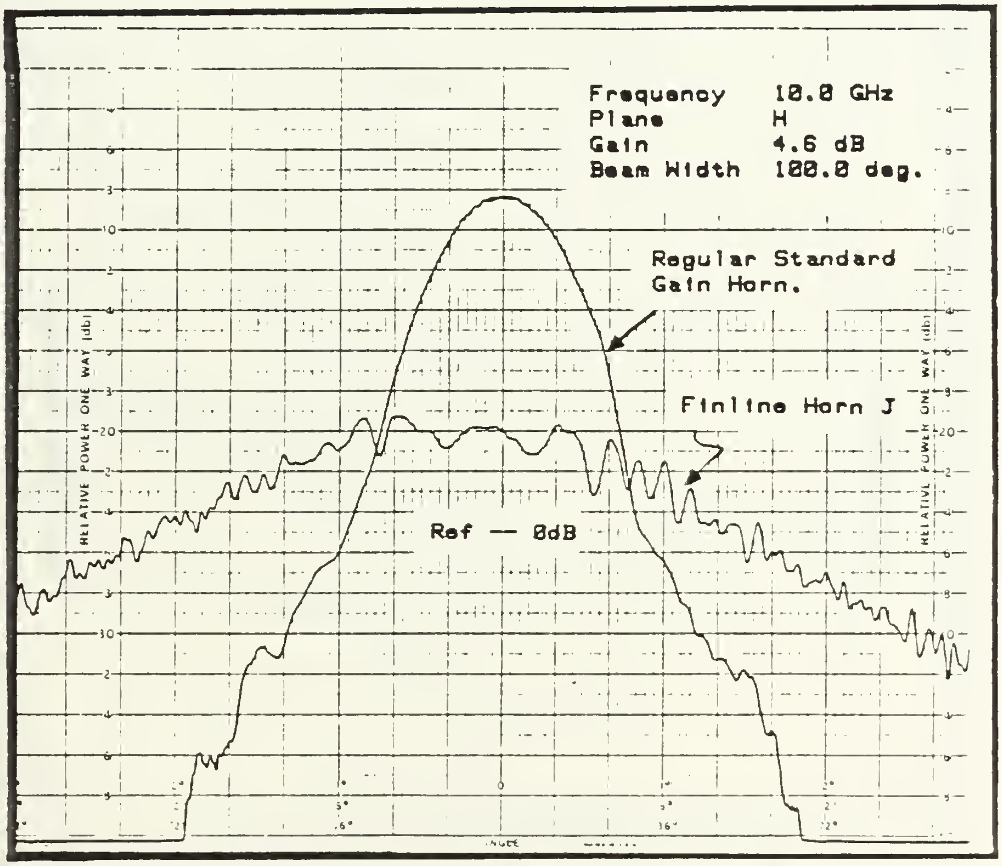

Figure A.23 H-Plane Radiation Pattern of Finline Horn "J".

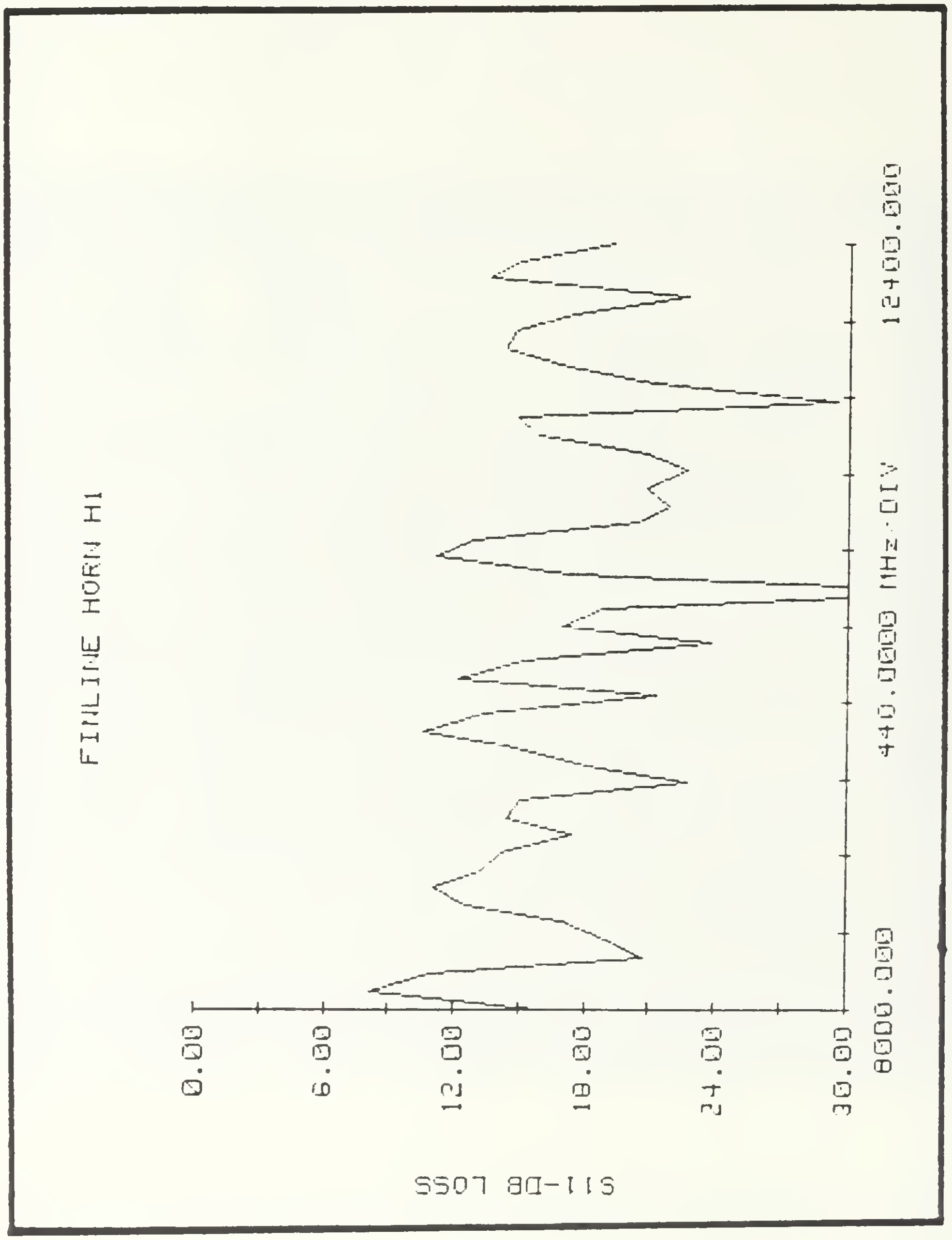

Figure A.24 Reflected Power of Finline Horn "H1".

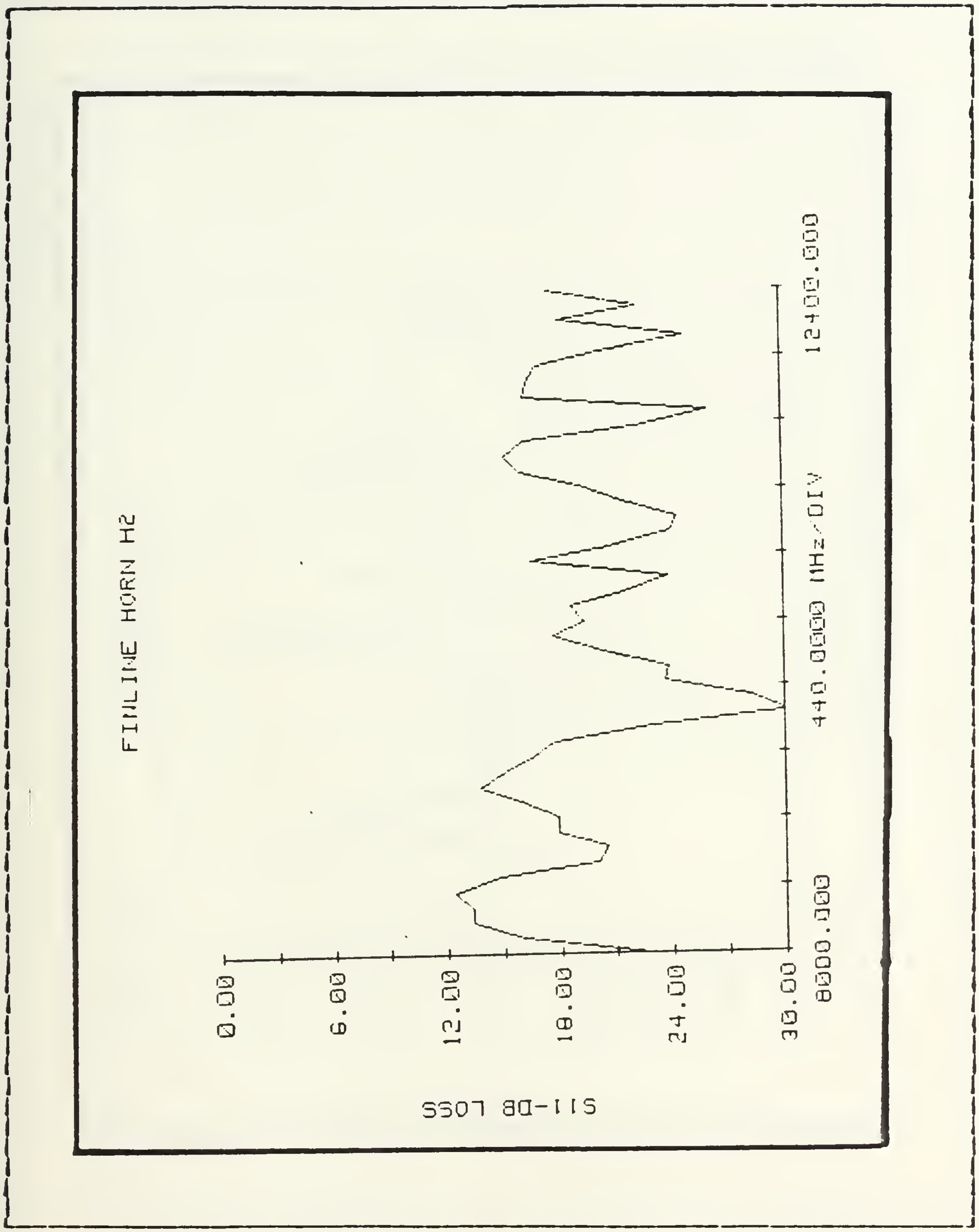

Figure A.25 Reflected Power of Finline Horn "H2".

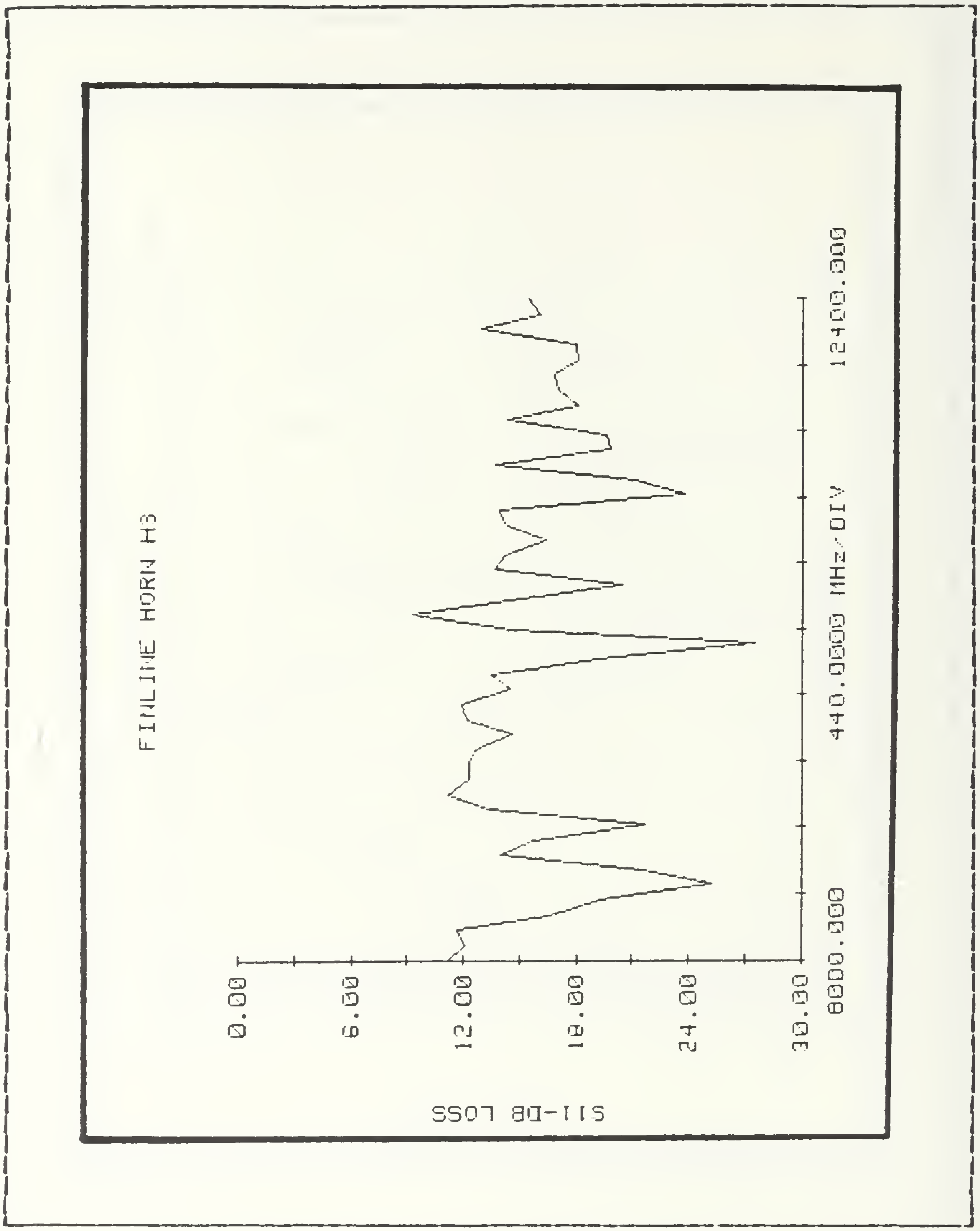

Figure A.26   Reflected Power of Finline Horn "H3".

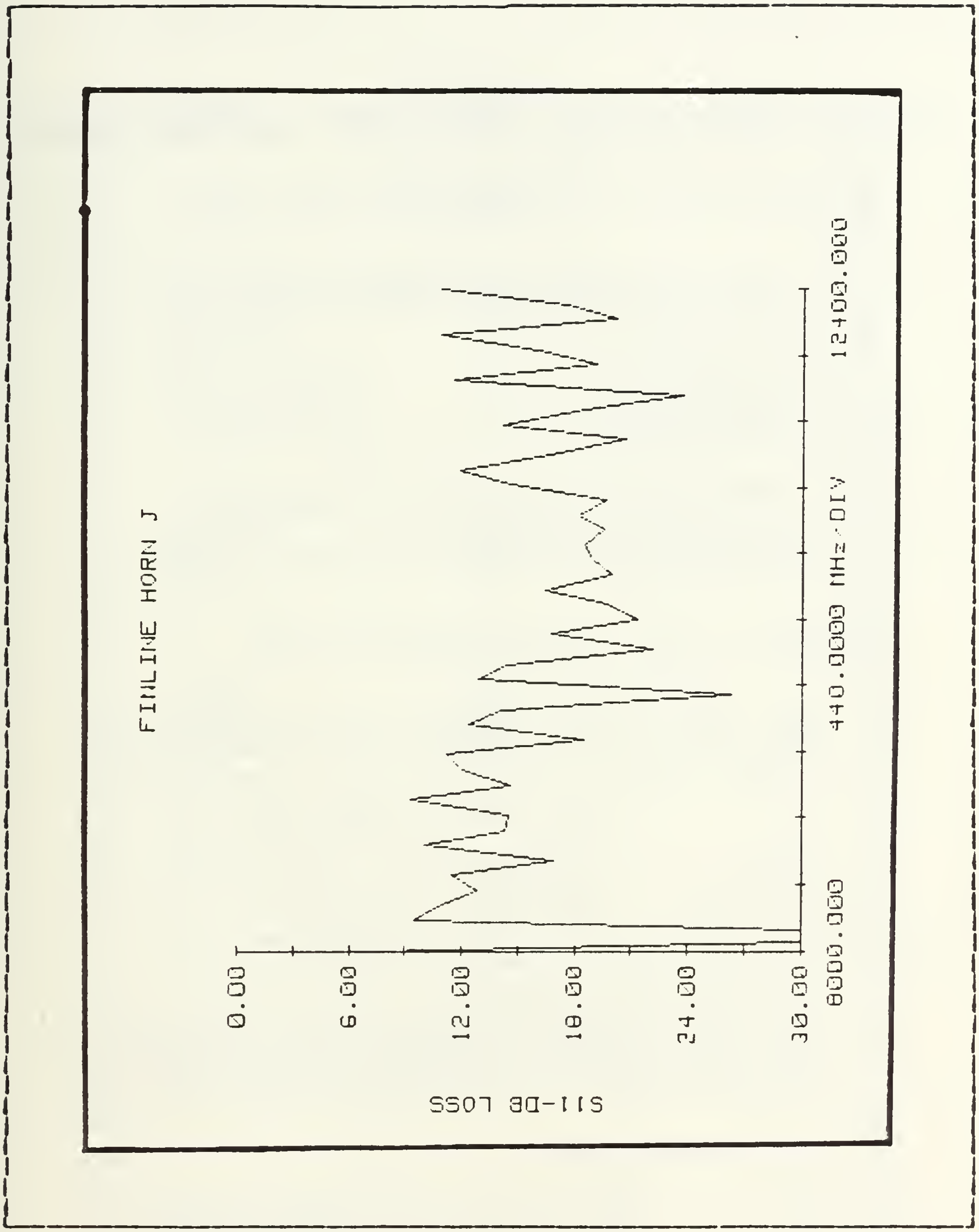

Figure A.27 Reflected Power of Finline Horn "J".

APPENDIX B

COMPUTER PROGRAM TO DRAW FINLINE HORN ON HP9845B PLOTTER

```
10    !                    FIN LIN HORN DESIGN               !
20    !                            BY                        !
30    !                    LCDR MUMTAZ UL HAQ                !
40    !                                                      !
50    !
60    !                     MSEE THESIS WORK                 !
70    !                 NAVAL POSTGRADUATE SCHOOL            !
80    !  (WRITTEN ON HP-9845B USING AN HP-9872C PLOTTER)     !
90    !
100   !
110   !
120   !
130   ! MISC. PROGRAMING INFO:
140   !
150   ! "MSCALE" ACCURATELY SCALES THE PLOTTER IN MILLIMETERS.
160   ! BY USING "MSCALE, ALL UNITS IN THIS PROGRAM ARE IN mm.
170   !
180   ! MSCALE 200,142.5  CENTERS DISPLAY ON  FULL SIZE PAPER !
190   ! MSCALE 116.576,91.77  CENTERS DISPLAY ON SMALL PAPER !
200   !
210   CLIP -102,140,-40,30    ! WHEN USED LIMITS PEN TRAVEL AS SHOWN.
220   ! FRAME ! WHEN USED DRAWS A BORDER AT CLIP LIMITS
230   !
240   !
250   !
260   PLOTTER IS "9872A"   !COORDINATES COMPUTER AND PLOTTER
270   DEG                  !ALL ANGLES ARE LISTED IN DEGREES
280   !
290   !
300   Xcenter=185         !CENTER OF DRAWING ON PAGE IN mm FROM LOWER LEFT.
310   Ycenter=120        !CENTER OF DRAWING ON PAGE IN mm FROM LOWER LEFT.
320   MSCALE Xcenter,Ycenter    !UNITS ARE mm FROM STATED ORGIN LOCATION
330   !
340   Pen=.35             !THIS IS THE PEN THICKNESS, AND IT IS CORRECTED
350   !                    FOR AUTOMATICALLY IN THE DRAWING.
360   Scale=1             !ENTIRE DRAWING IS SCALED TO THIS FACTOR
370   !
380   Mm=Scale             !SCALES ALL LISTED mm VALUES
390   In=25.4*Scale        !CONVERTS AND SCALES ALL LISTED inches VALUES
400   !
410   Linenumber=1         !FIRST DIGIT OF LINE TYPE CODE
420   Segmentsize=0        !SECOND DIGIT OF LINE TYPE CODE
430   !
440   !
450   !
460   ! THE FOLLOWING VARIABLES DESCRIBE THE ENTIRE DRAWING. THE REST OF THE
470   ! PROGRAM USES THESE VALUES EXCLUSIVELY TO CONSTRUCT THE DRAWINGS.
480   ! ANY CHANGE IN THESE VARIABLES WILL RESULT IN ALL ASSOCIATED PARAMETERS
490   ! IN THE DRAWING BEING ADJUSTED AUTOMATICALLY. ADJUSTING THESE VALUES
500   ! AND EVALUATING THE RESULTS IS A LIMITED USE OF CAD (COMPUTER AIDED
510   ! DESIGN).
520   !
530   !
540   ! USER DEFINED VARIABLES:
550   !
560   N=8               ! Determines the length of Horn. !
570   P=2               ! Determines the width of strip. !
580   M=3               ! Determines the length for transition. !
590   Hangle=10.1       ! Half angle of finline Horn antenna. !
600   Er=2.54           ! Dielectric Constant. !
610   Freq=1.00E10      ! Operating Frequency. !
620   Hwa=1.25*Mm       ! Half width of slot. !
630   !
640   ! DIMENSIONS OF FIXTURE:
650   !
660   Hwb=5.05*Mm       ! Half of Inside dimension of waveguide. !
```

```
670   Hwd=4*Mm          ! Extented flange of waveguide. !
680   Hlb=66.15*Mm      ! Length of fin inside the waveguide. !
690   Hlc=77.1*Mm       ! Length of fin for transition. !
700   !
710   !
720   ! FOLLOWING VARIABLES ARE COMBINATION OF USER DEFINED VARIABLE,
730   ! AND DEFINE THE WHOLE DRAWING.
740   !
750   !
760   Lambdazero=3.0E11*Mm/Freq   ! Wavelength in air. !
770   Lamdad=Lambdazero/SQR(Er)   ! Wavelength in dielectric. !
780   Hle=N*Lamdad                ! Length of Horn flare from center. !
790   Hws=Lamdad/P                ! With of Horn strip. !
800   Hla=Hle-Hwa/SIN(Hangle)     ! Length of Horn flare from mouth. !
810   Hlax=Hla*COS(Hangle)        ! Horizontal length of Horn flare. !
820   Hlay=Hla*SIN(Hangle)        ! Half of Horn slot. !
830   Hwsx=Hws*SIN(Hangle)        ! Lateral offset distance at end of Horn. !
840   Hwsy=Hws*COS(Hangle)        ! Vertical offset distance at end of Horn. !
850   !
860   !
870   X0=0                        ! Set location of drawing with respect to,
880                               ! the origion. !
890   Xa=X0-Hlax-Hwsx             ! Outer edge of Horn opening. !
900   Xb=X0-Hlax                  ! Upper edege of Horn opening. !
910   Xc=X0-Hwsx                  ! Horn mouth. !
920   Xd=X0+Hlb                   ! Length of slot inside waveguide. !
930   Xe=X0+Hlb+Hlc               ! Length of transition. !
940   !
950   !
960   Y0=0                        ! Set location of drawing with respect to,
970                               ! the origion. !
980   Ya=Y0+Hwa                   ! Width of inside slot. !
990   Yb=Y0+Hwb                   ! Inner edge of waveguide. !
1000  Yc=Y0+Hwa+Hwsy              ! Upper edge of Horn flare at mouth. !
1010  Yd=Yb+Hwd                   ! Upper edge of tansition. !
1020  Ye=Y0+Hwa+Hlay              ! Heigth of outer edge of Horn. !
1030  Yf=Ye+Hwsy                  ! Heigth of upper outer edge of Horn. !
1040  !
1050  !
1060  FOR Hfill=1 TO 5 STEP 2     ! Fill in the Horn. !
1070  Penn=Pen*Hfill
1080  Hangle1=45-Hangle           ! Uesed to determined the offset at the,
1090                              ! end of Horn. !
1100  Hangle2=(180-Hangle)/2      ! Used to determine offset at the mouth of Horn
. !
1110  Hangleb=ATN((Hwb-Hwa)/Hle) ! Used to determine offset at the transition. !
1120  Penoffset1h=Penn/2*COS(Hangle1)*SQR(2)  ! Correct point 2 in x direction,
1130                              ! and point 3 in y direction. !
1140  Penoffset2h=Penn/2*SIN(Hangle1)*SQR(2)  ! Correct point 2 in y direction,
1150                              ! and point 3 in x direction. !
1160  Penoffset3h=Penn/2/TAN(Hangle2)    ! Correct point 1 in x direction. !
1170  Penoffset4h=Penn/2*TAN(Hangleb/2)  ! Correct point 10 in x direction. !
1180  Penoffset5h=Penn/2/TAN(45+Hangleb/2)    ! Correct point 9 in y direction. !
1190  Penoffset6h=Penn/2/TAN(45+Hangle/2)     ! Correct point 4 in y direction. !
1200  !
1210  !
1220  ! FOLLOWING LINES DEFINES THE X CO-ORDINATE OF HORN POINT BY POINT. !
1230  !
1240  !
1250  X1h=Xc+Penoffset3h
1260  X2h=Xa+Penoffset1h
1270  X3h=Xb+Penoffset2h
1280  X4h=Xo-Penn/2
1290  X5h=Xo-Penn/2
1300  X6h=Xd+Penn/2
1310  X7h=Xd+Penn/2
1320  X8h=Xe-Penn/2
```

```
1330  X9h=Xe-Penn/2
1340  X10h=Xd-Penoffset4h
1350  !
1360  !
1370  ! FOLLOWING LINES DEFINES THE Y CO-ORDINATE OF HORN POINT BY POINT. !
1380  !
1390  !
1400  Y1h=Ya+Penn/2
1410  Y2h=Ye+Penoffset2h
1420  Y3h=Yf-Penoffset1h
1430  Y4h=Yc-Penoffset6h
1440  Y5h=Yb-Penn/2
1450  Y6h=Yb-Penn/2
1460  Y7h=Yd-Penn/2
1470  Y8h=Yd-Penn/2
1480  Y9h=Yb+Penoffset5h
1490  Y10h=Ya+Penn/2
1500  !
1510  !
1520  ! FOLLOWING LINES DRAW THE HORN FOR LARGE FIXTURE. !
1530  !
1540  !
1550  FOR Image=0 TO 2 STEP 2
1560  LINE TYPE Linenumber,Segmentsize    ! Plotter select dotted line with,
1570                                      ! overlap to draw Horn. !
1580  Im=1-Image
1590  MOVE X1h,Y1h+Im
1600  DRAW X2h,Y2h+Im
1610  DRAW X3h,Y3h+Im
1620  DRAW X4h,Y4h+Im
1630  DRAW X5h,Y5h+Im
1640  DRAW X6h,Y6h+Im
1650  DRAW X7h,Y7h+Im
1660  DRAW X8h,Y8h+Im
1670  DRAW X9h,Y9h+Im
1680  DRAW X10h,Y10h+Im
1690  DRAW X1h,Y1h+Im
1700  IF Hfill>1 THEN GOTO 1990
1710  X0arc=Xc+Hwa/TAN(Hangle)
1720  Y0arc=Y0
1730  LINE TYPE 4,.4*Scale   ! Select linetype to draw phase front and,
1740                         ! transition outline. !
1750  FOR Beta=0 TO Hangle STEP 2
1760  !
1770  ! FOLLOWING LINES ARE THE EQUATIONS THAT DEFINE PARALLEL PHASE FRONT,
1780  ! LENSE OUTLINES. !
1790  Aarc=1-COS(Beta)
1800  Barc=1-COS(Hangle)
1810  Carc=1/SQR(Er)-COS(Beta)
1820  Darc=COS(Hangle)-1/SQR(Er)
1830  Earc=COS(Beta)*(1-SQR(Er))
1840  B=Hle*(Aarc+Barc*Carc/Darc)/Earc    ! Thickness of lens. !
1850  Hrad=Hle+B+Pen                      ! Radius from center of flare to edge,
1860                                      ! of lens. !
1870  Xarc=X0arc-Hrad*COS(Beta)           ! X Position of arc. !
1880  Yarc=Y0arc-Hrad*SIN(Beta)           ! Y Position of arc. !
1890  IF Beta=0 THEN MOVE Xarc,Yarc
1900  DRAW Xarc,Yarc*Im*-1                ! Draws outline for lens. !
1910  NEXT Beta
1920  !
1930  ! FOLLOWING LINES DRAW OUTLINE FOR TRANSITION FROM WAVEGUIDE TO SLOTLINE.
!
1940  !
1950  Xbh=Xe+M*Lamdad
1960  Yba=Y0-.01*Lamdad
1970  MOVE Xe,Yb+Im
```

```
1980  DRAW Xbh,Yba*Im
1990  NEXT Image
2000  NEXT Hfill
2010  !
2020  !
2030  LINE TYPE 1
2040  !
2050  Xheading=X0-3*In
2060  Yheading=Ye+.5*In
2070  CSIZE .1*In
2080  MOVE Xheading,Yheading
2090  LABEL "FINLINE HORN by LCDR MUMTAZ UL HAQ"
2100  PEN 0
2110  MOVE 5000,500
2120  END
```

APPENDIX C

IBM COMPUTER PROGRAM TO CALCULATE FAR FIELD PATTERN

```
$JOB            IX,XREF,EXT
C
C     ******************************************************************
C     *                                                                *
C     *    THIS PROGRAM PERFORMS FOLLOWING FUNCTIONS.                  *
C     *    A, READ INPUT IN PHASE(DEGREE) AND MAGNITUDE(BD)            *
C     *       MEASURED AT FOUR DIFFERENT LOOP POSITIONS.               *
C     *    B, CONVERTS ALL PHASE AND MAGNITUDE IN TO REAL AND          *
C     *       IMAGINARY FORM AND CALCULATE RESULTANT PHASE AND         *
C     *       MAGNITUDE.
C     *    C, NORMALISES THE MEASURED AND CALCULATED PHASE AND         *
C     *       MAGNITUDE.                                               *
C     *    D, PERFORM THE FOURIER TRANSFORM ON THE RESULTANT           *
C     *       PHASE AND MAGNITUDE.                                     *
C     *    E, NORMALISES THE TRANSFIRMED MAGNITUDE(LINEAR),            *
C     *       MAGNITUDE(DB), AND PHASE(DEGREE).                        *
C     *                                                                *
C     *                                                                *
C     *                          MUMTAZ UL HAQ                         *
C     *                          LCDR PAKISTAN NAVY                    *
C     *                                                                *
C     ******************************************************************
C
C     ************** VARIABLE DEFINATIONS *****************************
C
C     K          NUMBER OF STEP FOR FOURIER TRANSFORM
C     STEP       ARRAY OF MEASUREMENT STEP ON FACE OF ANTENNA
C     MAD        RESULTANT MAGNITUDE IN DB ON FACE OF ANTENNA
C     PHA        RESULTANT PHASE IN DEGREE ON THE FACE OF ANTENNA
C     NPHA       NORMALISED RESULTANT PHASE IN DEGREE
C     NMAD       NORMALISED RESULTANT MAGNITUDE IN DE
C     NMAL       NORMALISED RESULTANT MAGNITUDE(LINEAR)
C     MADF       MEASURED MAGNITUDE IN DB ON FACE OF ANTENNA LOOP FACING
C                0 DEGREE POSITION
C     PHAF       MEASURE PHASE IN DEGREE ON FACE OF ANTENNA LOOP FACING
C                0 DEGREE POSITION
C     MALF       CALCULATED MAGNITUDE (LINEAR) FOR LOOP FACING 0 DEGREE
C                POSITION
C     NMADF      NORMALISED MAGNITUDE IN DB LOOP FACING 0 DEGREE POSITION
C     NPHAF      NORMALISED PHASE IN DEGREE LOOP FACING 0 DEGREE POSITION
C     NMALF      NORMALISED MAGNITUDE (LINEAR) LOOP FACING 0 DEGREE
C                POSITION
C     MADB       MEASURED MAGNITUDE IN DB ON FACE OF ANTENNA LOOP FACING
```

```
C               180 DEGREE POSITION
C       PHAB    MEASURE PHASE IN DEGREE ON FACE OF ANTENNA LOOP FACING
C               180 DEGREE POSITION
C       MALB    CALCULATED MAGNITUDE (LINEAR) FOR LOOP FACING 180 DEGREE
C               POSITION
C       NMADB   NORMALISED MAGNITUDE IN DB LOOP FACING 180 DEGREE POSITION
C       NPHAB   NORMALISED PHASE IN DEGREE LOOP FACING 180 DEGREE POSITION
C       NMALB   NORMALISED MAGNITUDE (LINEAR) LOOP FACING 180 DEGREE
C               POSITION
C       MADU    MEASURED MAGNITUDE IN DB ON FACE OF ANTENNA LOOP FACING
C               90 DEGREE POSITION
C       PHAU    MEASURE PHASE IN DEGREE ON FACE OF ANTENNA LOOP FACING
C               90 DEGREE POSITION
C       MALU    CALCULATED MAGNITUDE (LINEAR) FOR LOOP FACING 90 DEGREE
C               POSITION
C       NMADU   NORMALISED MAGNITUDE IN DB LOOP FACING 90 DEGREE POSITION
C       NPHAU   NORMALISED PHASE IN DEGREE LOOP FACING 90 DEGREE POSITION
C       NMALU   NORMALISED MAGNITUDE (LINEAR) LOOP FACING 90 DEGREE
C               POSITION
C       MADD    MEASURED MAGNITUDE IN DB ON FACE OF ANTENNA LOOP FACING
C               270 DEGREE POSITION
C       PHAD    MEASURE PHASE IN DEGREE ON FACE OF ANTENNA LOOP FACING
C               270 DEGREE POSITION
C       MALD    CALCULATED MAGNITUDE (LINEAR) FOR LOOP FACING 270 DEGREE
C               POSITION
C       NMADD   NORMALISED MAGNITUDE IN DB LOOP FACING 270 DEGREE POSITION
C       NPHAD   NORMALISED PHASE IN DEGREE LOOP FACING 270 DEGREE POSITION
C       NMALD   NORMALISED MAGNITUDE (LINEAR) LOOP FACING 270 DEGREE
C               POSITION
C       FPHA    PHASE OF FOURIER TRANSFORM OF RESULTANT
C       FMAL    MAGNITUDE OF FOURIER TRANSFORM OF RESULTANT
C       NFPHA   NORMALISED PHASE OF FOURIER TRANSFORM OF RESULTANT
C       NFMAL   NORMALISED MAGNITUDE OF FOURIER TRANSFORM OF RESULTANT
C       NFMAD   NORMALISED MAGNITUDE OF FOUIER TRANSFORM IN DB
C       LAMDA   WAVELENGTH IN MM
C       SS      STEP SIZE IN MM
C
C       **************** VARIABLE DECLARATIONS ********************
C
        INTEGER  IWK(6),I,L,M,N,J
        COMPLEX*8 A(32)
        REAL*8   RE,IM
        REAL*8   FPHA(32),FMAL(32),NFPHA(32),NFMAL(32),NFMAD(32)
        REAL*8   STEP(50),PHA(50),MAD(50),MAL(50),NPHA(50),NMAD(50),A1,A2
        REAL*8   NMAL(50),RPHA,RMAD,RMAL
        REAL*8   PHAF(50),MADF(50),MALF(50),NPHAF(50),NMADF(50),NMALF(50)
        REAL*8   A1F,A2F,REF,IMF
        REAL*8   PHAB(50),MADB(50),MALB(50),NPHAB(50),NMADB(50),NMALB(50)
        REAL*8   A1B,A2B,REB,IMB
        REAL*8   PHAU(50),MADU(50),MALU(50),NPHAU(50),NMADU(50),NMALU(50)
```

```
      REAL*8   A1U,A2U,REU,IMU
      REAL*8   PHAD(50),MADD(50),MALD(50),NPHAD(50),NMADD(50),NMALD(50)
      REAL*8   A1D,A2D,RED,IMD,K
      REAL*8   BEAM,LAMDA,SS,Q,PI,AMAG(32),APHA(32)
C
      LAMDA = 30.0
      SS = 5.00
      N = 32
      L = 32
      M = 5
      K = 0.0
      J = N/2
      PI = 57.295779
      RPHA = -360.0
      RMAL = 1.0E-10
      RMAD = 100.0
C
C     ******************** INPUT INFORMATION *********************
C
      DO 10 I = 1,N
         READ (5,600) STEP(I),MADF(I),PHAF(I),MADB(I),PHAB(I),MADU(I),
     *PHAU(I),MADD(I),PHAD(I)
         MALF(I) = 10.0 ** (-1.0*MADF(I)/10.0)
         MALB(I) = 10.0 ** (-1.0*MADB(I)/10.0)
         MALU(I) = 10.0 ** (-1.0*MADU(I)/10.0)
         MALD(I) = 10.0 ** (-1.0*MADD(I)/10.0)
         A1F = DCOS (PHAF(I)/PI)
         A2F = DSIN (PHAF(I)/PI)
         A1B = DCOS (PHAB(I)/PI)
         A2B = DSIN (PHAB(I)/PI)
         A1U = DCOS (PHAU(I)/PI)
         A2U = DSIN (PHAU(I)/PI)
         A1D = DCOS (PHAD(I)/PI)
         A2D = DSIN (PHAD(I)/PI)
         REF     = MALF(I) * A1F
         IMF     = MALF(I) * A2F
         REB     = MALB(I) * A1B
         IMB     = MALB(I) * A2B
         REU     = MALU(I) * A1U
         IMU     = MALU(I) * A2U
         RED     = MALD(I) * A1D
         IMD     = MALD(I) * A2D
         RE      = REF + REB + REU + RED
C        RE      = REF + REB
         IM      = IMF + IMB + IMU + IMD
C        IM      = IMF + IMB
         MAL(I)  = DSQRT(RE**2 + IM**2)
         MAD(I)  = -10.0 * (DLOG10(MAL(I)))
         PHA(I)  = (DATAN(IM/RE))*PI
         IF (RE .GE. 0.0 ) GO TO 2
```

```
            IF (IM .GE. 0.0 ) GO TO 1
               PHA(I) = (PHA(I)-180.0)
            GO TO 2
 1          CONTINUE
            PHA(I) = PHA(I) + 180.0
 2       CONTINUE
         MALF(I) = DSQRT(REF**2 + IMF**2)
         MADF(I) = -10.0 * (DLOG10(MALF(I)))
         PHAF(I) = (DATAN(IMF/REF))*PI
         IF (REF .GE. 0.0 ) GO TO 4
            IF (IMF .GE. 0.0 ) GO TO 3
               PHAF(I) = (PHAF(I)-180.0)
            GO TO 4
 3          CONTINUE
            PHAF(I) = PHAF(I) + 180.0
 4       CONTINUE
         MALB(I) = DSQRT(REB**2 + IMB**2)
         MADB(I) = -10.0 * (DLOG10(MALB(I)))
         PHAB(I) = (DATAN(IMB/REB))*PI
         IF (REB .GE. 0.0 ) GO TO 6
            IF (IMB .GE. 0.0 ) GO TO 5
               PHAB(I) = (PHAB(I)-180.0)
            GO TO 6
 5          CONTINUE
            PHAB(I) = PHAB(I) + 180.0
 6       CONTINUE
         MALU(I) = DSQRT(REU**2 + IMU**2)
         MADU(I) = -10.0 * (DLOG10(MALU(I)))
         PHAU(I) = (DATAN(IMU/REU))*PI
         IF (REU .GE. 0.0 ) GO TO 8
            IF (IMU .GE. 0.0 ) GO TO 7
               PHAU(I) = (PHAU(I)-180.0)
            GO TO 8
 7          CONTINUE
            PHAU(I) = PHAU(I) + 180.0
 8       CONTINUE
         MALD(I) = DSQRT(RED**2 + IMD**2)
         MADD(I) = -10.0 * (DLOG10(MALD(I)))
         PHAD(I) = (DATAN(IMD/RED))*PI
         IF (RED .GE. 0.0 ) GO TO 11
            IF (IMD .GE. 0.0 ) GO TO 9
               PHAD(I) = (PHAD(I)-180.0)
            GO TO 11
 9          CONTINUE
            PHAD(I) = PHAD(I) + 180.0
 11      CONTINUE
         A(I) = DCMPLX (RE,IM)
 10   CONTINUE
C
C     ******** PROGRAM TO NORMALISE THE MAG. AND PHASE **********
```

```
C
      DO 20 I = 1,N
         IF (.NOT. MAD(I) .LE. RMAD) GO TO 20
         RMAD = MAD(I)
20    CONTINUE
      DO 30 I = 1,N
         IF (.NOT. MAL(I) .GE. RMAL ) GO TO 30
         RMAL = MAL(I)
30      CONTINUE
      DO 40 I = 1,N
         IF (.NOT. PHA(I) .GE. RPHA) GO TO 40
         RPHA = PHA(I)
40    CONTINUE
      DO 21 I = 1,N
         IF (.NOT. MADF(I) .LE. RMAD) GO TO 21
         RMAD = MADF(I)
21    CONTINUE
      DO 31 I = 1,N
         IF (.NOT. MALF(I) .GE. RMAL ) GO TO 31
         RMAL = MALF(I)
31      CONTINUE
      DO 41 I = 1,N
         IF (.NOT. PHAF(I) .GE. RPHA) GO TO 41
         RPHA = PHAF(I)
41    CONTINUE
      DO 22 I = 1,N
         IF (.NOT. MADB(I) .LE. RMAD) GO TO 22
         RMAD = MADB(I)
22    CONTINUE
      DO 32 I = 1,N
         IF (.NOT. MALB(I) .GE. RMAL ) GO TO 32
         RMAL = MALB(I)
32      CONTINUE
      DO 42 I = 1,N
         IF (.NOT. PHAB(I) .GE. RPHA) GO TO 42
         RPHA = PHAB(I)
42    CONTINUE
      DO 23 I = 1,N
         IF (.NOT. MADU(I) .LE. RMAD) GO TO 23
         RMAD = MADU(I)
23    CONTINUE
      DO 33 I = 1,N
         IF (.NOT. MALU(I) .GE. RMAL ) GO TO 33
         RMAL = MALU(I)
33      CONTINUE
      DO 43 I = 1,N
         IF (.NOT. PHAU(I) .GE. RPHA) GO TO 43
         RPHA = PHAU(I)
43    CONTINUE
      DO 24 I = 1,N
```

```
         IF (.NOT. MADD(I) .LE. RMAD) GO TO 24
         RMAD = MADD(I)
   24    CONTINUE
         DO 34 I = 1,N
         IF (.NOT. MALD(I) .GE. RMAL ) GO TO 34
         RMAL = MALD(I)
   34      CONTINUE
         DO 44 I = 1,N
         IF (.NOT. PHAD(I) .GE. RPHA) GO TO 44
         RPHA = PHAD(I)
   44    CONTINUE
         DO 50 I = 1,N
            NMAD(I)  = RMAD-MAD(I)
            NMAL(I)  = MAL(I)/RMAL
            NPHA(I)  = PHA(I)-RPHA
            NMADF(I)  = RMAD-MADF(I)
            NMALF(I)  = MALF(I)/RMAL
            NPHAF(I)  = PHAF(I)-RPHA
            NMADB(I)  = RMAD-MADB(I)
            NMALB(I)  = MALB(I)/RMAL
            NPHAB(I)  = PHAB(I)-RPHA
            NMADU(I)  = RMAD-MADU(I)
            NMALU(I)  = MALU(I)/RMAL
            NPHAU(I)  = PHAU(I)-RPHA
            NMADD(I)  = RMAD-MADD(I)
            NMALD(I)  = MALD(I)/RMAL
            NPHAD(I)  = PHAD(I)-RPHA
   50    CONTINUE
C
C
C        ** PROGRAM TO COMPUTE FOURIER TRANSFORM AND NORMALISE IT **
C
         CALL FFT2C (A,M,IWK)
C
         DO 60 I = 1,N
            AMAG(I)  = CABS(A(I))
            RE = REAL(A(I)) + 1.0E-8
            IM = AIMAG(A(I))
            APHA(I)  = DATAN2(IM,RE)* PI
            FMAL(I)  = AMAG(I)
            FPHA(I)  = APHA(I)
   60    CONTINUE
C
         RPHA = -360.0
         RMAL = 1.0E-10
         RMAD = 0.0
         DO 70 I = 1,N
         IF (.NOT. FMAL(I) .GE. RMAL) GO TO 70
         RMAL = FMAL(I)
   70    CONTINUE
```

```
      DO 80 I = 1,N
         IF (.NOT. FPHA(I) .GE. RPHA) GO TO 80
         RPHA = FPHA(I)
80    CONTINUE
      DO 90 I = 1,N
         NFPHA (I) = FPHA (I)-RPHA
         NFMAL (I) = FMAL (1) /RMAL
         NFMAD (I) = 10.0*(DLOG10(NFMAL(I)))
90    CONTINUE
C
C     ********************* OUTPUT DATA ************************
C
      WRITE (6,500)
      DO 100 I = 1,N
         WRITE (6,510) STEP(I),PHA(I),MAD(I)
100   CONTINUE
      WRITE (6,500)
      DO 110 I = 1,N
        WRITE(6,520) STEP(I),NMADF(I),NMADB(I),NMADU(I),NMADD(I),NMAD(I)
110   CONTINUE
      WRITE (6,500)
      DO 120 I = 1,N
        WRITE(6,530) STEP(I),NPHAF(I),NPHAB(I),NPHAU(I),NPHAD(I),NPHA(I)
120   CONTINUE
      WRITE (6,500)
      DO 130 I = 1,N
        WRITE(6,540) STEP(I),NMALF(I),NMALB(I),NMALU(I),NMALD(I),NMAL(I)
130   CONTINUE
      WRITE (6,500)
      DO 140 I = 1,N
        WRITE(6,550) STEP(I),MADF(I),MADB(I),MADU(I),MADD(I),MAD(I)
140   CONTINUE
      WRITE (6,500)
      DO 150 I = 1,N
        WRITE(6,560) STEP(I),PHAF(I),PHAB(I),PHAU(I),PHAD(I),PHA(I)
150   CONTINUE
      WRITE (6,500)
      DO 210 I = 1,N
         WRITE(6,580) K,NFPHA(I),NFMAD(I),NFMAL(I)
         K= K+1
210   CONTINUE
      WRITE (6,500)
      K = N/2
      J =J+1
      DO 220 I = J,N
         Q = (K*LAMDA)/(N*SS)
         IF (.NOT. Q .LE. 1.0) GO TO 215
            BEAM = (DARSIN(-1.0*Q))*PI
            WRITE (6,590) BEAM,NFMAD(I)
215      CONTINUE
```

```
          K = K-1
  220  CONTINUE
       K = 0
       DO 230 I = 1,J
          Q = (K*LAMDA)/(N*SS)
          IF (.NOT. Q .LE. 1.0) GO TO 225
             BEAM = (DARSIN(Q))*57.298
             WRITE (6,590) BEAM,NFMAD(I)
  225     CONTINUE
          K =K+1
  230  CONTINUE
       WRITE (6,500)
       STOP
  500  FORMAT ('1')
  510  FORMAT (' ',3F8.2)
  520  FORMAT(' ',6F10.3)
  530  FORMAT(' ',6F10.3)
  540  FORMAT(' ',6F10.5)
  550  FORMAT(' ',6F10.3)
  560  FORMAT(' ',6F10.3)
  580  FORMAT(' ',4F10.5)
  590  FORMAT(' ',2F10.3)
  600  FORMAT(9F8.2)
       END
```

LIST OF REFERENCES

1. Paul,J.Meier,"Millimeter Integrated Circuits Suspended in the E-Plane of Rectangular Waveguide," IEEE Transation on Microwave Theory and Techniques, pp. 726-732, October 1978.

2. Arvind,K.Sharma,"Empirical Expression for Fin Line Design," IEEE Transactions on Microwave Theory and Techniques, pp. 350-355, 1983.

3. W.A.Hammening,"Implementing a Near-Field Antenna Test Facility," Microwave Journal, pp. 44-55, September 1979.

4. C.F.Stubenrauch,and A.C.Newell,"Some Recent Near Field Measurement at NBS," Microwave Journal, pp. 37-42, November 1980.

5. John,R.Musitano, FinLine Horn Antenna, M.S.Thesis, Naval Postgraduate School, Monterey, California, 1984.

6. W.A.Hammening,"A Laser Based, Near Field Probe Position Measurement System," Microwave Journal, pp. 91-101, October 1979.

7. D.W.Hess,"Spherical Near Field Antenna Measurements Improved Through Expanded Software Feature," MSN & CT, pp. 64-83, March 1985.

8. Kenneth,R.Grimm,"Antenna Analysis by Near-Field Measurement," Microwave Journal, pp. 43-45, April 1976.

9. L.Thourel,The Antenna, pp. 239 - 250, John Wiley&sons Inc,1960.

10. Om.P.Gandhi.Microwave Engineering and Application, Pergamon press, 1984.

11. Adalbert Beyer and Ingo Wolff,"FinLine Taper Design Made Easy," IEEE Transactions on Microwave Theory and Techniques, pp. 493-496, 1985.

12. Henry Jasik,Antenna Engineering HandBook, pp. 10.1-10.17, McGraw-Hill, 1961.

13. A.Z.Fradin,Microwave Antennas, pp. 3-22, Pergamon press, 1961.

14. Skolink, M.I, Radar HandBook, pp. 10.1-10.17, McGraw-Hill, 1970.

15. Jordan, E.C and Balmain, K.G, Electromagnetic Waves and Radiating systems, p. 503, Prentice-Hall Inc., 1968.

16. James, W. Rowley, FinLine Magic Tee, M.S. Thesis, Naval Postgraduate School, Monterey, California, 1985.

BIBLIOGRAPHY

Harry Syrigos and others, "Planer Waveguide Yields mm-wave Monopulse Comparators," _Microwaves and RF_, March 1984.

INITIAL DISTRIBUTION LIST

		No. Copies
1.	Defence Technical Information Center Cameron Station Alexandria, Virginia 22304-6145	2
2.	Library, Code 0142 Naval Postgraduate School Monterey, CA 93943-5100	2
3.	Department Chairman, Code 62 Department of Electrical Engineering Naval Postgraduate School Monterey, CA 93943-5100	1
4.	Professor Jefferey B. Knorr, Code 62Ko Department of Electrical Engineering Naval Postgraduate School Monterey, CA 93943-5100	2
5.	Professor Hung-Mou Lee, Code 62Lh Department of Electrical Engineering Naval Postgraduate School Monterey, CA 93943-5100	1
6.	LCDR Mumtaz ul Haq PN 4 Chauburji Park Multan Road Lahore Pakistan	2
7.	LCDR James W. Rowley USN 6691 675th Avenue West Oak Harbor, Washington 98277	1

216629

Thesis
H20473 Haq
c.1 Finline horn antennas.